Development of Techniques for Rapidly Assessing the Local Air Quality Impacts of Airports

by

Gideon Lee

B.S. Mechanical Engineering
University of California, Berkeley, 2010

SUBMITTED TO THE DEPARTMENT OF AERONAUTICS AND ASTRONAUTICS
IN PARTIAL FULFILLMENT OF THE REQUIREMENTS FOR THE DEGREE OF

MASTER OF SCIENCE IN AERONAUTICS AND ASTRONAUTICS
AT THE
MASSACHUSETTS INSTITUTE OF TECHNOLOGY

SEPTEMBER 2012

Signature of Author.....
Department of Aeronautics and Astronautics
September 2012

Certified by.....
Steven R.H. Barrett
Assistant Professor of Aeronautics and Astronautics
Thesis Supervisor

Accepted by.....
Eytan H. Modiano
Professor of Aeronautics and Astronautics
Chair, Graduate Program Committee

Development of Techniques for Rapidly Assessing the Local Air Quality Impacts of Airports

by

Gideon Lee

Submitted to the Department of Aeronautics and Astronautics
on August 23, 2012 in Partial Fulfillment of the
Requirements for the Degree of Master of Science in
Aeronautics and Astronautics

Abstract

The combustion of fossil fuels for aviation activity harms air quality and human health near airports through the production of $PM_{2.5}$. Currently, dispersion models can assess these local-scale (distances ~10 km) impacts, calculating long-term (annual) average concentrations of $PM_{2.5}$. However, these models typically require hours to complete an analysis for one site, hindering their use for assessing local-scale impacts over national or global extents.

In this thesis, approximations are used to develop and apply the Rapid Dispersion Modeling System (RDMS) for calculating annual average concentrations of $PM_{2.5}$. RDMS accuracy and speed were compared to a preexisting dispersion model, the AMS-EPA Regulatory Model (AERMOD). Meteorological, emissions, runway, and taxiway/terminal data for simulations were obtained from various sources. The RDMS was applied to obtain local-scale $PM_{2.5}$ concentrations and exposures for the year 2006 for 191 U.S. airports that accounted for 95% of U.S. air passenger traffic. The resulting local-scale $PM_{2.5}$ concentrations were combined with results from the Community Multiscale Air Quality (CMAQ) regional-scale model to account for primary and secondary $PM_{2.5}$. Cases accounting for both landing-takeoff (LTO)-only and full-flight emissions were considered. Finally, premature mortalities at both regional and local scales were estimated by applying a concentration-response function to the combined concentrations.

On average, RDMS over-predicts AERMOD concentrations by ~5% but reduces total simulation time by ~99.5% when only the rapid dispersion calculation (RDC) is considered. Including the calculation of dispersion parameters required by the RDC, RDMS saves ~95% of the simulation time required by AERMOD. Over all airports at the local scale, RDMS-modeled concentrations of $PM_{2.5}$ accounted for 38-66 premature mortalities, 43-65% of total local-scale premature mortalities for the LTO case and 8-13% for the full-flight case. At the regional scale, RDMS-modeled $PM_{2.5}$ accounted for 34-50% of premature mortalities for the LTO case and 4-7% for the full-flight case. Inclusion of RDMS-modeled local-scale variations increased local-scale premature mortality estimates by 16-27% for the LTO case and 1-2% for the full-flight case. Inclusion of local-scale variations increased regional premature mortality estimates by 8-12% for the LTO case and 1% for the full-flight case.

Thesis Supervisor: Steven R.H. Barrett
Title: Assistant Professor of Aeronautics and Astronautics

Acknowledgements

I would like to thank my research and thesis adviser for the past two years, Professor Steven Barrett, for his continual guidance, patience, and good humor during my work on this project, without which completing this research would not have been possible. I especially appreciate Steven's help in finding solutions to all those unexpected issues that arose during the development of RDMS, knowing that the opportunity to work closely with one's research adviser is not an opportunity that all graduate students have. Thank you, Steven.

I also thank those that I've had the opportunity to work and spend time with the past two years. Akshay, thank you for always keeping an open ear for helping me figure things out with research and graduate school life; Steve, thanks for taking care of the project so that I could focus on the research; Sergio, thanks for providing me with memorable quotes (although I wish you were wrong when you said "theses don't write themselves"); Kevin, thanks for sharing graduate school experiences with me.

I'm grateful for the continuing support of my family and close friends, who have helped me during this challenging experience of graduate school at MIT. Thanks, Mom and Dad, for always encouraging me to pursue my career interests whatever that may be, and for providing financial support when I needed it. To Tina, and Tammy, I'm sincerely grateful to have you as friends. Thank you both for your care, understanding, and advice that have helped me through difficult situations these past two years.

This project was funded by the U.S. Federal Aviation Administration. The AEDT Airport Database used in this work was provided by the U.S. DOT Volpe Center. The AERMOD dispersion model and AERMET meteorological preprocessor were provided by the U.S. Environmental Protection Agency. Meteorological data were provided by the U.S. NOAA National Climatic Data Center. Any opinions, findings, and conclusions expressed in this thesis are those of the author and do not necessarily reflect the views of the U.S. FAA, U.S. DOT Volpe Center, U.S. EPA, or U.S. NOAA NCDC.

Contents

List of Figures

List of Tables

List of Equations

List of Acronyms

Organizational Terms

DOT	Department of Transportation
EPA	Environmental Protection Agency
(ETC/ACM)	European Topic Center for Air Pollution and Climate Change Mitigation
FAA	Federal Aviation Administration
ICAO	International Civil Aviation Organization
LAE	Laboratory for Aviation and the Environment
NAAQS	National Ambient Air Quality Standards
NASA	National Aeronautics and Space Administration
NCDC	National Climatic Data Center
NSR	New Source Review
PSDH	Project for the Sustainable Development of Heathrow
PSD	Prevention of Significant Deterioration
SLAMS	EPA State and Local Air Monitoring Stations
SEDAC	Socioeconomic Data and Applications Center
WHO	World Health Organization

Computer Models and Data

ADMS™	Atmospheric Dispersion Modelling System
AEDT	Aviation Environmental Design Tool
AERMOD	AMS-EPA Regulatory MODel
CFD	Computational Fluid Dynamics
CMAQ	Community Multiscale Air Quality
CTM	Chemistry Transport Model
EDMS	Emissions and Dispersion Modeling System
GEOS-Chem	Goddard Earth Observing System - Chemistry
GRUMPv1	Global Rural-Urban Mapping Project, version 1
IGRA	Integrated Global Radiosonde Archive
ISD/ISHD	Integrated Surface Database/Integrated Surface Hourly Database
LASAT™	Lagrangian Simulation of Aerosol Transport
LSM	Lagrangian Stochastic Model
MATLAB®	MATrix LABoratory
MM5	PSU/NCAR Mesoscale Model
MOZART	Model for OZone And Related chemical Tracers
OML Model	Operationelle Meteorologiske Luftkvalitetsmodeller Model
RDC	Rapid Dispersion Calculation
RDMS	Rapid Dispersion Modeling System
SVG	Scalable Vector Graphics
SQL	Structured Query Language
TOMCAT/SLIMCAT	Toulouse Off-line Model of Chemistry And Transport/ Single Layer Isentropic Model of Chemistry And Transport
WRF	Weather Research and Forecasting Model

Pollutants

$PM_{2.5}$	Particulate Matter with aerodynamic diameter of 2.5 μm
BC	Black Carbon
CO	Carbon Monoxide
CO_2	Carbon Dioxide
EC	Elemental Carbon
HC	Hydrocarbon
NO_x	Nitrogen Oxides
PEC	Primary Elemental Carbon
POA	Primary Organic Aerosol
PSO_4	Primary Sulfates
RSP	Respirable Suspended Particles
SO_2	Sulfur Dioxide
SO_4	Sulfates
UFP	Ultra-Fine Particles

Technical Terms

CP	Cardiopulmonary
CRF	Concentration-Response Function
FTIR	Fourier Transform Infrared Spectroscopy
GLP	Ground-Level Primary
LC	Lung Cancer
LDAA	Lateral Dispersion Averaging Approximation
LIDAR	LIght Detection And Ranging
LTO	Landing Take-Off
TIM	Time In Mode
ULS	Ultra-Low Sulfur

Airports

EGLL	London Heathrow Airport
KATL	Hartsfield-Jackson Atlanta International Airport
KAVL	Asheville Regional Airport
KBOS	Logan International Airport (Boston)
KELP	El Paso International Airport
KEWR	Newark Liberty International Airport
KGCN	Grand Canyon National Park Airport
KJFK	John F. Kennedy International Airport (New York)
KLAX	Los Angeles International Airport
KLGA	LaGuardia Airport (New York)
KPIT	Pittsburgh International Airport
KPVD	T.F. Green Airport (Providence)
LSZH	Zurich Airport
VHHH	Hong Kong International Airport

1. Introduction

Civil air transport is an important component of the global economy, contributing 4.5% of world economic output in 1998 according to the International Civil Aviation Organization (ICAO) [1]. Demand for air transport is closely linked with economic development [1]. As economies worldwide develop, demand for air transport is expected to grow as well. For example, passenger traffic is projected to grow at an average rate of 4.8% per year through 2036 [2].

As with other transportation modes, such as ground and ship transport, aviation relies on the combustion of fossil fuels. Emissions from fuel combustion impact the global climate and air quality. Although aviation's contribution to anthropogenic emissions of greenhouse gases and pollutants compared to that of other sources is relatively small (ICAO estimates 13% of global transport CO_2 emissions come from aviation, while 74% come from road transport [2]), growth in the aviation sector means that emissions of greenhouse gases and pollutants could increase correspondingly if measures regulating aviation fuel and technology do not mitigate such effects.

1-1 Airborne Pollution at Airports

Aviation activities at airports contribute to the degradation of air quality in surrounding areas through the emission of air pollutants. ICAO estimates that "for a typical urban environment, airport emissions represent approximately 10% of total regional emissions in the vicinity of airports" where "the term 'region' refers to the local communities surrounding the airport (i.e. within 50 km)" [2]. Airborne pollutants associated with aircraft have a variety of adverse health impacts, some of which are summarized in Table 1.

Inhalation of airborne pollutants causes a variety of ill effects in humans [3]. In epidemiological studies on these effects, negative impacts are divided into those resulting from short-term exposure and long-term exposure to pollutants. Short-term exposure can result from events such as smoggy days, fires, dust clouds, and day-to-day variations and are generally temporary in nature. For example, Pope and Dockery report on studies of short-term exposure that relate daily exposure to particulate matter (PM) to mortalities in cities [4]. Short-term (acute) health impacts of exposure to pollutants include eye irritation, headaches, and nausea [3]. Long-term exposure, on the other hand, is measured over periods of months and years [4]. Long-term

Pollutant	Health Effects
Carbon Monoxide (CO)	Headaches, reduced mental alertness, heart attack, cardiovascular diseases, impaired fetal development, death.
Sulfur Dioxide (SO_2)	Eye irritation, wheezing, chest tightness, shortness of breath, lung damage.
Nitrogen Dioxide (NO_2)	Susceptibility to respiratory infections, irritation of the lung and respiratory symptoms (e.g., cough, chest pain, difficulty breathing).
Ozone (O_3)	Eye and throat irritation, coughing, respiratory tract problems, asthma, lung damage.
Lead (Pb)	Anemia, high blood pressure, brain and kidney damage, neurological disorders, cancer, lowered IQ.
Particulate Matter (PM)	Eye irritation, asthma, bronchitis, lung damage, cancer, heavy metal poisoning, cardiovascular effects.

Table 1. Health effects of criteria pollutants. Adapted from [3].

Air Pollutant	Guideline Amount	Averaging Time
$PM_{2.5}$	10 μg/m^3	Annual
	25 μg/m^3	24-hr
PM_{10}	20 μg/m^3	Annual
	50 μg/m^3	24-hr
Ozone	100 μg/m^3	8-hr
NO_2	40 μg/m^3	Annual
	200 μg/m^3	1-hr
SO_2	20 μg/m^3	24-hr
	500 μg/m^3	10-min

Table 2. WHO air quality guidelines for four major pollutants. Adapted from [5].

health impacts include decreased lung capacity, lung cancer, respiratory disease, and premature death [3]. According to Pope and Dockery, "long-term repeated exposures have larger, more persistent cumulative effects than short-term transient exposures" [4].

Due to their negative health impacts, airborne pollutant levels are regulated by agencies such as the U.S. Environmental Protection Agency (EPA). The World Health Organization (WHO) has established guidelines for exposure to air pollutants, five of which are listed in Table 2.

Concentrations of pollutants are frequently expressed in μg (mass) of pollutant present per m^3 (volume) of air. Population-weighted concentrations provide another metric of exposure that can be calculated with the following formula:

$$\text{Pop} - \text{weighted Concentration} = \sum_{\text{areas}} \frac{\text{Concentration} \times \text{Population in Area}}{\text{Total Population}}$$

This formulation is included in studies that use computer models [6–8], in which the population-weighted concentration is approximately proportional to health impacts as measured

by increased early death risk. Population-weighted concentrations place greater emphasis on areas that are more heavily populated as these areas will have higher health impacts.

1-2 $PM_{2.5}$

Of the pollutants listed, fine particulate matter ($PM_{2.5}$) is especially harmful to human health [4]. Fine particulate matter consists of small particles and liquid droplets of different chemical composition that have an aerodynamic diameter of 2.5 μm or less. When inhaled by humans, these particles can bypass respiratory defenses to reach the lungs and enter the bloodstream, causing negative health effects. For its latest guidelines, the WHO reviewed several studies on long-term exposure to $PM_{2.5}$ and concluded that "robust associations were reported between long-term exposure to $PM_{2.5}$ and premature mortality." [5]

$PM_{2.5}$ comes from a variety of natural and anthropogenic sources. $PM_{2.5}$ can be emitted directly or can form in the atmosphere due to the reaction of chemical precursors and existing compounds in the atmosphere. The former are termed "primary" particulate matter and the latter are called "secondary" particulate matter [9]. Although $PM_{2.5}$ consists of a variety of species, a few compounds contribute the most to concentrations in the United States [10], [11]. Some of these compounds are listed in Table 3.

$PM_{2.5}$ Species	**Example Sources**	**Primary/Secondary**
Black Carbon	Combustion of fossil fuels, forest fires	Primary
Organic Carbon	Gas emissions from combustion	Primary
Sulfates	Sulfur dioxide emissions from combustion	Both
Nitrates	Nitrogen oxide emissions from combustion	Secondary
Crustal Particles - Soil and Ash	Dust storms, construction sites, ash pits	Primary

Table 3. Major $PM_{2.5}$ species in the United States. Information from [10], [11].

Sources of $PM_{2.5}$ attributable to aviation activities include emissions from aircraft, auxiliary power units, ground support equipment, ground access vehicles, buildings that combust fuel for heating and power, and road traffic around airports [12]. The location of airports, temporal variations in aviation traffic and meteorology, presence of other emissions sources, and population patterns distribute the negative health effects of aviation $PM_{2.5}$ non-uniformly.

1-3 Methods for Studying Aircraft Impacts on Air Quality Near Airports

To aid in the evaluation of measures to mitigate these effects, researchers have pursued different approaches to assessing the air quality impacts of aviation and aircraft in particular. In this section, some of these methods are briefly described.

1-3-1 Characterization of Aircraft Emissions

Aircraft emissions contribute a significant proportion of total airport emissions from all sources near airports, with one study at Zurich airport estimating that aircraft contributed 70-87% of airport-related NO_x, HC, CO, PM, and CO_2 [13]. However, emissions of particulate matter are not as well understood as other pollutants for several reasons. Particulate matter does not consist of a single chemical species, but is an umbrella category for liquid and solid airborne particles of different size, number, and composition. Furthermore, the formation of particulate matter from aircraft engine exhaust involves a variety of chemical and microphysical processes for which a complete understanding has not yet been reached in the literature.

Current estimates of aircraft PM emissions rely on emission indices, which express the amount of pollutants per mass of fuel burned (typically in g pollutant/kg fuel). The ICAO has developed emission indices for a variety of engine types and thrust settings, for the purpose of approximating pollutant emissions under ideal laboratory settings [14]. To quantify aircraft emissions near airports, often only emissions during landing and take-off (LTO) are considered and are defined as emissions below an altitude of 3000 ft above field elevation.

To estimate emissions from aircraft operations, emissions indices for particular engines and thrust settings are multiplied by assumed times spent in a particular thrust setting, called time-in-mode (TIM), and by the average fuel flow rate. The ICAO has also developed times-in-mode for assessing emissions at airports. As an example of a study using this approach to estimate emissions, Stettler used emission indices from the ICAO databank and the U.S. Federal Aviation Administration's (FAA) Emissions and Dispersion Modeling System (EDMS) with some modification to estimate aircraft emissions in the UK [15].

Although the ICAO database is useful for approximating aircraft emissions, it does not account for real-world operations and conditions that can influence the emissions of pollutants. As ICAO notes, "In assessing, for example, total aircraft emissions at a specific airport, consideration must be given to the appropriateness of the prescribed thrusts, the times in mode and the reference conditions" [14]. Furthermore, Stettler notes that "the standard ICAO

certification LTO cycle is generally not representative of operations at airports" [15]. For practical air quality analysis, computer models that scale air quality linearly with emissions would yield different results depending on particular emissions methods used.

These factors motivate studies to better quantify emissions from aircraft. Schafer used an optical method, Fourier Transform Infrared Spectroscopy (FTIR), to passively observe infrared radiation emanating from aircraft exhausts [16]. The observations are used to infer the temperature and concentration of gaseous compounds within the plume. Several studies incorporated the use of on-site mobile laboratories to collect aircraft plumes for analysis [17–20]. The plumes are sampled, then laboratory equipment is used to analyze chemical composition and size and number distribution of particulate matter. Moniruzzaman developed a model that accounts for jet fuel chemistry, engine parameters, atmospheric conditions, and aerosol microphysics and predicts the time evolution, formation history, and emissions index of gas and soot particle exhausts [21]. Studies to better understand aircraft emissions of particulate matter can improve future estimates of aircraft impacts on local air quality.

1-3-2 Aircraft Plume Dynamics

After aircraft engines exhaust pollutants, a variety of physical and chemical processes occur that transport particulate matter through the atmosphere and transform precursors into $PM_{2.5}$. Regulatory models such as the AMS-EPA Regulatory Model (AERMOD) [22] were developed for the treatment of emissions from stationery sources such as power plant stacks. However, aircraft plumes possess several characteristics that differ from plumes from industrial sources. For example, Barrett notes that aircraft plumes emanate from accelerating sources, are unsteady, are subject to the effects of ground impingement and trailing vortices, and buoyantly rise differently from industrial stacks [23]. While aircraft plumes disperse into the atmosphere, chemical reactions occur among compounds in the plumes and surrounding air which influence levels of particulate matter. These effects motivate the study of aircraft plumes to improve understanding and improve current models that predict particulate matter pollution specifically from aircraft.

Furthermore, incorporation of plume dynamics has been shown to affect estimates of aviation-attributable pollution in global models, in which simulation estimates of aircraft-induced NO_x were reduced by 20-40% by incorporating plume effects [24], [25]. Barrett notes

that regulatory models such as AERMOD over-predicted observed annual mean concentrations of NO_x at monitors near London Heathrow Airport (EGLL) by 40% [23].

Taking an observational approach, Bennett used a Light Detection and Ranging (LIDAR) technique to obtain shapes of aircraft plumes of different aircraft at Heathrow Airport [26]. These observations supported theoretical work describing aircraft plumes during take-off [26]. Schafer also used an optical technique, FTIR, to observe plume structures and characterize species using absorption spectra [16].

Using computer simulations, Wu developed a model based on the method of moments to address large and small-scale turbulent mixing of aerosols in aircraft plumes [27]. This model was used to conclude that micro-scale mixing can account for a 40% difference in predictions of aerosol number density, which would affect estimates of particulate matter away from the aircraft plume. Similarly, Wong developed and verified a one-dimensional plume model incorporating plume chemistry, wake dilution, and aerosol microphysics to predict the formation of sulfates in aircraft plumes [28]. The model was used to study nucleation of liquid aerosols within aircraft plumes [28]. Studies of aircraft plume dynamics complement studies of aircraft emissions by enabling better understanding of how emissions are transported and reacted with the atmosphere immediately after exhaust.

1-3-3 Direct Monitoring

To ensure compliance with air quality regulations and assess health impacts of air pollution, environmental agencies such as the EPA and state and local agencies regularly monitor air quality through nationwide monitoring networks. These networks allow agencies to assess the concentrations of pollutants, including $PM_{2.5}$, in populated areas. For example, the EPA's State and Local Air Monitoring Stations (SLAMS) network comprises approximately 4,000 monitors nationwide and are mostly concentrated in urban areas, as Figure 1 illustrates. Data from monitors are also used to validate air quality models that can predict concentrations in locations that are not monitored.

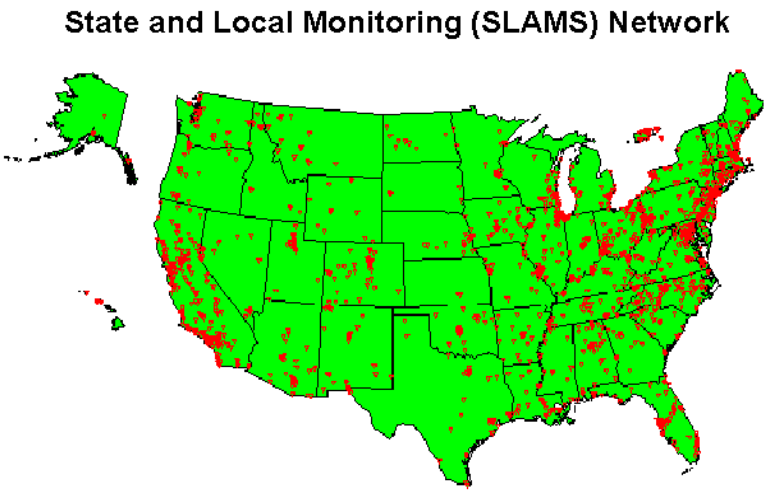

Figure 1. Location of EPA SLAMS network air quality monitoring stations [29].

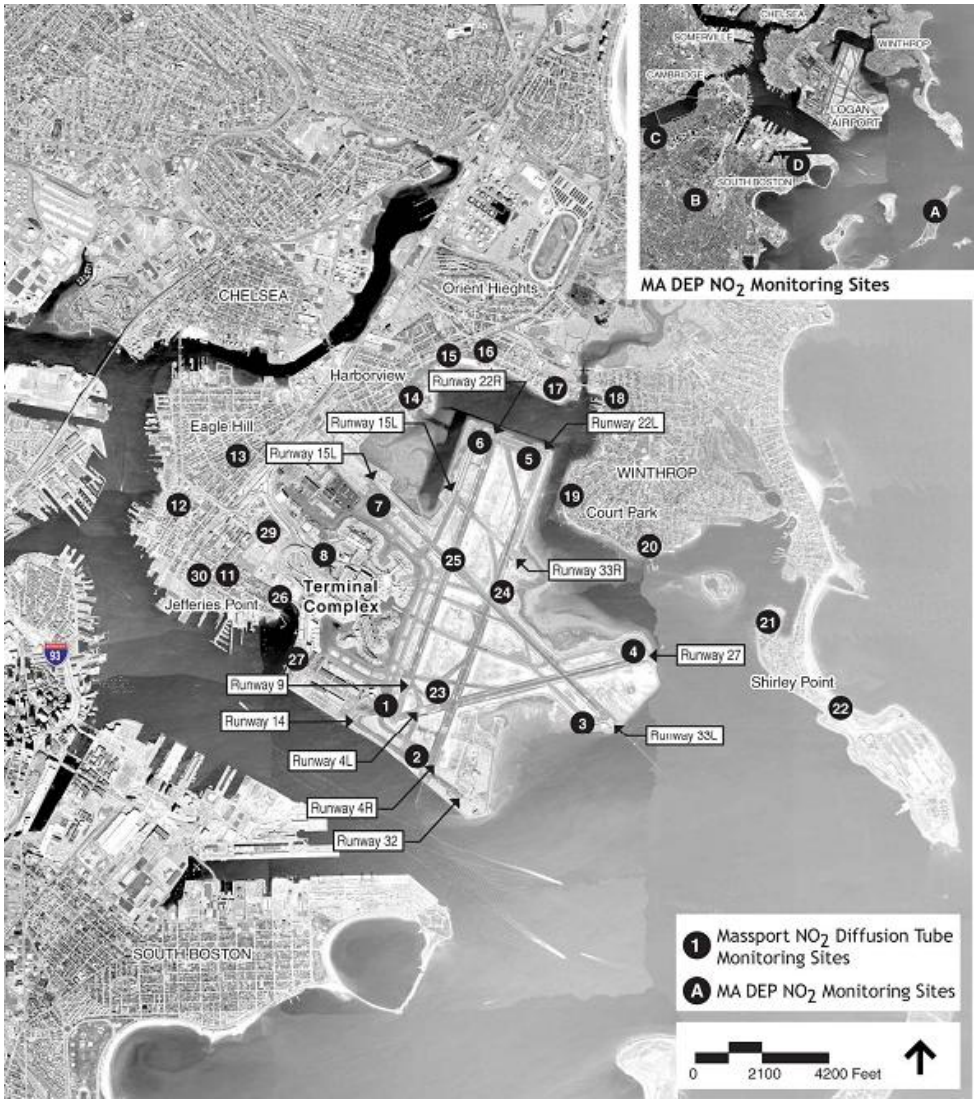

Figure 2. Massport NO_2 monitoring sites [30].

Although these networks cover a wide area, they are not designed specifically for the measurement of air pollution from airports. Those monitors that are closest to airports may be located sparsely as illustrated in Figure 2 for Boston Logan International Airport (KBOS) [30]. To improve assessment of airport air quality and validation of air quality models, several research groups quantified airport contributions to local air pollution concentrations by setting up monitors separate from air quality networks. Airport operators at Los Angeles International Airport (KLAX), Boston Logan International Airport (KBOS) (Figure 2), and Zurich Airport (LSZH) also conducted studies addressing airport air quality [31–33].

Hu and Carr monitored concentrations of ultra-fine particles (UFP, particulate matter with aerodynamic diameter of <100 nm) and lead, respectively, both upwind and downwind of runways [34], [35]. Both found elevated levels of pollutants downwind of the airport, indicating that emissions from aircraft takeoffs could increase local concentrations of pollutants in residential areas. Similarly, Westerdahl and Zhu monitored concentrations of UFP, black carbon (BC), and $PM_{2.5}$ near a large international airport (KLAX) [36], [37] and reached similar conclusions. Hu also indicated that levels of ultra-fine particles were elevated more than levels of black carbon perhaps indicating that particles originating from aircraft are smaller than those from other sources [34]. Hsu and Dodson performed monitoring studies at Theodore Francis Green Airport in Providence (KPVD) [38], [39].

Although monitors enable direct quantification of pollutant concentrations near airports, the number of monitors is limited by available resources and are restricted to monitoring specific locations and species. Furthermore, monitors can only quantify pollutants at the current time, such that the effect of future policies or aviation growth on local air quality cannot be estimated. Monitors also cannot easily separate aviation contributions to pollution concentrations from contributions from other sources such as power plants, motor vehicles, and natural sources, although many techniques for source apportionment have been developed [40].

1-3-4 Regression Models

One method for source apportionment is to relate monitored concentrations statistically to meteorological and emissions variables in the vicinity of the monitor. Regression models attempt to show the relative contributions of different factors such as time-varying emissions, location, and wind speed and direction to local concentrations of pollutants such as particulate matter.

With knowledge of the monitor location, wind speed, direction, concentrations, and locations of potential emissions sources, regression analysis can estimate which factors contribute the most to local air pollution.

Yu used a nonparametric regression method to show the relative contributions of sources of CO, NO_x, SO_x, and respirable suspended particles (RSP) based on wind speed and direction at KLAX and Hong Kong International Airport (VHHH) [41]. The nonparametric method did not assume a mathematical relationship between the predictor variables - wind speed and direction - and the variable of interest - concentrations at the monitor. Yu concluded that aircraft could be a major source of sulfur dioxide (SO_2) based on these results [41].

Dodson developed a regression model to estimate contributions of wind speed, direction, mixing height, and flight activity to concentrations of black carbon (BC) around KPVD. Dodson concluded that aircraft departures accounted for approximately 25% of observed BC concentrations at monitoring sites near the airport [39]. Similarly, Hsu developed a regression model to determine contributions to concentrations of UFP at KPVD, concluding that LTO activities contribute 6.6-9.8% of UFP near a major runway and 1.8-4.7% farther away [38]. The results from both of these studies exhibited large variability in results that reflect the difficulty in attributing particle pollution to sources using statistical methods.

A variant of the regression modeling approach used in the Project for the Sustainable Development of Heathrow (PSDH) employed empirical data to map air pollution concentrations by relating them to some measure of the emissions source. This empirical model differs from the other studies by determining concentrations at locations apart from the monitors [42]. This approach relied on emissions source data that were at a finer scale than concentration data [42].

1-3-5 Computer Models

Observations of pollutant concentrations, both from aircraft plumes and from air quality monitors, provide real data but do not provide predictive capability. Computer models provide the ability to estimate pollutant concentrations and subsequent health impacts for locations that are not monitored for different aviation scenarios, such as for different aviation policies, technology, and climate change. Furthermore, because computer models model emissions sources, they can be used to estimate contributions of different sources to total pollution (source apportionment). Computer models are also not restricted to simulating pollution as it disperses with time; some models can simulate backwards in time in cases where information about the

strength of pollutant sources is desired [43–45]. These kinds of model simulations are called "inverse" simulations, whereas simulations that model pollutant dispersion in time are called "forward" simulations.

To serve their regulatory purposes, air quality models typically provide ways to address different types of sources. For example, AERMOD is used by the EPA to regulate sources of local air pollution, such as power plants, through New Source Review (NSR) and Prevention of Significant Deterioration (PSD) applications. AERMOD can simulate the different types of sources listed in Table 4.

Source Type	Example
Point	Industrial stacks, isolated vents
Area	Storage piles, slag dumps, lagoons
Volume	Building roof monitors, multiple vents, conveyor belts
Open Pit	Surface coal mines, rock quarries

Table 4. Source types in AERMOD. Information from [46].

Computer models for predicting air quality near airports can be roughly divided into three categories by their treatment of pollutant dispersion: Gaussian models, Eulerian models, and Lagrangian models. Holmes reviewed different kinds of dispersion models and added two categories: Computational Fluid Dynamics (CFD) models and models that include aerosol dynamics [47]. The European Topic Centre on Air and Climate Change (ETC/ACM) compiled a list of different atmospheric dispersion models and their capabilities [48].

1-3-6 Gaussian Models

Gaussian models such as AERMOD [22] and the Atmospheric Dispersion Modelling System (ADMS™) [49] calculate concentrations downwind of pollutant sources, assuming a shape for the pollutant plumes. An example Gaussian plume is illustrated in Figure 3. As a pollutant plume travels away from the source (in this case, an industrial stack), concentrations vary according to a Gaussian distribution in the directions perpendicular to the prevailing plume direction. Concentrations are calculated at "receptor" points, geographic locations of interest (such as points in populated areas) away from the emissions sources.

Often the plume shape is averaged over hourly meteorological conditions rather than attempting to simulate the turbulent fluctuations in plume dispersion at shorter time scales. Over this time period the plume is assumed to emit pollutants steadily; thus this particular approach is called a steady-state Gaussian plume model.

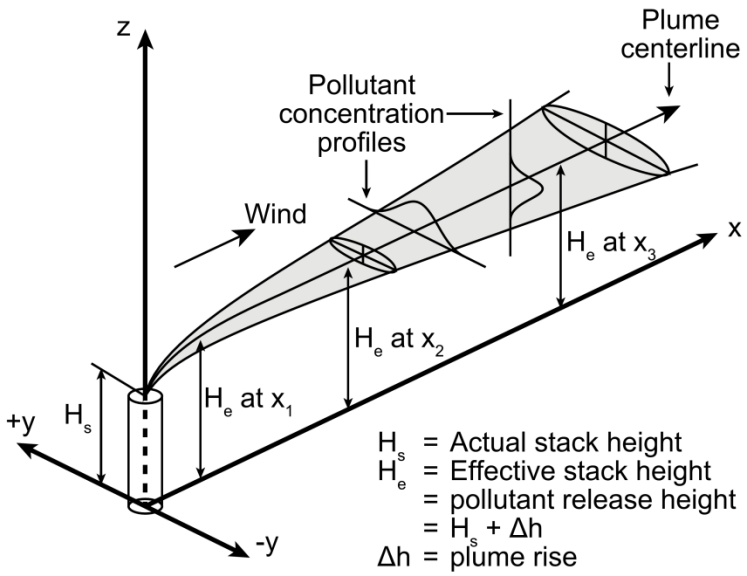

Figure 3. Illustration of Gaussian plume used in Gaussian dispersion models [50].

Gaussian models have been applied to estimating air quality impacts of aviation emissions. Carr used AERMOD to estimate concentrations of lead emissions resulting from piston-engine aircraft near a general aviation airport [35]. This study suggested that the use of leaded aviation gasoline can cause exceedance of national ambient air quality standards (NAAQS) for lead in the vicinity of airports [35]. Carruthers used ADMS™ along with modifications to account for aircraft plume effects as part of PSDH to determine the impact of Heathrow Airport on local air quality [51]. Also, the FAA's EDMS air quality tool for assessing air quality near airports uses AERMOD to perform dispersion calculations [12].

1-3-7 Eulerian Models

Eulerian models employ a fixed coordinate system to calculate the transport and transformation of pollutants and pollutant precursors in the atmosphere. Typically, three-dimensional regions of the atmosphere are subdivided into grid cells, and emissions, concentrations, and chemical and transport processes are modeled within and between the grid cells. Because Eulerian models discretize the atmosphere into grid cells rather than specific geographical receptor points, concentrations at specific points are often estimated using the concentration of the grid cell that the receptor point is located in. The grid-cell nature of Eulerian models also aids in its combination with spatially-averaged population data in estimating health impacts.

Though many Eulerian models exist, two used in atmospheric research are described below.

The Community Multiscale Air Quality (CMAQ) model, which is used by the EPA for regional analysis, simulates "multiple air quality issues, including tropospheric ozone, fine particles, toxics, acid deposition, and visibility degradation" with an Eulerian approach. Among some of the processes that CMAQ models are advection, diffusion, deposition, gas and aqueous-phase chemical reactions, and photolysis [52].

CMAQ is widely used in air quality studies. For example, Yim used CMAQ to estimate that combustion emissions cause ~13,000 premature deaths per year in the UK [8]. Woody used CMAQ to assess the impact of U.S. LTO emissions on $PM_{2.5}$ concentrations in the United States and Levy estimated the health impacts of such emissions [6], [53]. At the local scale, Unal estimated the impact of Hartsfield-Jackson Atlanta International Airport (KATL) on local air quality using CMAQ [54].

GEOS-Chem is a global model based on assimilated meteorological observations from the NASA Goddard Earth Observing System. As with CMAQ, GEOS-Chem is capable of simulating a variety of processes including atmospheric chemistry, deposition, advection, and aerosol physics for different spatial and temporal scenarios [55].

Barrett used GEOS-Chem with population data from the WHO to conclude that aircraft cruise emissions account for ~8,000 premature mortalities worldwide. Furthermore, Barrett concluded that in addition to LTO emissions, cruise emissions should be included in assessing aviation impacts on air quality [7]. Leibensperger used GEOS-Chem to assess the sensitivity of worldwide PM levels to anthropogenic emissions of NO_x and CO [56]. Previous work within the Laboratory for Aviation and the Environment (LAE) involved the development of GEOS-Chem Adjoint to determine emissions contributions to concentrations of pollutants using inverse model runs [45].

CMAQ and GEOS-Chem are just two examples of Eulerian models. Because these models simulate atmospheric chemistry, they are sometimes referred to as chemistry transport models (CTMs). Other examples of CTMs are the MOZART model [57] and the TOMCAT/SLIMCAT model [58].

1-3-8 Lagrangian Models

Lagrangian models model the dispersion of particulate matter by simulating the transport of large numbers of particles. Whereas Gaussian models assume a dispersion profile for the pollution plume, and Eulerian models address transport and transformation within and among discrete grid cells, Lagrangian models attempt to model the physical processes that affect pollution from their source to their final location where they impact human health. Large numbers of individual particles are "released" from pollution sources, and their trajectories are calculated based on atmospheric conditions.

The Lagrangian Simulation of Aerosol Transport (LASAT™) model developed by Janicke Consulting models the dispersion of a variety of particulate species and forms the basis for the German regulatory model AUSTAL2000 [59]. LASAT™ was also used by EUROCONTROL in a study comparing Eulerian, Lagrangian, and Gaussian approaches to modeling air quality near airports [60].

Das developed a Lagrangian stochastic model (LSM) for stratified turbulence in the atmosphere and applied it to calculate concentrations of CO around a runway [44]. The model developed by Das can perform both forwards and inverse simulations. Gray developed a Lagrangian air quality model for elemental carbon (EC) and used it to determine that EC concentrations in Los Angeles were dominated by emissions from diesel engines in 1982 [61].

1-4 Common Issues in Assessing the Impact of Aircraft Emissions on Local Air Quality

In summary, a review of the literature on air quality near airports reveals experimental, mathematical, and simulation-based methods for assessing the impact of aircraft emissions. Experimental methods include those that seek to better understand particulate matter emissions from engines in real-world conditions, how they evolve immediately in the plume, and methods that investigate local concentrations through air quality monitoring. Statistical methods include regression models and empirical models that relate observed concentrations to measures of aircraft activity and meteorology (to a limited extent). Simulation-based methodologies use computer models to solve equations describing physical and chemical processes in the atmosphere. The different methods discussed previously are summarized in Table 5.

Approach to Studying Aircraft Impacts		**Sources**
Aircraft Emissions Characterization		[12], [15–21], [49], [59]
Aircraft Plume Dynamics		[16], [24–28]
Direct Monitoring		[29], [31–40]
Regression Models		[38], [39], [41], [42]
Dispersion and other Computer Models	Gaussian	[12], [22], [35], [49], [51]
	Eulerian	[6–8], [45], [52–56]
	Lagrangian	[44], [59–61]
	Other References	[43–45], [47]

Table 5. Methods for studying aircraft impacts on air quality.

1-4-1 Limitations of Atmospheric Dispersion Models

The atmosphere is a complex fluid system that exhibits processes at both small and large spatial and temporal scales. Seinfeld and Pandis separated atmospheric processes roughly into four categories, which are listed in Table 6 [62]. Examples of the scale of some processes are shown in Table 7.

The computational resources required to simulate pollutant dispersion often require that computer models focus on atmospheric processes that are important at small or large length scales, depending on the model. The Eulerian models CMAQ and GEOS-Chem are frequently used to simulate atmospheric processes at regional and global scales while Gaussian, Lagrangian, and regression models are typically used at urban scales. At an even finer scale, Riddle used the computational fluid dynamics (CFD) package FLUENT™ to analyze pollutant dispersion around

Scale Category	Description	Examples
Microscale	Phenomena occurring on scales of the order of 0-100 m	Meandering and dispersion of a chimney plume, complicated flow regime in the wake of a large building
Mesoscale	Phenomena occurring on scales of tens to hundreds of kilometers	Land-sea breezes, mountain-valley winds, migratory high and low-pressure fronts
Synoptic Scale	Phenomena occurring on scales of hundreds to thousands of kilometers	Motions of whole weather systems
Global Scale	Phenomena occurring on scales exceeding 5×10^3 km	n/a

Table 6. Four scale categories of atmospheric processes [62].

Phenomenon	Length Scale, km
Urban air pollution	1-100
Regional air pollution	10-1000
Acid rain/deposition	100-2000
Toxic air pollutants	0.1-100
Stratospheric ozone depletion	1000-40,000
Greenhouse gas increases	1000-40,000
Aerosol-climate interactions	100-40,000
Tropospheric transport and oxidation processes	1-40,000
Stratospheric-tropospheric exchange	0.1-100
Stratospheric transport and oxidation processes	1-40,000

Table 7. Spatial scales of atmospheric chemical phenomena [62].

a complex group of buildings and compared them to results from the Gaussian model ADMS™ [63].

In preliminary work conducted within LAE, for example, calculations of mean annual concentration of $PM_{2.5}$ for airports consisting of 1-7 area sources using AERMOD took up to 6 hours to complete. The CMAQ regional air quality model often takes weeks on powerful computer servers to complete simulations. Clearly, detailed analyses required to assess air quality for multiple sources over space and time can require much computational resources.

1-4-2 Quality of Available Data and Validation

Computer models rely on available, accurate data to predict air quality around airports. However, not all necessary data are available due to real world constraints. For example, efforts to characterize emissions from real aircraft aim to improve on using data from the ICAO databank to estimate emissions. As Unal noted, "emissions inventories have long been noted for being one of the most ... uncertain aspect [*sic*] of air quality modeling" and that "this uncertainty inhibits accurate air quality modeling" [54].

Air quality monitors near airports are frequently sparsely located, with a few located for long-term monitoring purposes and not specifically for assessment of airport air quality. Compounding the problem, monitor data exhibit large variability, adding difficulty to ensuring that models accurately predict concentrations.

Data availability for assessing airport air quality also depends on efforts by environmental agencies, airport operators, and scientists to collect such data for particular airports and regions. For example, Figure 4 shows the locations of stations in the U.S. National Climatic Data Center's (NCDC) Integrated Global Radiosonde Archive (IGRA), a database of upper-air soundings for use in the current work. The maps shows that data are available at higher spatial density in Europe and Asia, while available stations in South America, Africa, and Australia are more sparse.

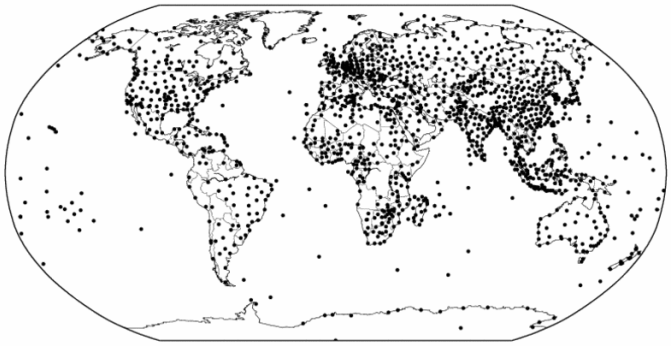

Figure 4. Locations of all stations in IGRA [64].

Models that predict air quality are frequently used by regulatory agencies such as the EPA and FAA to assess the environmental effects of technological, operational, and policy changes. Although larger-resolution models such as CMAQ can capture these effects at larger scales, due to computational constraints they cannot simulate local variations near airports. Models designed for assessing local variations can be used to assess impacts of aircraft; however to perform analyses over many airports and scenarios would multiply the time and computational resources required to perform these analyses. Thus it is desired to have a tool that can enable simulation of local variations in air quality near airports but with less computational resources.

1-5 Focus of Thesis - the Rapid Dispersion Modeling System

The focus of this thesis will be to develop and apply the Rapid Dispersion Modeling System (RDMS) based on approximations developed by Barrett [65], [66]. RDMS addresses the problem of computational resources in simulating dispersion of PM for a large number of airports. The RDMS builds on top of preexisting dispersion models that can perform detailed calculations involving: meteorological data; emissions types, sources, and temporal profiles; terrain; and dispersion formulae that account for different physical processes.

At airports, emissions of aircraft occur at taxiways and runways. Consequently, previous studies have modeled aircraft emissions as two-dimensional area sources or three-dimensional volume sources [35], [66]. The calculations for these types of sources are more computationally intensive than those for simple point sources (e.g. industrial stacks). The RDMS operates by using fast calculations done for point sources and applying them to area sources, achieving time savings at the expense of some accuracy. Effects of meteorology, terrain, and dispersion are accounted for with a set of dispersion parameters, which are then used by the RDMS to calculate long-term (annual) mean concentrations of particulate matter attributable to area sources.

This thesis presents RDMS results for aviation-attributable, annual average $PM_{2.5}$ concentrations associated with ground-level aircraft emissions at 191 U.S. airports for the year 2006. These 191 airports were chosen to account for approximately 95% of passenger traffic and 90% of aircraft fuel burn at the ground level in the United States. RDMS results were also combined with results from the CMAQ model to obtain concentrations and health impacts of $PM_{2.5}$ at local and regional scales. Details of RDMS in its current development and its limitations are discussed. Future developments and analyses will be addressed.

2. Methods

In this section, the formulation of the RDMS will be addressed, followed by a discussion of model inputs for this study, methods for combining the RDMS with CMAQ results, and methods for calculating local and regional scale health impacts.

2-1 Structure of the Rapid Dispersion Modeling System (RDMS)

The overall structure of the RDMS in Figure 5 illustrates the types of data required for the calculation of mean annual concentrations of $PM_{2.5}$ around an airport and where they enter into the process. These data sources will be discussed further. The rapid dispersion calculation described by Barrett [66] uses outputs from a conventional dispersion model in the form of point-source dispersion parameters to calculate long-term averages. For further discussion, the RDMS will refer to the entire process in Figure 5 while the methods developed by Barrett will be described as the rapid dispersion calculation (RDC). Both terms may be used interchangeably to describe the mean annual $PM_{2.5}$ results calculated using the rapid dispersion process.

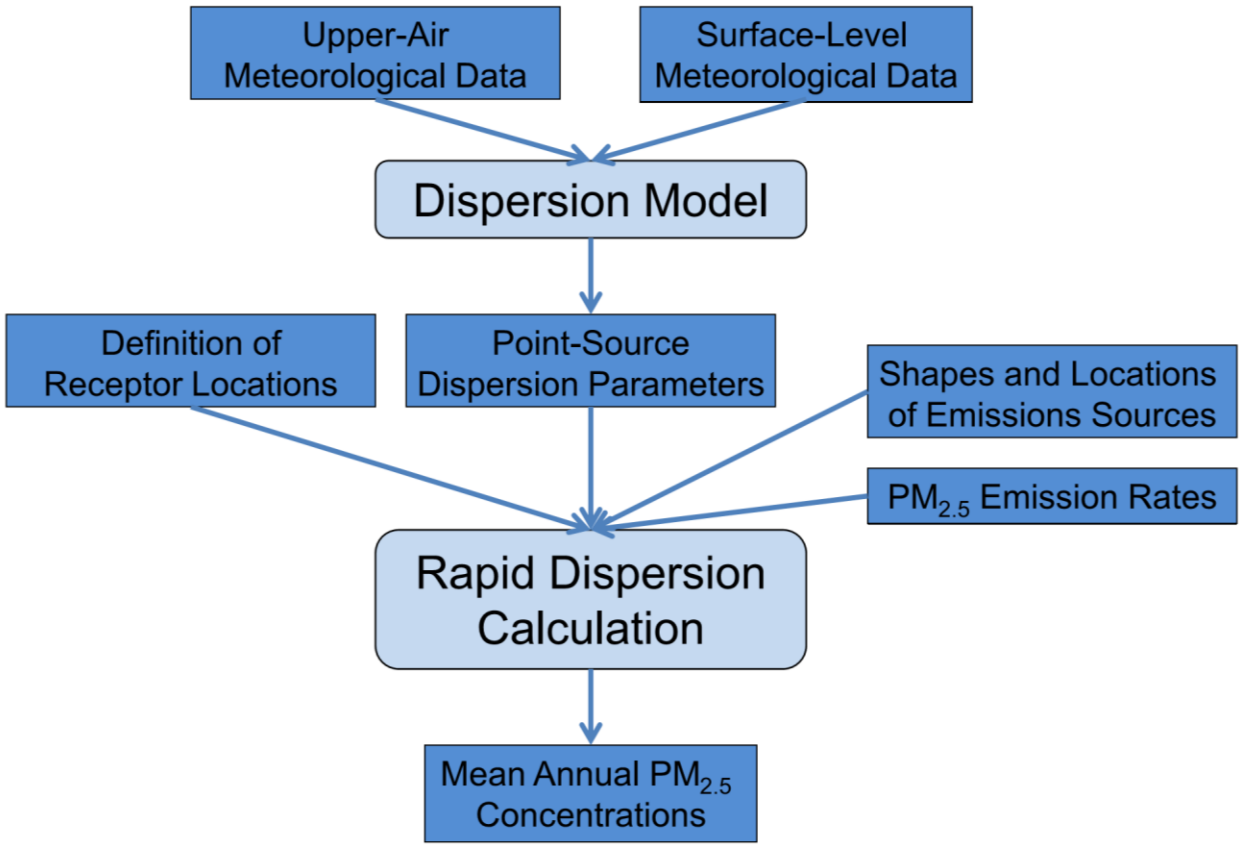

Figure 5. Overall structure of Rapid Dispersion Modeling System.

2-2 Choice of Dispersion Model

For this work, the AMS/EPA Regulatory Model (AERMOD) was used as the dispersion model for several reasons. AERMOD incorporates recent scientific knowledge of air dispersion and is the model used by the EPA for regulatory applications. AERMOD has also been validated against several observational air quality studies [22]. Furthermore, the FAA uses AERMOD to calculate dispersion of air pollution sources from airport sources as part of its EDMS model [12]. Finally, AERMOD is freely available to the public and well-documented, aiding in its use as a research tool. Although AERMOD was chosen for this work, other dispersion models such as ADMS™ or LASAT™ could be equally useful.

2-3 Description of Methods to Calculate Long-Term Average Concentrations

In this section, methods used by traditional dispersion models will be described and compared to the RDC. Three approaches will be described: time-series integration, statistical approaches, and the RDC.

2-3-1 Time-Series Integration

In steady-state Gaussian dispersion models such as AERMOD, pollutants are assumed to disperse away from their source in a plume as illustrated in Figure 3. Pollutant concentrations assume a Gaussian profile in both directions perpendicular to the plume centerline. For a point source such as an industrial stack, the basic equation for Gaussian dispersion (Equation 1) describes the concentration at a point in terms of source emission rate of pollutant, location, and parameters describing the width of the plume. This basic equation is sometimes referred to as a Gaussian dispersion kernel.

In practice, AERMOD and other Gaussian models account for other factors that influence dispersion. For example, AERMOD addresses convective and stable boundary layer conditions, urban and rural areas, terrain, the influence of buildings, and different types of sources [22].

In time-series integration, A Gaussian model calculates concentrations at locations of interests (receptors) individually, using the Gaussian formulation for each pollution source. Meteorological variables such as wind speed and direction are typically provided at the hourly level because the assumption that concentrations vary according to a Gaussian profile does not account for instantaneous turbulent effects. In reality, pollutants are subject to real-time conditions in the atmosphere. To perform a calculation of annual average concentration at a

$$c(x,y,z) = \frac{q}{2\pi u \sigma_y \sigma_z} \exp\left(-\frac{y^2}{2\sigma_y^2}\right)\left[\exp\left(-\frac{(z-h)^2}{2\sigma_z^2}\right) + \exp\left(-\frac{(z+h)^2}{2\sigma_z^2}\right)\right]$$

x	Direction of advection of the plume
y	Horizontal direction
z	Vertical direction
q	Source strength
u	Mean horizontal wind speed in the x direction
h	Stack height
σ_y, σ_z	Horizontal and vertical standard deviations of the plume in the y and z directions
Note that the plume spread increases with distance from the stack so that σ_y, σ_z depend on x	

Equation 1. Basic Gaussian Plume Equation and variables [42].

receptor, Gaussian models utilize hourly data for the entire year (8760 h), calculating the concentration at a receptor at every hour, then averaging the results.

For calculating long-term averages around airports, the computational resources required to perform a time-series integration can multiply quickly. Airports typically consist of multiple sources of pollution (e.g. building emission sources, auxiliary power units, ground support equipment, aircraft). Furthermore, modifications within Gaussian models to address different types of sources such as area or volume sources add complexity compared to modeling all sources as point sources. More than one receptor is necessary to enable understanding of how impacts are spatially distributed. For combination with population data to assess health impacts, receptors are often defined at regular spatial intervals surrounding the airport; for example, extending out a certain distance at a certain resolution (e.g. 20 km at 400 m resolution in this study). To calculate the mean annual concentrations in this example would require roughly 10,201 × 8,760 × N Gaussian dispersion calculations, where N represents the number of pollution sources. Although computers can perform calculations quickly, these simulations can still take several hours to complete [67].

2-3-2 Statistical Approaches

Because time-series integration calculates concentrations at detailed temporal resolution, it can account for cases in which emissions and meteorological conditions are correlated in its estimation of long-term averages. For example, emissions from human activity are higher during daylight hours than evening hours and meteorological conditions are different for day and night. If emissions and meteorology are treated independently, however, statistical approaches can

estimate long-term average concentrations more computationally efficiently than time-series integration can.

In the steady-state plume assumption, each hour is treated independently of others, such that the concentrations at receptors solely depend on meteorological conditions within that hour [68]. Thus meteorological conditions can be sampled for the year to develop a joint probability density function describing the relative impact an emissions source has in a particular direction and set of meteorological conditions. Barrett describes the statistical approach with Equation 2 [66].

$$\langle \chi(\boldsymbol{x}) \rangle = \int \int \int \int p(\theta, \boldsymbol{m}, q) q \chi_p\big(\theta, \boldsymbol{m}, \boldsymbol{x} - \boldsymbol{x}(\boldsymbol{t})\big) dq d\boldsymbol{t} d\theta d\boldsymbol{m}$$

$\langle \chi(\boldsymbol{x}) \rangle$	Long-term average concentration at spatial location $\boldsymbol{x}$
$\boldsymbol{x}$	Receptor spatial location
$p(\theta, \boldsymbol{m}, q)$	Joint probability density function
θ	Direction of receptor relative to source component
$\boldsymbol{m}$	Meteorological variables
q	Source strength
$\boldsymbol{t}$	Source component - parameterization depends on type of source (e.g. point, line, area, volume)
χ_p	Gaussian dispersion formula (kernel) for a point source

Equation 2. Statistical calculation of long-term average concentration [66].

The statistical approach captures the effects of yearly meteorological conditions through the calculation of the probability density function. After this is calculated, the integration to calculate concentrations proceeds without the hourly iterations (8760 iterations in the time-series approach).

The statistical approach requires that emissions and meteorology are independent; to account for temporal correlations, a correction factor may be applied post-calculation. Although the statistical approach is more or equally efficient than a time-series approach [66], Barrett notes that some applications "such as detailed analysis of specific pollution episodes associated with low wind conditions" [66] still require a time-series approach.

2-3-3 RDC - Lateral Dispersion Averaging Approximations

To simplify the calculation of long-term average concentrations, the rapid dispersion calculation uses two approximations. Before applying these approximations, the dispersion kernel is assumed to be separable into vertical (relative to the ground) and horizontal (perpendicular to the predominant plume direction) components as shown in Equation 3 [66]. Note that the basic Gaussian plume equation (Equation 1) can be separated in this way.

$$\chi_p(\boldsymbol{m}, x, y) = \underbrace{\chi_v(\boldsymbol{m}, x)}_{\text{vertical}} \underbrace{\chi_l(\boldsymbol{m}, x, y)}_{\text{lateral}}$$

Equation 3. Separation of dispersion kernel into vertical and lateral components [66].

Both approximations are illustrated in Figure 6. The first approximation, termed "receptor lateral dispersion averaging approximation" (receptor LDAA) [66] assumes that the average impact a source has in a particular direction does not change across the width of the pollutant plume emanating in that direction [67]. This enables consideration of the vertical dispersion component only. The second approximation, termed "source LDAA", assumes that the average impact a source has on a receptor does not change across angles extending upwind from the receptor to the source [66]. Both of these approximations reduce the number of calculations by enabling consideration of just the impact a source has in the direction of the receptor. Quantifying the impact involves parameterization of the vertical dispersion which will be discussed in the next section. Barrett also notes that the smoothing effect of lateral dispersion can be replicated to some extent by smoothing calculated parameters across angles upwind of the receptor [66].

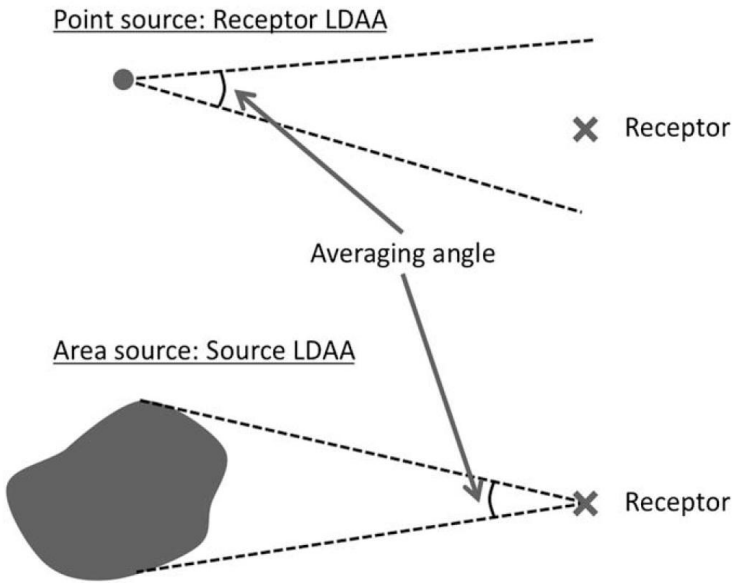

Figure 6. Graphical depiction of Receptor and Source LDAA with angles over which the two-dimensional dispersion parameters are smoothed [66].

2-3-4 RDC - Parameterization of Impacts Through Dispersion Model Calculation

Barrett describes in [66] a method to quantify the effect of vertical dispersion using existing dispersion models. This approach is advantageous because existing dispersion models such as AERMOD account for a variety of effects beyond the basic plume equation. During parameterization, long-term average concentrations are calculated at regular distances and directions for a point source using time-series integration. This point source calculation captures the effects of meteorology, dispersion, and temporal emissions on long-term averages but requires less time to perform than a multiple-area-source calculation. After long-term averages are calculated, parameters are derived according to a power-law fit (Equation 4) [66]. The power-law fit is performed either locally (at a particular distance and direction), or as will be discussed in the validation section, for all distances at one direction in this study.

$$\chi_v(x) = \frac{A}{x^s}$$

Equation 4. Power-law fit for vertical dispersion parameterization [66].

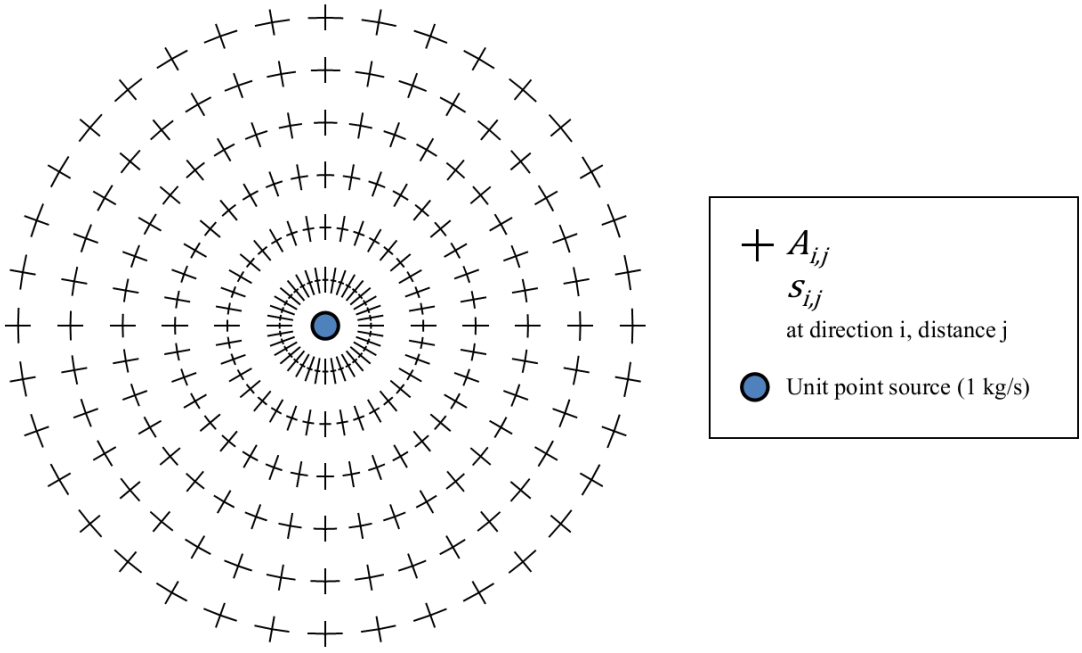

Figure 7. Dispersion parameters are calculated at regular intervals around a unit point source.

Figure 7 illustrates the end result of parameterization. Parameters describing long-term dispersion away from a unit point source are calculated and ready to be applied towards calculation of long-term averages from area sources.

2-3-5 RDC - Application of Dispersion Parameters to Area Sources

Barrett describes in [66] a mathematical derivation of formulae to calculate long-term average concentrations, given source emissions strengths and the dispersion parameters based on a unit point source. The overall process is illustrated in Figure 8.

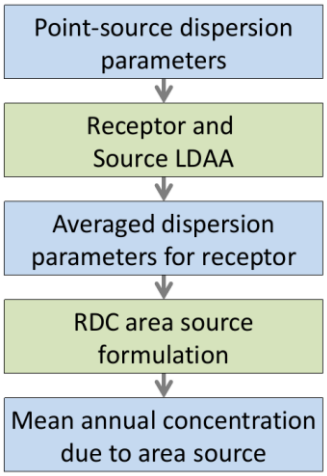

Figure 8. The use of point-source dispersion parameters in calculating concentrations from area sources.

Before applying the dispersion parameters to the area-source formulation, parameters are smoothed out according to the relative position and orientation of the receptor to each area source. As shown in Figure 9, for a particular receptor, an averaging angle is calculated based on the size, position, and orientation of the area source. The averaging angle does not extend fully to the edges of the area source for receptors; this assumes that edges of the area source have relatively little effect on concentrations at the receptor. Dispersion parameters for the directions are then averaged to quantify the average effect the area source has on the receptor. The averaged dispersion parameters are then input to the area source formulation. The process is repeated for each receptor and area source.

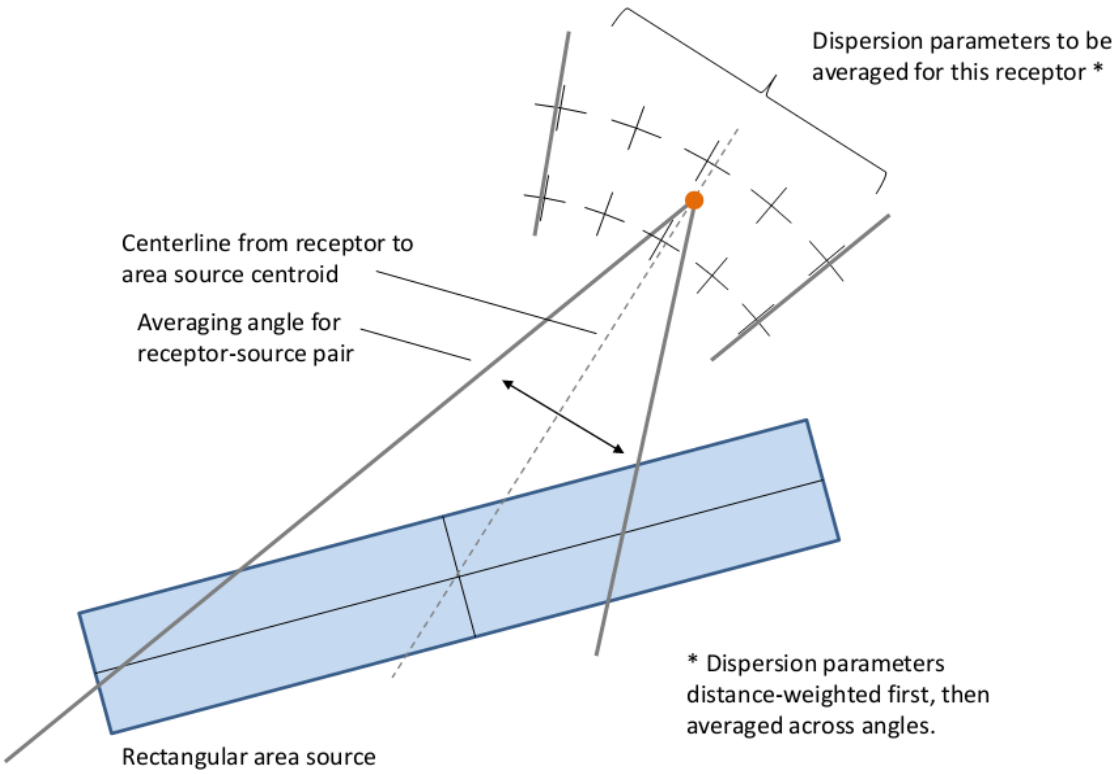

Figure 9. Source LDAA based on the relative position of sources and receptors. Note that the averaging angle used in this work does not extend fully to the edges of the area source.

The essence of the rapid dispersion calculation is parameterizing effects of meteorology, dispersion, and temporal emissions for a point source then applying these parameters directly to obtain a one-time calculation of long-term averages from area sources. In contrast to time-series integration, the rapid dispersion calculation requires much less calculation and thus reduces computation time by orders of magnitude [66].

2-4 Model Inputs

In the following sections, inputs within the Rapid Dispersion Modeling System (RDMS) are described in detail. For this study, model inputs for a set of 191 U.S. airports were developed and the methodology for these model inputs will be described. Table 8 summarizes the model inputs and Figure 5 provides a flowchart illustrating the overall process.

Model Input	Description	Input to:	Sources for U.S. Analysis
Upper-Air meteorological data	Year-long, twice-daily observational data describing upper-air meteorological conditions at upper-air sounding locations	Dispersion Model	NCDC IGRA database
Surface meteorological data	Year-long, hourly observation data describing surface meteorological conditions at airports	Dispersion Model	NCDC ISD database
Dispersion parameters	Parameters describing concentration as a function of distance and direction	RDC	n/a
Shapes and locations of emissions sources	Rectangular area sources approximating airport runways, taxiways, and terminals	RDC	AEDT database, FAA airport diagrams
$PM_{2.5}$ emissions rates	Total ground-level $PM_{2.5}$ emissions rates from aircraft only, assigned to area sources	RDC	AEDT 2006 simulation results
Receptor grid	2-D locations of points where long-term average concentrations are calculated	RDC	n/a

Table 8. Overview of RDMS model inputs.

Each model input will first be described, then advantages and disadvantages of using the model input will be discussed as well as any alternatives for future improvements.

2-4-1 Meteorological Data

Two types of meteorological data are required for input into AERMOD for the calculation of point-source dispersion parameters: upper-air soundings; and surface observations. Upper-air data were obtained from the National Climatic Data Center (NCDC) Integrated Global Radiosonde Archive (IGRA) which contains upper-air soundings for approximately 1,500 globally distributed stations (Figure 10a) [64]. Surface observations were obtained from the NCDC Integrated Surface Database (ISD) which contains observations for approximately 20,000 stations worldwide (including many airports) (Figure 10b) [69].

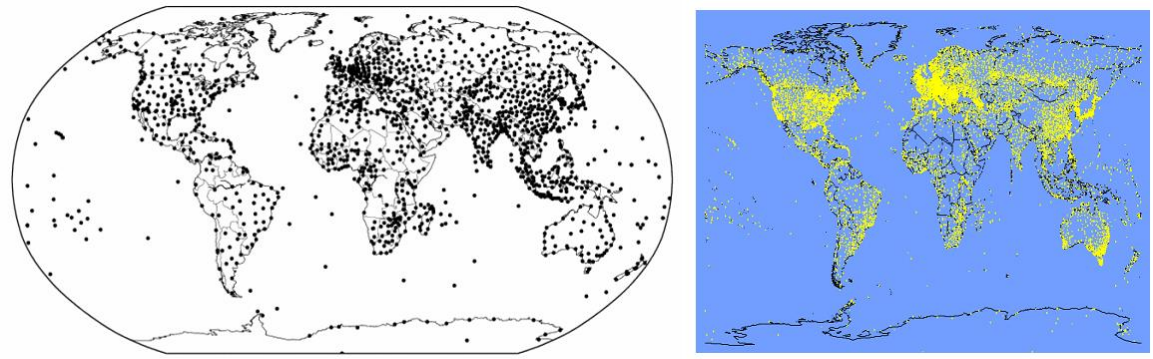

a) b)

Figure 10. a) Station locations in the Integrated Global Radiosonde Archive (IGRA) [64];
b) Station locations in the Integrated Surface Database (ISD) [69].

AERMOD requires both types of meteorological data to calculate atmospheric boundary layer parameters for dispersion calculations. AERMOD uses a meteorological preprocessor, AERMET, that performs quality control of raw meteorological data, and calculates dispersion parameters required by the RDC. AERMET requires data to be in a particular format. Although AERMET is designed to handle ISD data directly, upper-air data required conversion from IGRA to NCDC TD-6201 format.

Using the NCDC observations offered the advantage of representing meteorological conditions realistically. Many surface stations in the ISD database are located at airports and thus represent meteorological conditions closely. Upper-air stations in the IGRA database are more sparsely located but are not needed at as fine a spatial scale as surface stations. The worldwide coverage of both databases reduces the amount of development needed to perform worldwide analyses because the meteorological data exist in a consistent format.

However, using these two databases presents some issues in the modeling of air quality impacts near airports. Observational data are restricted to past years, and cannot account for future meteorological trends (such as those resulting from future climate change). Furthermore, data are not available for all sites equally. In Figure 10, upper-air stations are more sparsely located in South America, Africa, and Australia than in North America, Europe, and Asia. Although this difference in sparsity is partly due to population patterns (for example, Central Australia is largely unpopulated), for some airports this results in far distances to the nearest upper-air station. For example, the closest upper-air stations for some airports in South America are up to 1,000 km away from the airports and in different geographical regions. Such data may not accurately reflect the upper-air conditions near the airports.

To address these issues, modeled meteorological data may be used in future work. Models such as the Weather Research and Forecasting Model (WRF) [70] or MM5 mesoscale model [71] may be used to simulate meteorological fields needed for dispersion modeling specifically at airport locations. Isakov evaluated the use of weather models for input to AERMOD and concluded that "comprehensive [meteorological] models ... have the potential of providing adequate meteorological inputs for currently used short-range dispersion models such as AERMOD." [72] Other studies have used modeled meteorological data in air quality models [6], [53], [73].

2-4-2 Dispersion Parameters

The calculation of point-source dispersion parameters was described previously. Issues with their calculation are discussed here.

Dispersion calculations for determining dispersion parameters only require that long-term averages be obtained at directions and distances from a point source. However, the user of a preexisting dispersion model must exercise judgment in deciding what modeled effects to account for. Models such as AERMOD are sophisticated and can simulate (among other things) the effects of terrain. AERMOD also allows the user to specify parameters such as surface roughness. Figure 11 shows the variation in concentration with respect to distance for a point source in one direction using meteorological data from Hartsfield-Jackson Atlanta International Airport (KATL). Increasing the surface roughness decreases the predicted concentrations at farther distances because of decreased dispersion. This example highlights the need for the user of a dispersion model to understand which parameters are most relevant to modeling.

In this work, a surface roughness of 0.01 m was used for all point-source runs. In future work, the sensitivity of point-source runs to surface roughness could be assessed and appropriate values chosen by specific site or held constant for model consistency. The effects of modeling terrain could also be assessed.

To calculate dispersion parameters, concentrations are calculated at regular distance and direction intervals relative to the point source and parameters are fit according to a power law (Equation 4). Thus, the dispersion parameter values can vary depending on the extent and spacing of the concentrations used for their calculation. Because dispersion parameters are used eventually to calculate long-term concentrations from area sources, changing the resolution of point-source receptor locations can affect predictions of $PM_{2.5}$ exposure and health impacts. This

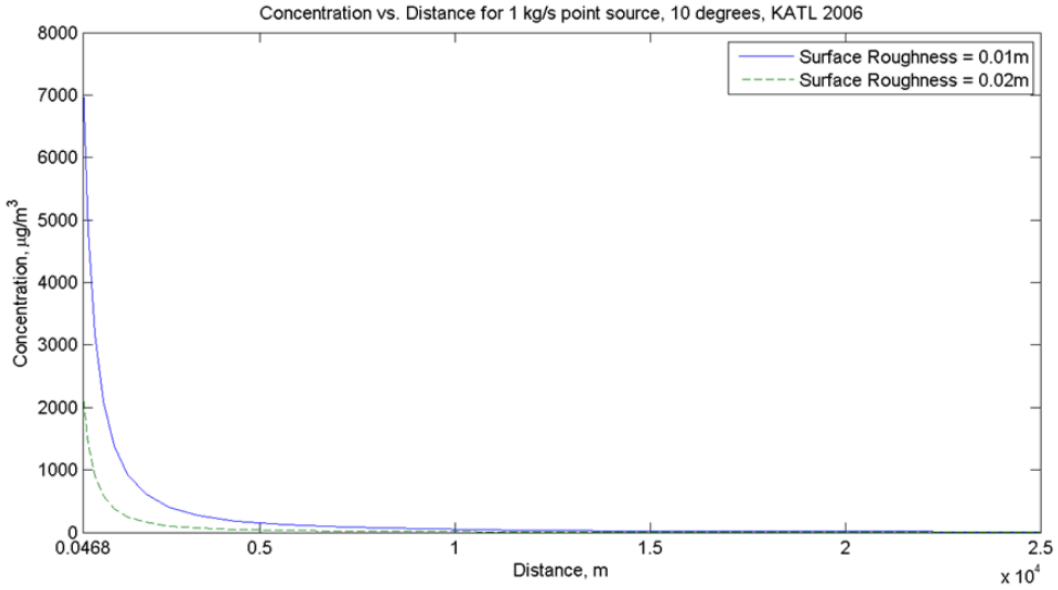

Figure 11. Comparison of point-source concentrations at 10 degrees for an annual average unit emissions rate (1 kg/s) for different surface roughness.

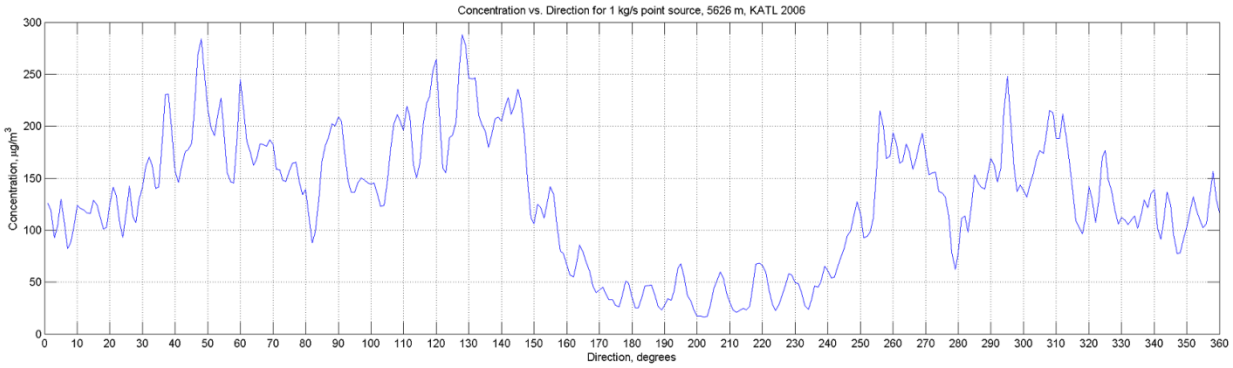

Figure 12. Variation of concentration with respect to angle at a fixed distance.

is especially true for the choice of directions. Figure 12 shows the variation of concentration with respect to direction for KATL, at 5326m away from the point source. Even in 10-degree intervals (the resolution typically provided by meteorological data), concentrations can vary greatly.

In this study, the error associated with interpolating concentration values from the 10-degree values compared to simulating them motivated simulating concentrations at finer scale. For example, the interpolated concentration at 5326m and 224 degrees for KATL is a factor of 2.6 higher (+160%) than that shown in Figure 12. To address this problem, AERMOD was run using a built-in randomization routine to create 1-degree wind directions from 10-degree meteorological data, and concentration values were calculated at 1-degree intervals (360 total).

As with other regression fits, the power-law fit used to calculate dispersion parameters can be performed over any number of points greater than two. Based on the results of a validation study to be discussed in detail in 3-1-1, power-law fits were calculated across all distances in each direction (to be referred to as "one-fit" parameters). Calculation of parameters in this way resulted in agreement with AERMOD within 5% on average. The metric used for this figure (mean(RDC)/mean(AERMOD)) will be discussed in 2-5-3. This method proved better than other methods of calculating dispersion parameters, likely because AERMOD-predicted concentrations already exhibit a power-law variation with respect to distance (Figure 13). For future work, localized fits can still be used for cases where the dispersion model does not generate concentration values that follow such a power-law variation with respect to distance.

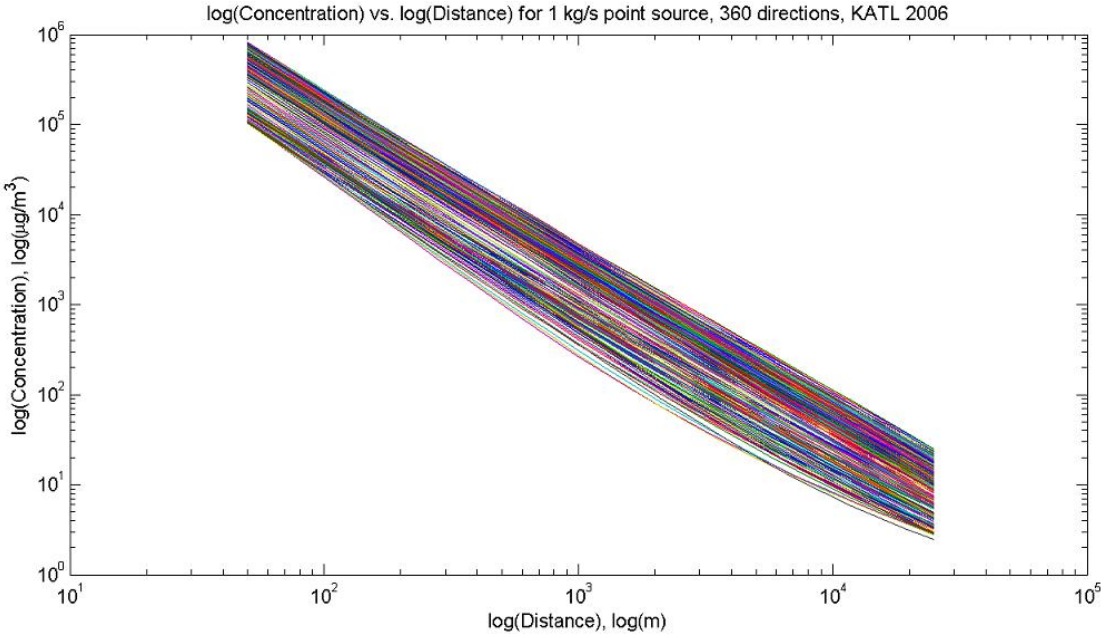

Figure 13. AERMOD-predicted concentrations indicate power-law variation.

After calculating dispersion parameters at different distances and angles, a smoothing operation was applied to capture some of the smoothing effect of lateral dispersion. As described by Barrett, this can be accomplished by averaging dispersion parameters over angles [66]. In this work, a 17-degree Gaussian averaging window was applied to each direction to smooth the dispersion parameters based on Gaussian plume half-angles from Hanna [74]. In this study, this "smoothing" operation introduced an <1% change in the error quantity mean(RDC)/mean(AERMOD) while smoothing out spikes in the results, as shown in Figure 14 for Asheville Regional Airport (KAVL).

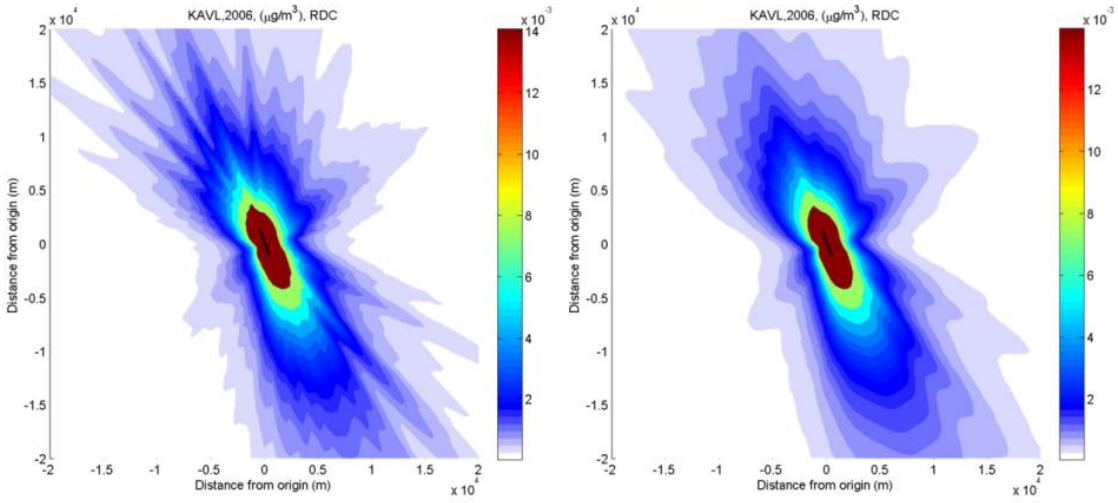

Figure 14. RDC results with unsmoothed and smoothed dispersion parameters.

2-4-3 Shapes and Locations of Emissions Sources

In the RDC, long-term average concentrations of $PM_{2.5}$ are calculated from rectangular emissions sources of constant, yearly-averaged emission rate. Only emissions from aircraft are accounted for presently and this affects the area-source representation of airports. As shown in the previous section, predicted concentrations can vary greatly within a few kilometers of the area source. Thus, to capture the spatial variation in concentrations near airports, multiple area sources are used rather than a single source or emissions placed at the airport center. For future work, the sensitivity of results to area source representation could be investigated.

For this study, aircraft-related emissions sources are divided into two types: runways; and terminals/taxiways. The procedure of obtaining a complete area source representation of airports is summarized in Figure 15.

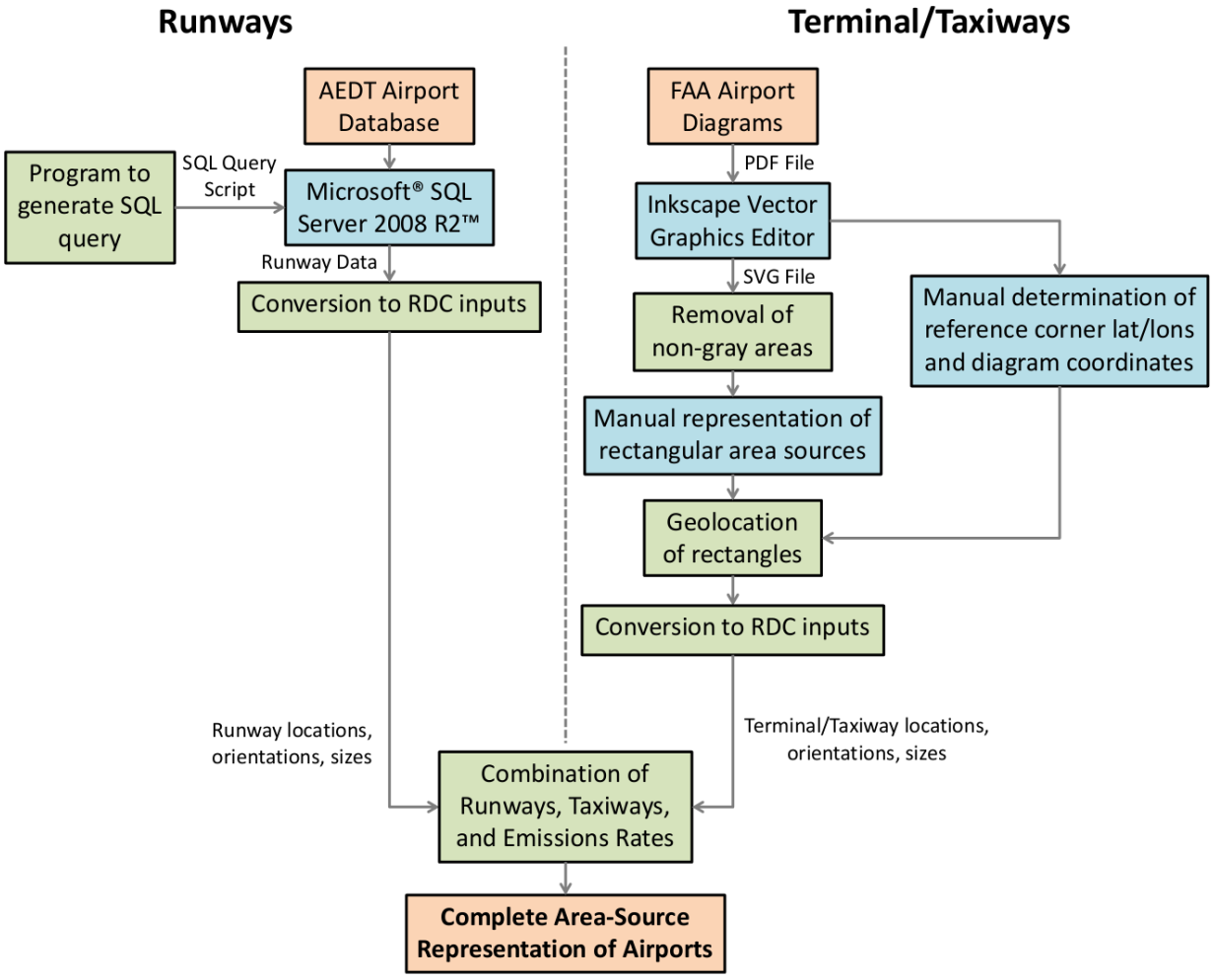

Figure 15. Overall process for obtaining complete area source representation of airports.

Runway data for RDMS were derived from the Aviation Environmental Design Tool (AEDT) Airport Database provided by the U.S. DOT Volpe National Transportation Systems Center [75]. Programs to generate queries to the SQL database extracted information about runways at approximately 13,000 airports and converted them into RDC inputs. Relevant variables from the database were an airport reference point (geographical location in lat/lon), the geographical location of each runway end at the airport, runway length, and runway width. As shown in Figure 16, this information was used to calculate a Cartesian-grid location (X,Y) relative to the airport reference point, length, width, and angle for each rectangular runway. Routines in the MATLAB® Mapping Toolbox™ [76] were used to calculate X,Y, length, and angle accounting for the Earth's elliptical shape. The width of each runway was assigned based on the airport database value. Note that although runway lengths were extracted from the airport database, these data were only used to validate the length calculated based on runway end locations. Runway lengths typically agreed within 5 m.

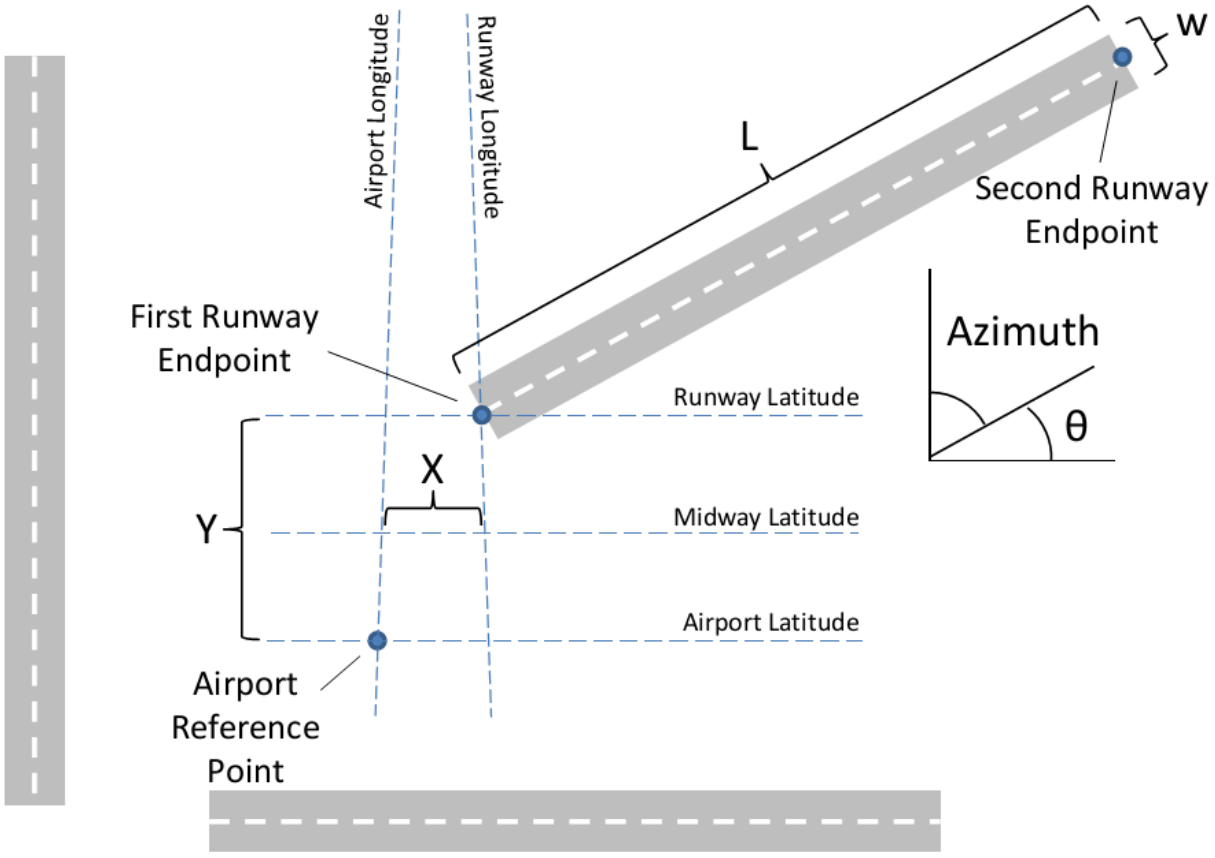

Figure 16. Method of determining runway area source parameters based on AEDT database inputs.

To obtain area-source representations of terminal areas and taxiways, a different approach was needed because the AEDT Airport Database does not include these areas. Furthermore, terminal areas are frequently irregularly shaped, requiring judgment about the best way to represent them with rectangles (Figure 17). Figure 15 shows the process for approximating these areas based on FAA airport diagrams.

Firstly, a collection of publicly-accessible airport diagrams for 191 U.S. airports were obtained from the FAA website [77] and converted into the Scalable Vector Graphics (SVG) format using Inkscape [78]. The open-source Inkscape software and SVG format allowed for modification and reading of vector shape coordinates. Thus, this combination of software and format enabled the drawing of shapes and systematic processing of their location, orientation, and size. After conversion, terminal and taxiway areas in grey were isolated and terminal/taxiway areas were approximated with rectangles manually. Without knowledge of which runways were used, judgment was exercised in excluding taxiways used by general aviation, which was not included in the emissions used for this study. Simultaneously, three reference points were identified and recorded to allow referencing of SVG page coordinates to geographical coordinates. These points were selected at corners of grid lines representing latitudes and longitudes and its page X, Y coordinate were also recorded. This process is illustrated in Figure 17.

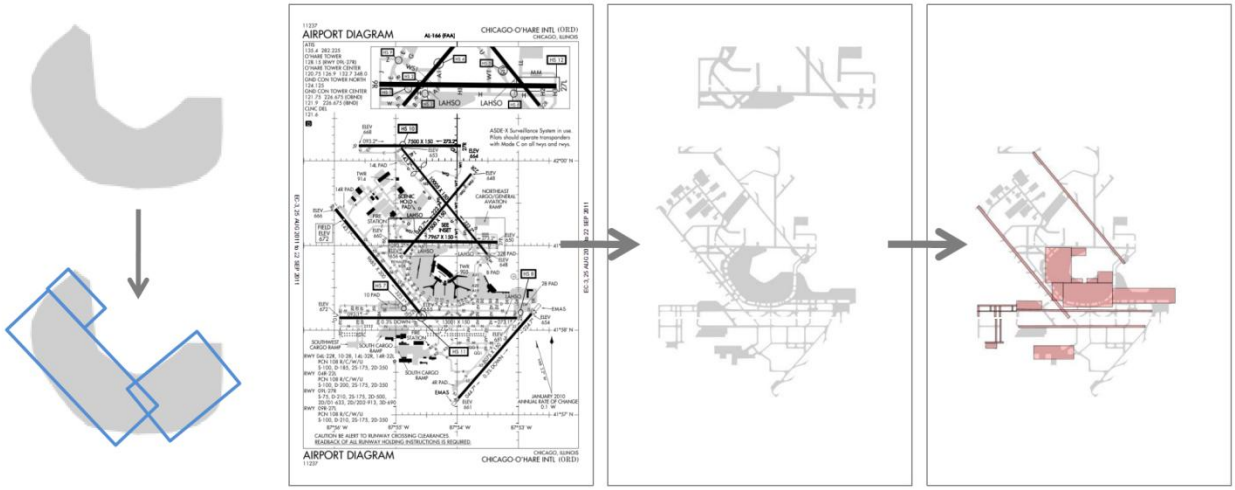

a) b) c) d)

Figure 17. Approximation of terminal/taxiway shapes using FAA airport diagrams: a) Irregular shapes are approximated with collections of rectangles for input into RDC; b) Complete FAA airport diagram converted into SVG format; c) Diagram with terminal, taxiway, and other grey areas isolated; d) Manual representation of terminal and taxiway areas.

The manual representation of rectangles, page coordinates, and corresponding geographical coordinates were processed to calculate each rectangular area source X,Y location, length, width, and angle. The terminal/taxiway area sources were located relative to the same airport reference point as the runway area sources. Finally, all area sources were combined to form a complete rectangular area-source representation of 191 U.S. airports.

Additional scripts were developed to check the airport area-source representations for accuracy. These scripts transformed the area sources into a Google Earth™ KML file [79] to superimpose the shapes on satellite imagery of the airports. The results show that area source representations align with the geographical locations of runways, terminals, and taxiways on satellite imagery, as shown in Figure 18 for Boston Logan International Airport (KBOS).

Figure 18. Complete area-source representation of Boston Logan International Airport (KBOS) superimposed on satellite imagery in Google Earth™. Runways are blue, terminals/taxiways are orange. Attribution: © 2012 Google.

Currently, the RDC is only capable of approximating ground-level point, line, and rectangular area sources [66]. It is not capable of handling volume sources although AERMOD possesses this capability [35]. Another study used volume sources to approximate runways rather than area sources [35].

Also due to this limitation, more irregular shapes such as terminal areas are currently represented using collections of rectangles that are manually drawn. For future work, methods using image processing may provide a more systematic way of approximating these shapes using rectangles. For example, Lee developed a method using genetic algorithms to approximate complex two-dimensional shapes with rectangles [80].

2-4-4 $PM_{2.5}$ Emissions Rates

The RDC requires a constant $PM_{2.5}$ emissions rate for each source. For this study, emissions were obtained from AEDT simulations for 2006. In AEDT, thousands of flights are simulated for each day of the year. Each flight is divided into flight modes corresponding to different stages of the flight. These emissions modes are listed in Figure 19. Emissions modes model the differences in thrust settings that affect quantities of $PM_{2.5}$ emitted by aircraft.

There are several limitations to the emissions rates that can be input to the RDC. Firstly, emissions for this work are restricted to the those emitted at ground level (zero elevation). Because the RDC is limited to modeling ground-level sources, full LTO emissions (those within an elevation of 3000 ft) from aircraft are not included in the emissions rates. To obtain the full impacts of aircraft near airports, the results of RDMS are combined with results from other models that can capture LTO emissions. More on this combination will be discussed in 2-6.

Secondly, because AERMOD and the RDC do not model the chemistry of the formation of secondary $PM_{2.5}$, only primary $PM_{2.5}$ emissions from aircraft are included in RDC emissions rates. The primary emissions species included in this work are primary elemental carbon (PEC), primary organic aerosol (POA), and primary sulfates (PSO_4) (Figure 19). Secondary $PM_{2.5}$ will be discussed as a future improvement to the model in 4-3.

Thirdly, AEDT only models emissions from commercial aircraft operations. Emissions from general aviation and other airport sources are not included within AEDT. Thus, these emissions are excluded from the RDC emissions rates. In future work, emissions from these sources could be modeled with separate area sources corresponding to the locations of these emissions.

Finally, RDC inputs a constant, yearly-averaged emissions rate for $PM_{2.5}$. RDC assumes that effects of temporal variations in emissions (for example, due to differing airport activity) are incorporated into the dispersion parameters already.

$PM_{2.5}$ emissions rates for area sources at each airport are found as follows. AEDT data describing flight segments are first filtered by flight mode and geographical location to reduce

the computational time of processing the AEDT data. Non-ground-level flight modes are skipped as well as those belonging to flights that do not list the United States as either the departure or arrival location. After segments are filtered, emissions for the three $PM_{2.5}$ species are summed for each flight mode. PEC and POA are extracted directly, while PSO_4 is calculated using Equation 5 [81].

$$SO_4 = \text{Fuel Burn} \times \frac{\text{FSC}}{1000} \times \frac{E}{100} \times \frac{96}{32}$$

SO_4	Mass of SO_4 emitted during flight segment, g
Fuel Burn	Mass of fuel burned during flight segment, kg
FSC	Fuel sulfur content, assumed value of 600 $mg/(kg - fuel)$ [82]
E	Mole fraction of sulfur emitted as S^{VI}, assumed value of 2% [81]
$96/32$	Molecular mass conversion factor from S^{VI} to SO_4

Equation 5. Formula for calculating emissions of primary sulfates from fuel burn [81].

Processing the AEDT data resulted in yearly totals of the three $PM_{2.5}$ species, separated by flight mode, for individual airports. Airport emissions totals were then combined, converted to average emissions rates (in kg/s), and assigned to either runway sources or taxiway sources. Emissions modes 0 and 10 corresponded to taxiing modes, while modes 1, 8, and 9 corresponded to runway modes. The airport taxiing total was area-weighted to the terminal/taxiway sources for the individual airport and the airport runway total was area-weighted to the runway sources. This method of assigning emissions is limited because it assumes that all runways are used equally. In practice, some runways are used more than others, and some runways may not be used at all. For future work, information about which runways are used most could be used to improve the distribution of airport emissions to the area sources.

At the end of this process, each of 191 U.S. airports had a complete area-source representation with runway and terminal/taxiway area sources and corresponding $PM_{2.5}$ emissions rates. This data was input into the RDC along with the dispersion parameters to calculate mean annual concentrations of $PM_{2.5}$ around these airports.

AEDT Emissions Mode	Description	Assigned to total for:
0	Taxi out	Terminals/Taxiways
1	Takeoff, ground roll	Runways
2	*Takeoff, airborne*	*Unassigned*
3	*Terminal climb*	*Unassigned*
4	*En route climb*	*Unassigned*
5	*Cruise*	*Unassigned*
6	*En route descent*	*Unassigned*
7	*Approach*	*Unassigned*
8	Landing, ground roll	Runways
9	Landing, ground roll with reverse thrust	Runways
10	Taxi in	Terminals/Taxiways

Emissions Species	Units
Fuel Burn	kg
Primary Sulfates (PSO_4)	g
Primary organic aerosol (POA)	g
Primary Elemental Carbon (PEC)	g

Airport-by-airport total $PM_{2.5}$ yearly average emissions rate
Runway total emissions rate
Terminals/Taxiways total emissions rate

Area-weight runways, taxiways separately

$PM_{2.5}$ emissions rate for each area source (kg/s)

Figure 19. Obtaining total $PM_{2.5}$ emissions from AEDT simulations.

2-4-5 Receptor Grid

Receptor points are locations where mean annual concentrations of $PM_{2.5}$ are calculated. In the RDC, receptor points are specified according to a Cartesian coordinate system in which the origin is placed at the airport reference point from the AEDT airport database. Points are specified in X, Y coordinates in meters. The conversion of these points to geographical locations follows the procedure described for determining the X,Y location of area sources. Although in this study, receptors are placed in a regular pattern, the RDC is capable of locating receptors at non-uniform locations (for example, if more receptors are desired to understand variations in a densely populated area).

Two issues arise in the specification of the receptors. Firstly, the local-scale impacts of airports extend over distances away from the airport requiring that receptor points extend far away enough to capture these impacts (i.e. until concentrations are negligible by some measure or the model is no longer valid). However, no precise value exists for the distance beyond which simulated impacts from airports are low enough to disregard. Such distance likely depends on the wind speed as higher wind speeds will disperse pollutants farther, creating higher concentrations. As a guideline, receptor grids could extend out to distances for which results vary by small amounts with respect to distance. Also, if results are to be combined with regional and global models, receptor grids could extend to the resolution of these models, thus resolving variations in concentration at smaller distances than the smallest distance possible with these models alone.

Secondly, the validity of the RDC results depends on distance. Since RDC only accounts for primary PM exposure, it does not account for secondary PM which could dominate air quality impacts far from the sources. Furthermore, RDC builds on preexisting dispersion models, which have a limited range of validity. For example, the EPA considers 50 km to be the range for which steady-state Gaussian plume models are applicable [83]. In comparison, the OML dispersion model used in Denmark is applicable for distances around 20 km from the source [84]. Though not included in this thesis, future work may address the validity of RDC by comparing results with modeled or observed concentrations from emissions sources.

In this work, receptors are placed on a 40 km by 40 km Cartesian grid at 400m intervals (101 x 101 receptor points total), in which the airport reference point is the center. In this grid, points at the edge are 20-30 km away from the origin. These values were chosen based on preliminary runs to capture impacts in areas surrounding airports while limiting the computational expense of calculating more concentration values. The extent of the domain is also within the general validity of dispersion models.

2-5 Validation of RDMS

In order to demonstrate the RDMS's ability to rapidly assess mean annual concentrations of $PM_{2.5}$ around airports, a validation study was performed comparing RDMS predictions to those of AERMOD. This validation study only serves to demonstrate that the RDMS can produce similar results (within a reasonable degree of error) to those of a time-series dispersion model at large savings in computational time. Studies were not performed testing the RDMS's accuracy compared to measured data, as has been done for models such as AERMOD, ADMS™, and

LASAT™. Since the RDMS is a method that builds on preexisting models, it would not be fair to compare RDMS directly to measured data without also assessing the accuracy of the dispersion model being used. RDMS enables the rapid assessment of long-term air quality impacts near airports at the expense of some accuracy. It is not suited for studies of short-term impacts.

2-5-1 Airports for Validation

For this validation study, fifteen U.S. airports were chosen based on their potential to demonstrate the RDMS's ability to model concentration variations. The airports were chosen to cover a variety of regions across the contiguous 48 states and based on the wind roses of the meteorological data used for simulations. As Figure 20 shows, the frequency of wind speeds and directions can vary among airports. Airports with low wind speeds and large directional variations were chosen to test the ability of the RDC to account for these variations. Other airports exhibited more uniformly distributed wind patterns, such as Pittsburgh International Airport (KPIT) in Figure 20.

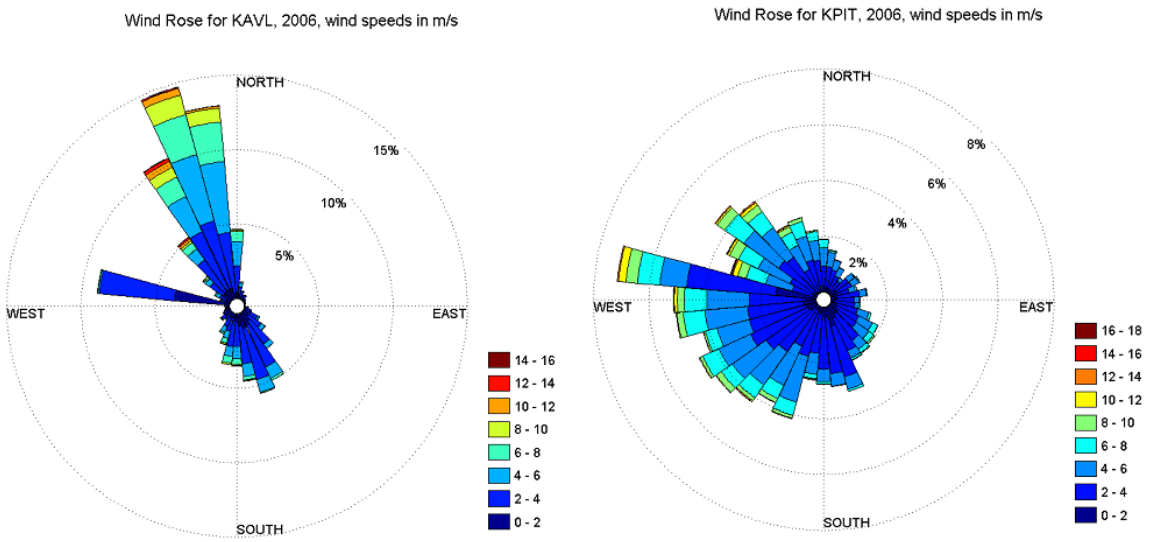

Figure 20. Wind roses for KAVL and KPIT for 2006.

Emissions rates, area sources, and receptor grids were specified for each airport and also input to AERMOD directly. For the validation study, the predicted mean annual $PM_{2.5}$ concentrations from RDMS were compared to AERMOD predictions in which area sources were input directly. The airports chosen contained different numbers of area sources, to attempt to

demonstrate the RDMS's time savings for airports of different sizes. Results for complete airports over 40 km by 40 km receptor grids were compared to demonstrate that AERMOD and RDC results agree despite errors adding up from the different area sources.

2-5-2 Method for Calculating Dispersion Parameters

The validation study also served to determine a procedure for calculating dispersion parameters that would result in agreement with AERMOD. Different methods of calculating the dispersion parameters are shown in Table 16 and Table 17 in Appendix A-2. Results using these different methods are also shown in Appendix A-2. As discussed before, calculating one dispersion parameter over all distances in each direction resulted in the best agreement.

2-5-3 RDC Error and Speed Evaluation

Three kinds of errors are reported in the validation results (Table 9).

Ratio error	$\text{Error} = \frac{\text{RDC}}{\text{AERMOD}}$
Percent relative to mean of domain	$\text{Error} = \frac{\text{RDC} - \text{AERMOD}}{\text{mean(AERMOD)}} \times 100\%$
Ratio of means	$\text{Error} = \frac{\text{mean(RDC)}}{\text{mean(AERMOD)}}$

Table 9. Three types of error reported.

The first quantity, ratio error, allows quantification of how much RDC over or under-estimates concentrations at each receptor. The second quantity shows how much RDC differs from AERMOD at each receptor, relative to a measure of the overall AERMOD values. The mean concentration value was chosen as this quantity is associated with health impacts. The third quantity relates how RDC will predict health impacts to how AERMOD will predict health impacts. Overall agreement between RDC and AERMOD will be expressed in terms of the ratio of means. Error quantities were calculated for all fifteen airports and reported in Appendix A-2.

Since RDMS and AERMOD require meteorological data, emissions rates, and area sources, the time to obtain these inputs is not included in comparing model performance. To compare RDMS to AERMOD, the time for RDMS to calculate dispersion parameters and calculate mean annual $PM_{2.5}$ concentrations is compared to the time for AERMOD to directly process meteorological data and calculate concentrations.

2-6 Combination with Regional Models

Air quality assessments for policy applications require the consideration of both primary and secondary $PM_{2.5}$. Because the RDMS only models the dispersion of ground-level, primary $PM_{2.5}$ emissions, RDMS results must be combined with results of other models that calculate concentrations of secondary $PM_{2.5}$. In this work, RDMS results were combined with regional results from the Community Multiscale Air Quality model (CMAQ) generated for a previous study for the U.S. [85]. Regional results used in this study considered both LTO and full-flight aircraft emissions cases. The method of combining results is summarized in Figure 21.

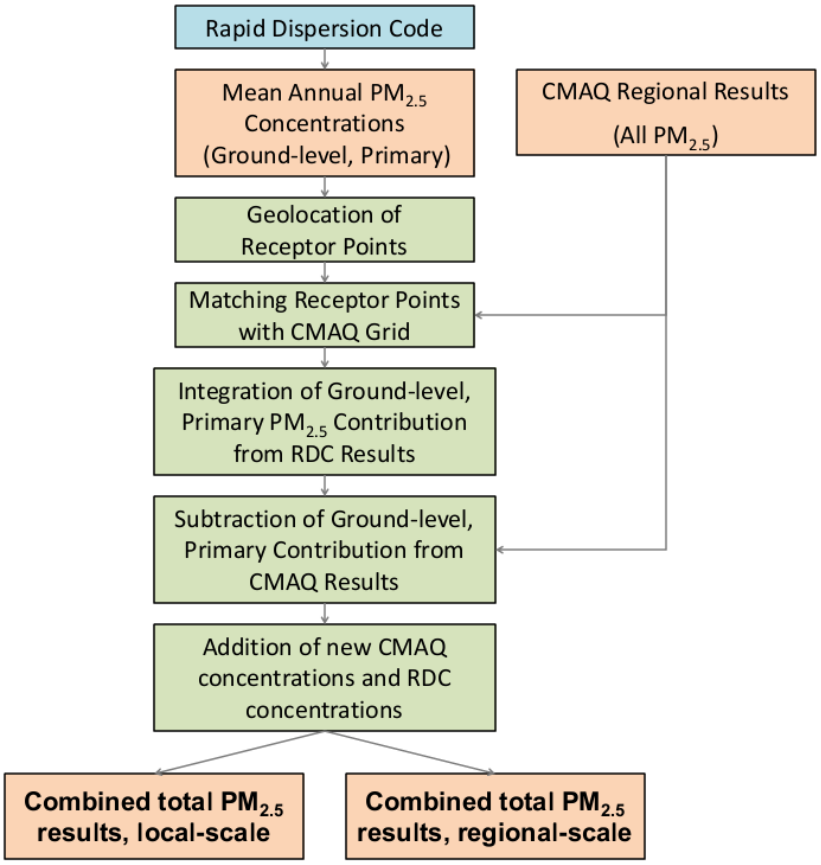

Figure 21. Summary of RDC-CMAQ combination process.

2-6-1 Emissions Consistency

Firstly, emissions files that were input to CMAQ and RDMS were checked for consistency. Both CMAQ and RDMS used emissions from AEDT for the year 2006. The three emissions species of interest were primary elemental carbon (PEC), primary organic aerosol (POA), and primary sulfates (PSO_4).

CMAQ emissions were specified for LTO and full-flight scenarios and were already gridded into 112 × 148 × 35 grid cells covering the United States. In contrast, emissions for RDMS were specified by airport totals. To ensure consistency between CMAQ and RDMS emissions, a process was developed to convert emissions developed for the RDMS to a grid-cell basis. The totals were then compared with those from CMAQ.

This procedure demonstrated that on average, CMAQ grid-cell total emissions were 8-14% higher than those developed for the RDMS. CMAQ grid-cell total emissions include emissions above the ground level but below the CMAQ grid cell height (~30m). Though not included in this study, in the future CMAQ grid cell emissions could be adjusted to include just ground-level modes for the purpose of this comparison, which would likely increase agreement between RDMS-developed emissions and CMAQ emissions. For this study, RDMS-developed emissions were taken to be consistent with those from CMAQ.

2-6-2 Spatial Consistency

CMAQ regional results (orders of 100 km) and RDMS local-scale (orders of 10 km) results are calculated within different domains and resolutions (Table 10). Furthermore, the RDMS and CMAQ results do not use the same coordinate system. The RDMS spatial domain is approximately aligned with latitudes and longitudes, but CMAQ uses a Lambert conformal conic projection. Before combining the concentration values from each model, the spatial location of points must be consistent.

Model	Domain	Spatial Region Covered by Domain	Resolution (Grid cell size)	Coordinate System
RDMS	40 km by 40 km	Area around each airport	400 m	Lat/Lon-aligned
CMAQ	4032 km by 5328 km	Contiguous United States	36 km	Lambert conformal

Table 10. Differences in RDC and CMAQ spatial parameters.

Using the airport reference point for each airport, the geographical location (lat/lon) of each RDC receptor point is calculated using routines in the MATLAB® Mapping Toolbox™. Then, the locations are converted to Lambert conformal conic coordinates to determine which CMAQ grid cell each receptor point lies in.

After performing this conversion, RDMS domains were plotted in Google Earth™ and compared to a plot of the regional grid. Figure 22 shows that different receptors within the

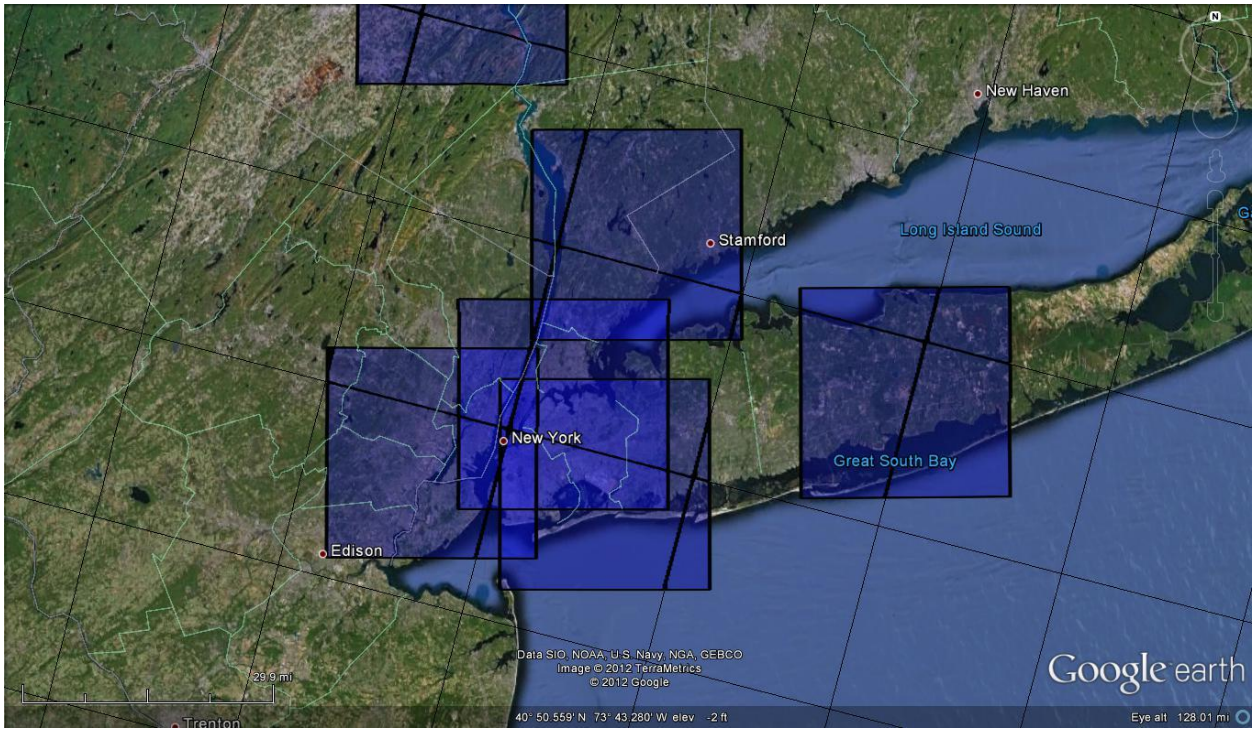

Figure 22. Overlap of RDMS domains with CMAQ grid cells around New York. The figure is oriented to due North. Lambert-conformal-based CMAQ grid cells are diagonally aligned, while RDMS domains are aligned with latitudes and longitudes. RDMS receptors are assigned to correct CMAQ grid cells. Attribution: Data SIO, NOAA, U.S. Navy, NGA, GEBCO; Image © 2012 TerraMetrics; © 2012 Google.

RDMS domain were assigned to different regional grid cells, and that the boundaries of these different assignments match the regional grid. Thus, the points were spatially consistent.

Figure 22 also shows that several RDMS domains may overlap with the same CMAQ grid cell. Such is the case for airports in close proximity, such as the New York airports (KJFK, KLGA, KEWR, etc.). However, the method for combining CMAQ regional concentrations with RDMS concentrations addresses this overlap.

2-6-3 Method of Combining Concentration Results

CMAQ concentrations are specified for the surface layer (~0-30m) and capture the effects of dispersion and formation of both ground-level and non-ground-level $PM_{2.5}$ emissions. Also, CMAQ concentration values include both primary and secondary $PM_{2.5}$. RDMS results only capture the dispersion of ground-level emissions of primary $PM_{2.5}$ (Figure 23). Though the total health impact from all four categories of $PM_{2.5}$ is desired, the RDMS models the health impact of ground-level, primary (GLP) $PM_{2.5}$ in further detail at the local scale. A method developed by

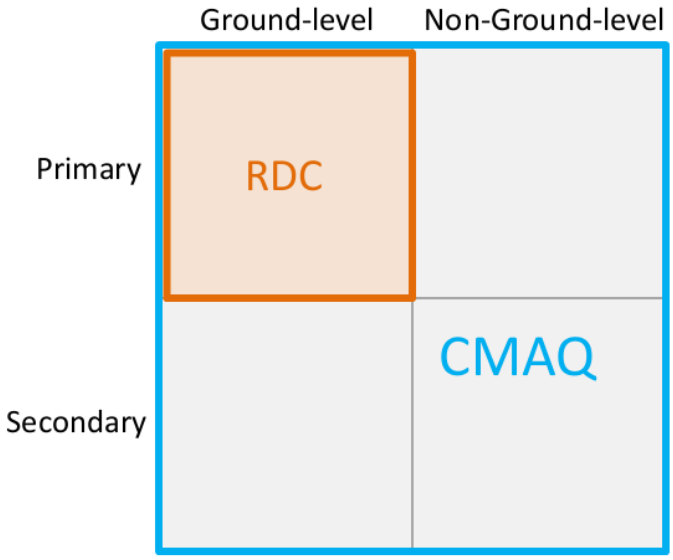

Figure 23. Categories of $PM_{2.5}$ emissions included in CMAQ and RDC simulations.

Isakov enables combination of local-scale RDMS results without double counting the effects of this PM category [86].

The process is shown in Figure 24 and Equation 6. For each airport, receptor points have already been assigned to CMAQ grid cells. Thus each CMAQ grid cell has been assigned receptor points from airports whose RDMS domains overlap the grid cell. Concentration values for all receptor points that overlap with the CMAQ grid cell are spatially integrated, giving the total ground-level, primary $PM_{2.5}$ contribution of RDMS-modeled airports to the CMAQ grid cell. This contribution is then subtracted from the CMAQ concentration value, such that a CMAQ value is obtained that contains PM except for the RDMS $PM_{2.5}$ component. Note that a conversion between 400 m and 36 km grid cell bases is necessary to ensure that concentrations are subtracted correctly. Finally, for each receptor point, this new CMAQ concentration value is added onto the receptor point value to obtain a total $PM_{2.5}$ concentration that accounts for all categories of PM.

This method accounts for multiple airports contributing to the same CMAQ grid cell, since the contributions from all airports are summed before being subtracted from the CMAQ concentration value. Also, this method accounts for cases in which the RDMS domain slightly overlaps a CMAQ grid cell. In these cases, the RDMS contribution that is subtracted out is minimal, reflecting that health impacts from this airport on a far away CMAQ grid cell are small.

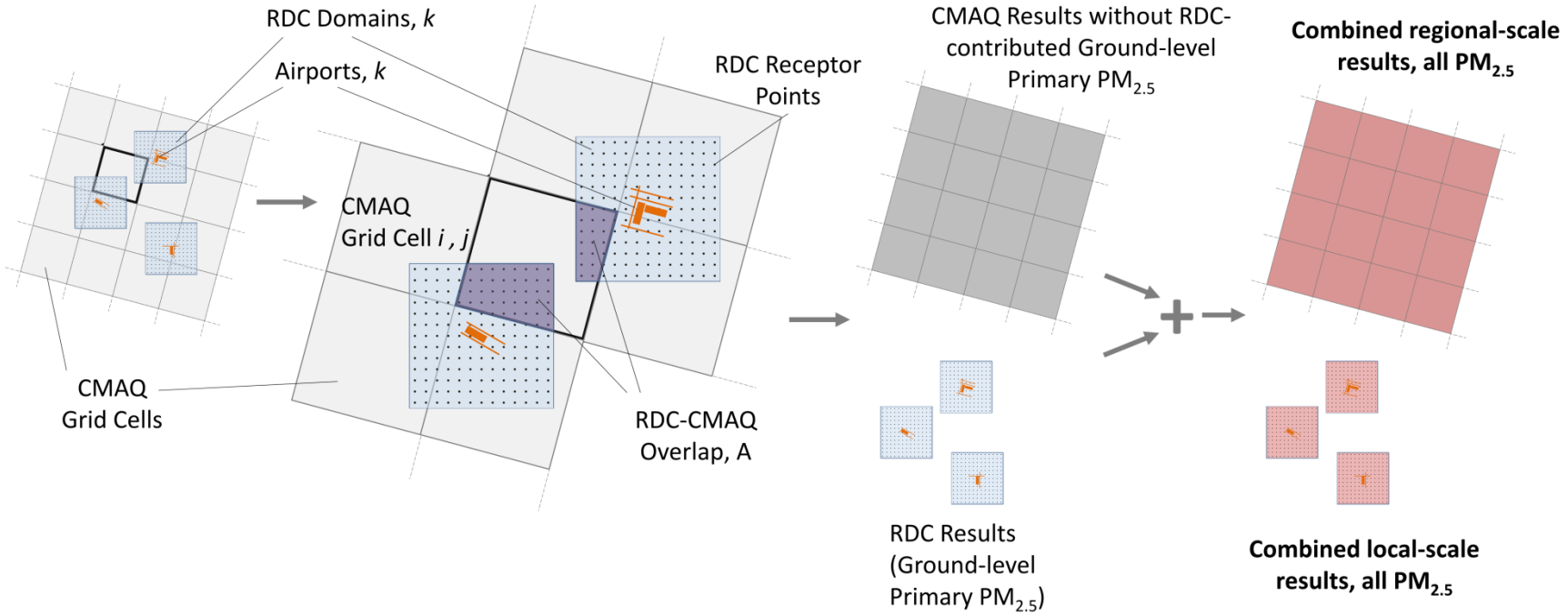

Figure 24. Estimation, subtraction, and re-addition of ground-level, primary $PM_{2.5}$ contributions from RDMS to CMAQ results.

$$\chi_{CMAQ,i,j,-GLP} = \chi_{CMAQ,i,j} - \frac{\int_A \chi_{RDC,GLP}\, dA}{A_{CMAQ}}$$

$$\frac{\int_A \chi_{RDC,GLP}\, dA}{A_{CMAQ}} \approx \frac{\sum_k \sum_{\text{receptors} \in A} \chi_{RDC,GLP} \times (400\text{ m})^2}{(36000\text{ m})^2}$$

i , j	CMAQ grid cell indices
$\chi_{CMAQ,i,j}$	Total CMAQ concentration
$\chi_{CMAQ,i,j,-GLP}$	CMAQ concentration without ground-level primary $PM_{2.5}$ contribution
A	Area where RDC domains and CMAQ grid cell overlap
A_{CMAQ}	CMAQ grid cell area, $(36000\text{ m})^2$
$(400\text{ m})^2$	RDC receptor area*
$\chi_{RDC,GLP}$	RDC concentration values at receptors (representing ground-level primary $PM_{2.5}$)
$\sum_k$	Sum over airports/RDC domains that overlap CMAQ grid cell i , j
$\sum_{\text{receptors} \in A}$	Sum over receptors that overlap with CMAQ grid cell i , j

Equation 6. Equations for subtraction of ground-level primary $PM_{2.5}$.
* Though the RDC does not calculate concentrations using a grid-cell approach, for integrating concentrations a "receptor area" is assumed to be the area immediately surrounding each receptor point with a uniform concentration of the receptor value.

2-6-4 Issues with the Combination Method

Before subtracting out contributions from the CMAQ concentration values, receptor values are summed to obtain an estimate of the total ground-level, primary $PM_{2.5}$ contribution that an airport has to a particular CMAQ grid cell. However, the RDC often produces clearly non-physical receptor values, especially close to domain center. These large spikes in concentration value result from using a power-law fit; both AERMOD and RDC generates large values near the center because concentration is calculated as an inverse power of distance. To address this issue, receptor values above the 99.5th percentile value (roughly 50 points near the center) are assigned the 99.5th percentile value. This value was chosen to allow for cases in which airport runways (and spikes in concentration values) extend beyond the immediate vicinity of the airport reference point (and origin of the RDMS 40 km domains).

As discussed previously, current research aims to improve understanding of the processes that determine the formation and spread of $PM_{2.5}$ within aircraft exhaust plumes. For example, Barrett estimated that including aircraft plume dynamics would result in a 40% reduction in predicted long-term average concentrations when compared to a dispersion model that assumes passive emissions sources [23]. To account for this, a correction factor of 0.6 was applied to the RDMS results before combining with the CMAQ results. Results are presented both without and with this correction factor.

For some regional grid cells, integrated RDMS contributions exceeded the CMAQ concentration value (which should incorporate all PM categories). This resulted in negative concentrations at some receptors. For these cases, a scaling factor was applied to the RDMS receptors within these grid cells such that the subtraction of integrated RDMS GLP $PM_{2.5}$ and re-addition of the local RDMS receptor value would result in a value ≥ 0. This factor was applied in such a way as to preserve mass: no concentration of $PM_{2.5}$ is created nor destroyed. Rather, less RDMS-modeled GLP $PM_{2.5}$ is subtracted, and less is added back. Thus the scaling factor adjusts some receptors to account less for local-scale variations to prevent non-physical negative concentration values. Of 820 regional grid cells that RDMS domains overlapped (Appendix A-1), this scaling procedure was applied to 26 grid cells (3%) in the LTO case and just 1 grid cell (0.1%) in the full-flight case.

Finally, consistent emissions between RDMS and CMAQ (or global models for future work) are crucial for ensuring that $PM_{2.5}$ concentrations can be combined. The emissions provided for

CMAQ did not include airport-by-airport totals used to generate gridded emissions. Although emissions were approximately consistent for the 191 airports in this study, in future work, airport-by-airport totals for global and regional models would ensure with more certainty that emissions input to the RDC and CMAQ were consistent.

2-7 Assessment of Health Impacts

After calculating mean annual concentrations of $PM_{2.5}$, health impacts were calculated using a similar method to Barrett [85] (to be referred to as "ULS study"). The overall process for calculating health impacts is shown in Figure 25. Health impacts are calculated at both the local-scale RDMS domain and at the regional scale. For both of these results, primary, secondary, ground-level, and non-ground-level $PM_{2.5}$ are accounted for by using the combined RDMS-CMAQ concentrations. Furthermore, a comparison is made between health impacts calculated without and with local-scale variations modeled by RDMS, for both local and regional scales.

$PM_{2.5}$ has a variety of cardiovascular and respiratory health impacts that are addressed in the epidemiological literature. Consistent with the ULS study, this study will focus on premature mortalities as this health endpoint dominates other health impacts. Furthermore, premature mortalities are assumed to result entirely from cardiopulmonary (CP) diseases and lung cancer (LC). More information about methodological assumptions in calculating health impacts are described in the ULS study [85].

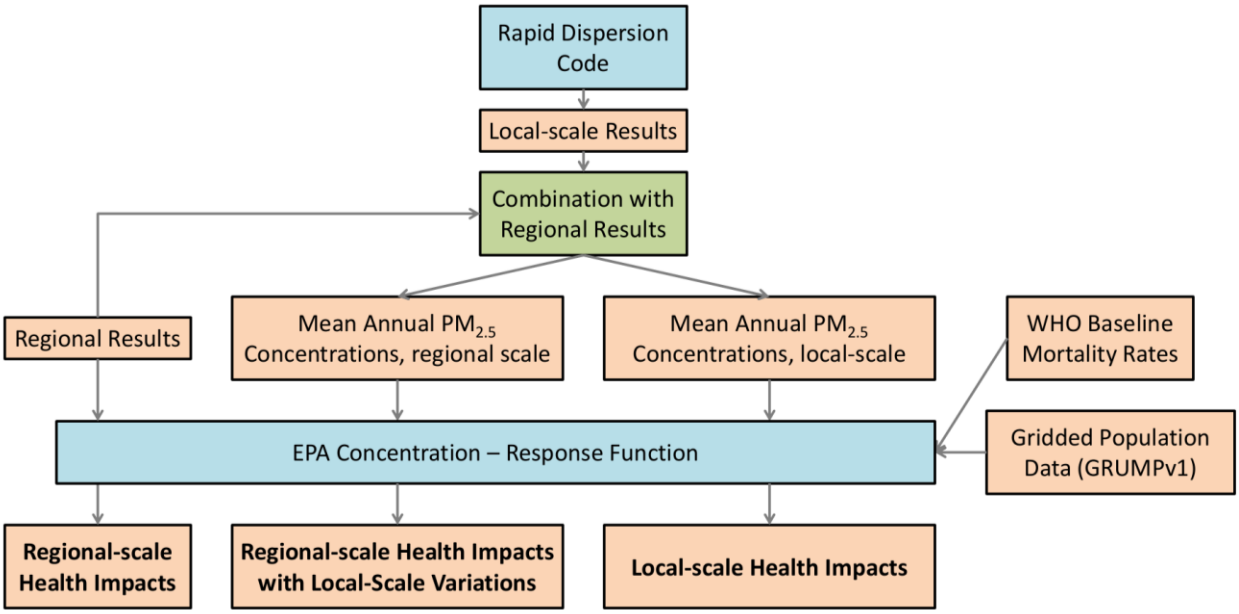

Figure 25. Overall process for calculating health impacts.

Health impacts can be calculated within computer models for each discretized grid cell with a population and concentration value. The total premature mortalities over all population grid cells in the United States is described by Equation 7, where values for fractional increases in mortality are from an EPA-derived concentration-response function based on a 1% / 1 μg/m^3 increase in all-cause mortalities due to long-term $PM_{2.5}$ exposure [85].

$$\Delta(\text{Premature Mortalities}) = \sum_{ij} [f_{k,30+} P_{ij} \Delta\chi_{ij} \beta_{US}^{CP} (B_{US}^{CP} + \gamma B_{US}^{LC})]$$

$\sum_{ij}$	Sum over all population grid cells
$f_{k,30+}$	Fraction of population over 30 years of age
P_{ij}	Population in grid cell i , j
$\Delta\chi_{ij}$	Aviation-attributable increase in $PM_{2.5}$ concentration, μg/m^3
β_{US}^{CP}	Fractional increase in mortality given one μg/m^3 increase in annual average $PM_{2.5}$, United States, cardiopulmonary disease
B_{US}^{CP}	Baseline per capita mortality rate, United States, cardiopulmonary disease
B_{US}^{LC}	Baseline per capita mortality rate, United States, lung cancer
γ	Ratio relating lung cancer risk to cardiopulmonary risk

Equation 7. Equation for calculating premature mortalities [85].

Population data were obtained from the GRUMPv1 database developed by the Socioeconomic Data and Applications Center at Columbia University (SEDAC) [87]. The population data for the United States were for the year 2000 at a 30 arc-second resolution (approximately 1 km at the equator).

Because the population data were available at a coarser resolution than that of the combined local-regional results, a procedure was developed to obtain a population density value for each receptor point. These density values were used to calculate population at the RDMS resolution, local-scale exposure, and estimates of premature mortality totals.

To estimate regional premature mortalities, these local-scale population density values were used to calculate an RDMS-only premature mortality adjustment to each grid cell, in a similar procedure used to calculate RDMS ground-level-primary contributions to each grid cell. These adjustments were then added to regional premature mortalities calculated based only on the concentrations with integrated RDMS contributions subtracted out. The end result was a regional premature mortality total accounting for local-scale variations, but not double-counting health impacts from RDMS-modeled GLP $PM_{2.5}$.

2-8 Summary

In this section, the RDMS was described as well as processing of inputs and outputs for the calculation of $PM_{2.5}$ exposure and health impacts for a set of 191 airports in the United States. The following results will be presented:

1) Comparison of RDMS to AERMOD
    a) Error statistics
    b) Comparison of calculation speed
2) Local-scale results
    a) Spatial variations of concentrations
    b) Spatial variations of health impacts
    c) Premature mortality estimates for 191 airports, without and with local-scale variations
3) Regional-scale results
    a) Spatial variations in regional concentrations
    b) Spatial variations in regional health impacts
    c) Regional premature mortality estimates, without and with local-scale variations

3. Results and Discussion

Results from the validation and study of 191 U.S. airports are presented and discussed below. First, the validation study results will show the agreement of RDMS-predicted annual average $PM_{2.5}$ concentrations with predicted concentrations from AERMOD. Then, concentrations and health impacts will be presented at the local scale and regional scale. For discussion purposes, the terms "RDMS" and "RDC" will be used interchangeably to describe the rapid dispersion results.

3-1 Comparison of RDMS and AERMOD

3-1-1 Overall Error Statistics

The differences in errors among different dispersion parameter calculation methods are shown in Table 21, Table 22, and Table 23 in Appendix A-2-3. These error totals are calculated over all 15 airports. For all three measures of error discussed in 2-5-3, calculating one dispersion parameter over all distances resulted in the best agreement between RDC and AERMOD. Comparing mean(RDC) to mean(AERMOD) shows that on average, RDC will over-predict AERMOD by +5% (Table 23).

The error between RDC and AERMOD-predicted concentrations can vary by airport (Table 20 in Appendix A-2-3). For mean(RDC)/mean(AERMOD), the error between RDC and AERMOD varies from -2% to +9% except for KAVL and KGCN. KAVL RDC results overestimate AERMOD by 11%, while KGCN RDC results overestimate AERMOD by 31%. The larger errors for these airports are due to large variations in wind speeds over wind directions, which cause averaging errors in the dispersion parameters. Nevertheless, for all airports, calculating over all distances still produces better agreement than other methods of calculating dispersion parameters.

3-1-2 Comparison of Calculation Speed

The RDC is designed to estimate long-term average $PM_{2.5}$ concentrations faster than traditional dispersion models can. For this validation study, the time to conduct simulations for the fifteen airports were compared (Table 24 in Appendix A-2-4). For discussion purposes, a "full AERMOD simulation" entails running AERMOD with raw meteorological data inputs, area source shapes, and emissions rates, to calculate annual average concentrations of $PM_{2.5}$ at

receptor points. Each full AERMOD simulation was conducted on a single processor on the same computer. Dispersion parameters were calculated for all airports in series on a single processor, then the RDC was run in series to generate results for all airports. Thus, the calculations used to compare AERMOD to RDC computational performance did not use any parallel processing that would bias the comparison.

On average, the time to perform the RDC simulation took 0.4% of the time to run a full AERMOD simulation. On average, the time to calculate dispersion parameters took 3.9% of the time to run a full AERMOD simulation. The most time savings recorded occurred for El Paso International Airport (KELP), for which the RDC took 0.35% of the time to perform an AERMOD simulation. The least time savings recorded occurred for Grand Canyon National Park Airport (KGCN), for which the RDC took 0.61% of the time to perform an AERMOD simulation. The time savings for both calculating dispersion parameters and running RDC increases with the number of area sources; Figure 26 shows that in general, airports with more area sources took proportionally less time than airports with fewer area sources. Overall, the time to run the RDC was much less than the time to calculate dispersion parameters (~10%), and the time to calculate dispersion parameters was much less than the time for a full AERMOD simulation (3.9%).

RDMS is designed to assess the local air quality impacts of airports for different policy, technology, and operational scenarios. The computational savings achieved by RDMS compared to running a dispersion model such as AERMOD would change if analyses required processing of different years of meteorological data. For the case in Table 24 in Appendix A-2-4 where only one scenario is considered for the year 2006, the total time to both calculate all dispersion parameters and run RDC simulations is about 4.3% of the total time to run AERMOD simulations. But dispersion parameters only need to be calculated once for a particular year, after which the RDC can use these parameters for different scenarios considered. In contrast, the times to run AERMOD would multiply by every scenario for every year considered. Thus, analyzing more scenarios that do not require the recalculation of dispersion parameters would increase the time savings from using RDMS.

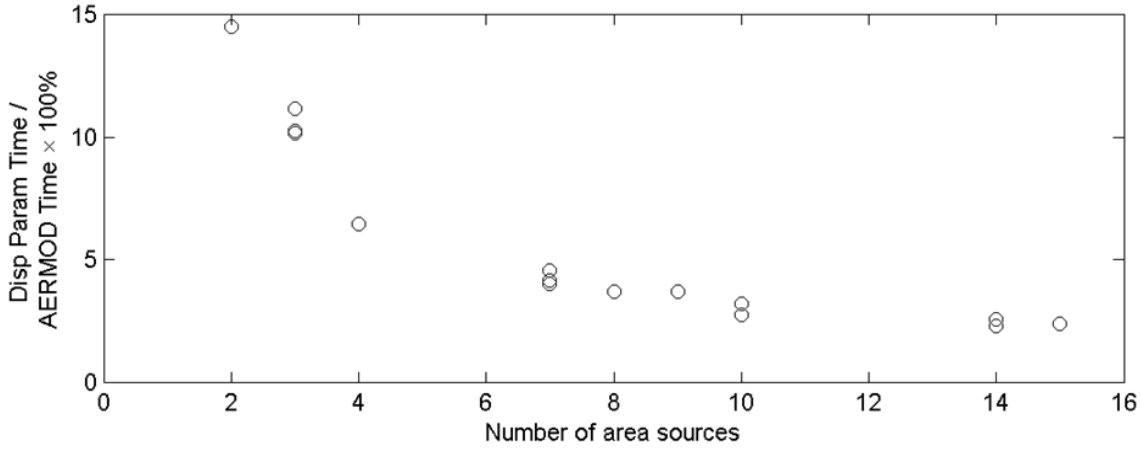

a)

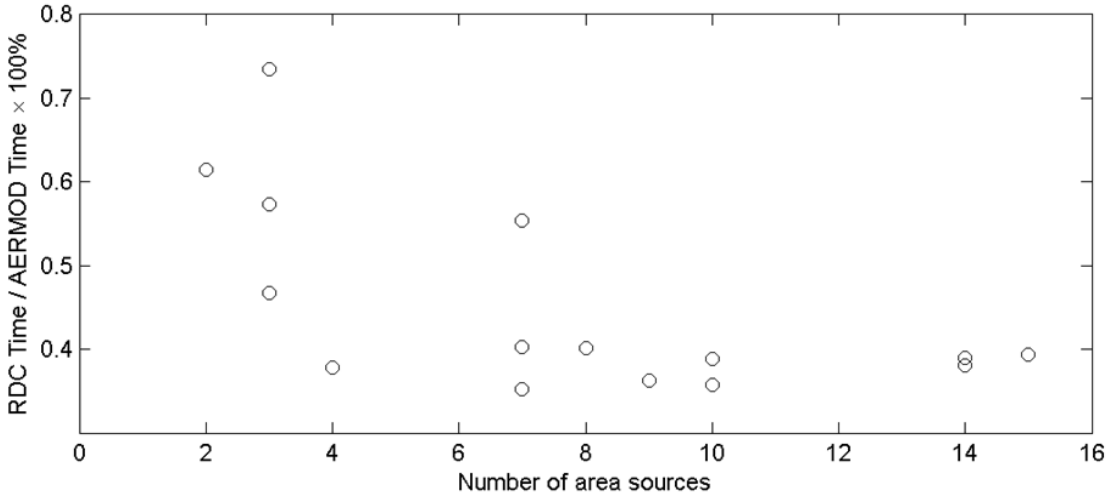

b)

Figure 26. Percentage of time relative to time to run AERMOD as a function of number of area sources, for a) calculating dispersion parameters b) rapid dispersion calculation.

3-1-3 Summary of Comparison of RDC to AERMOD

In summary, RDMS results overestimate AERMOD results by ~5% on average, while saving up to approximately 99.5% of the time to calculate long-term average $PM_{2.5}$ concentrations.

3-2 Local-Scale Results

In the following section, concentrations and health impacts at the local-scale will be presented and discussed for one airport, Boston Logan International Airport (KBOS). For simplicity, only figures for one airport will be shown. Additional airports are in Appendix A-4. The wind rose and RDMS-calculated mean annual $PM_{2.5}$ concentrations are shown in Figure 27. For this study, local-scale results cover a 40 km by 40 km Cartesian receptor grid surrounding each airport with the airport at the center.

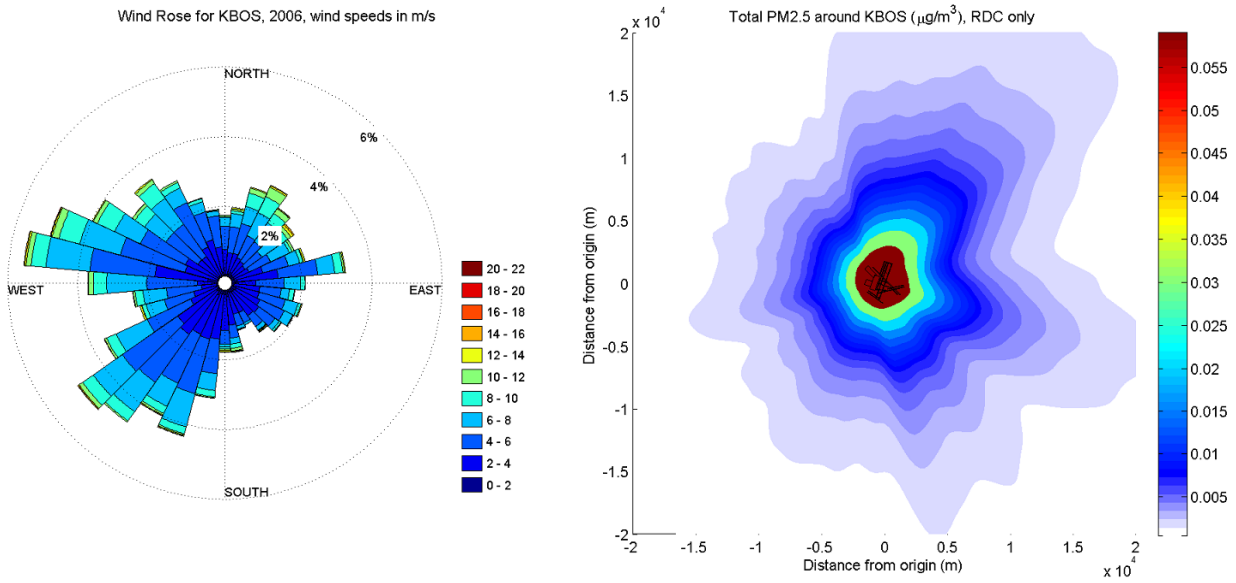

Figure 27. Wind rose and RDC results for Boston Logan International Airport (KBOS). Concentrations are higher in directions with prevailing winds.

Furthermore, premature mortality estimates for all 191 airports at the local-scale will be presented and discussed.

For both the local-scale and regional-scale results, concentrations and health impacts were generated without and with a plume correction factor accounting for aircraft plume dynamics. This correction will be referred to as a "plume factor adjustment" in all plots and discussion to follow.

3-2-1 Spatial Variations of Concentrations

Figure 28a and Figure 29a show local-scale variations of concentrations for RDC results only and RDC results combined with concentrations from CMAQ LTO and full-flight cases, where integrated ground-level-primary (GLP) $PM_{2.5}$ from the RDC has been subtracted out from the CMAQ concentrations prior to adding the results to avoid double-counting this category of $PM_{2.5}$. The concentration maps for Figure 28a and Figure 29a are spatially similar due to the uniform application of a constant plume factor adjustment over all receptors.

Comparing the RDC results to the wind rose for KBOS shows that concentrations are higher in prevailing wind directions. However, winds in other directions are significant over the year and this is reflected in the spread nature of the concentration results. Other airports with more unidirectional winds showed high concentrations in these directions and small concentrations elsewhere.

In Figure 28a and Figure 29a, the boundaries of the specific CMAQ grid cells combined with the RDC results are clear. CMAQ grid cells and RDC domains are not aligned in the same way: RDC domains are aligned to compass directions (i.e. N-S, E-W) but CMAQ grid cells follow a Lambert conformal conic projection. For all 191 airports, this caused the CMAQ grid cells to be aligned at an angle to the RDC domains. Furthermore, RDC domains did not fully encompass CMAQ grid cells, nor the opposite. This partial overlapping of domains and grid cells was accounted for in the calculation of RDC contributions to CMAQ grid cells.

The concentration results show that long-term average concentrations of ground-level-primary $PM_{2.5}$ decrease with distance away from the airport. However, contributions of non-GLP $PM_{2.5}$ can cause concentrations far from the airport to vary, as illustrated by the noticeable differences in concentrations between adjacent CMAQ grid cells. The results suggest that accounting for both ground-level-primary and other categories (primary, secondary, and non-ground-level) is important for assessing total levels of $PM_{2.5}$.

3-2-2 Spatial Variations of Health Impacts

Figure 28b and Figure 29b show $PM_{2.5}$ exposure surrounding KBOS. The discrete population grid cells reflect the local population distribution.

The exposures shown in the RDC-only portions of these plots reflect those from RDMS-modeled concentrations only and do not reflect grid-cell-by-grid-cell scaling to prevent negative concentrations from combining with regional results. This is to show the exposure that would be calculated from just running RDMS. However, of 820 grid cells that overlapped RDMS domains, a scaling factor was applied to 26 (3%) for the LTO case and 1 (0.1%) for the full-flight case. In contrast, the combined RDC-LTO and RDC-full-flight portions of Figure 28b and Figure 29b and premature mortality estimates reflect the application of these scaling factors.

For the RDC-only case, exposure is generally limited to near-airport populations approximately within 10 km. For the combined cases, exposure extends farther out, reflecting levels of $PM_{2.5}$ that are modeled by CMAQ but not the RDC. Especially for the case of combined RDC-full flight concentrations, exposure extends to the boundaries of the RDC domain. Exposure is highest in the more densely population middle regions.

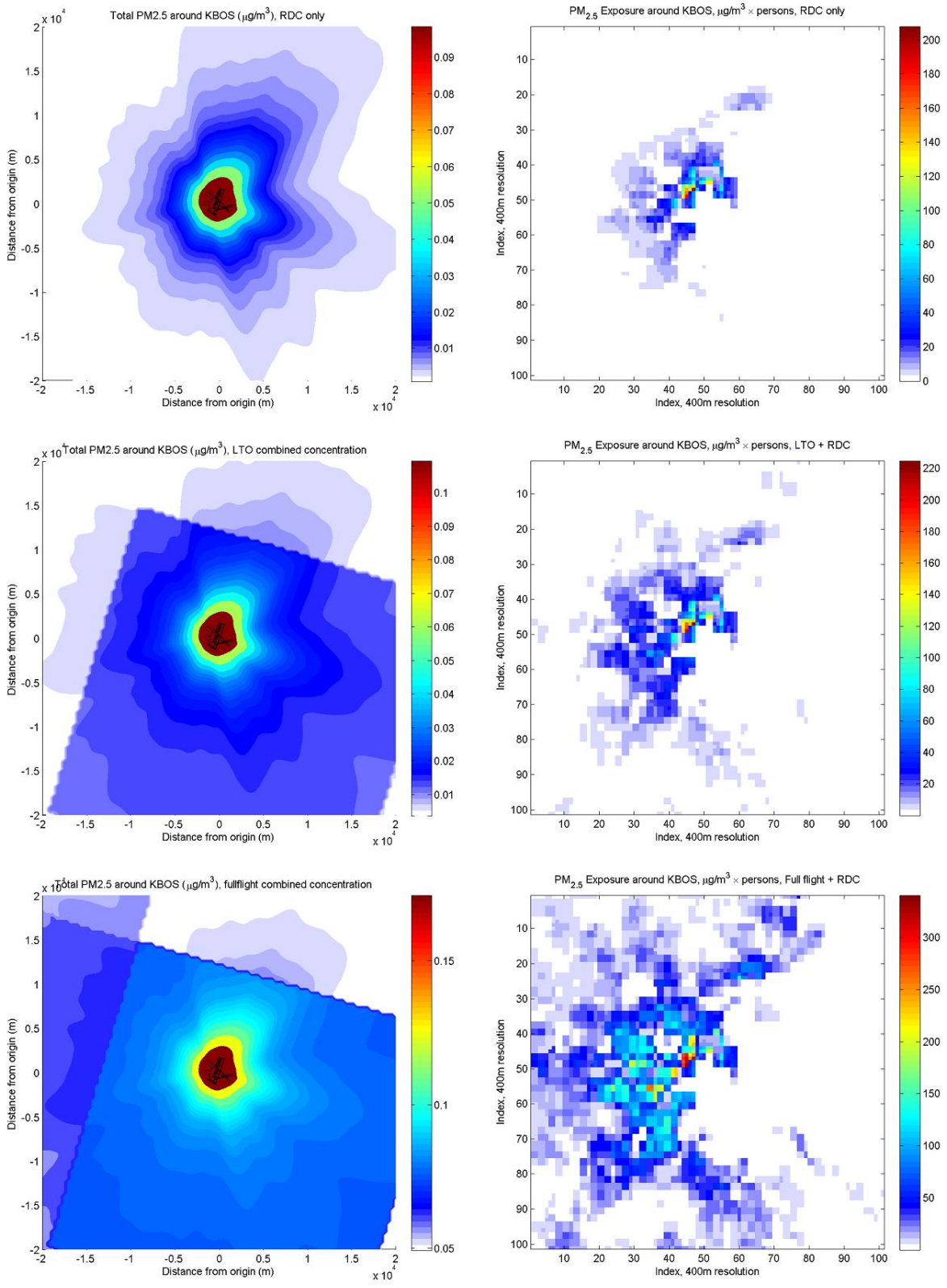

a) b)

Figure 28. Plots of a) RDC-only and combined RDC-CMAQ $PM_{2.5}$ concentration values; b) Spatial variation of local $PM_{2.5}$ exposure. Without plume factor adjustment.

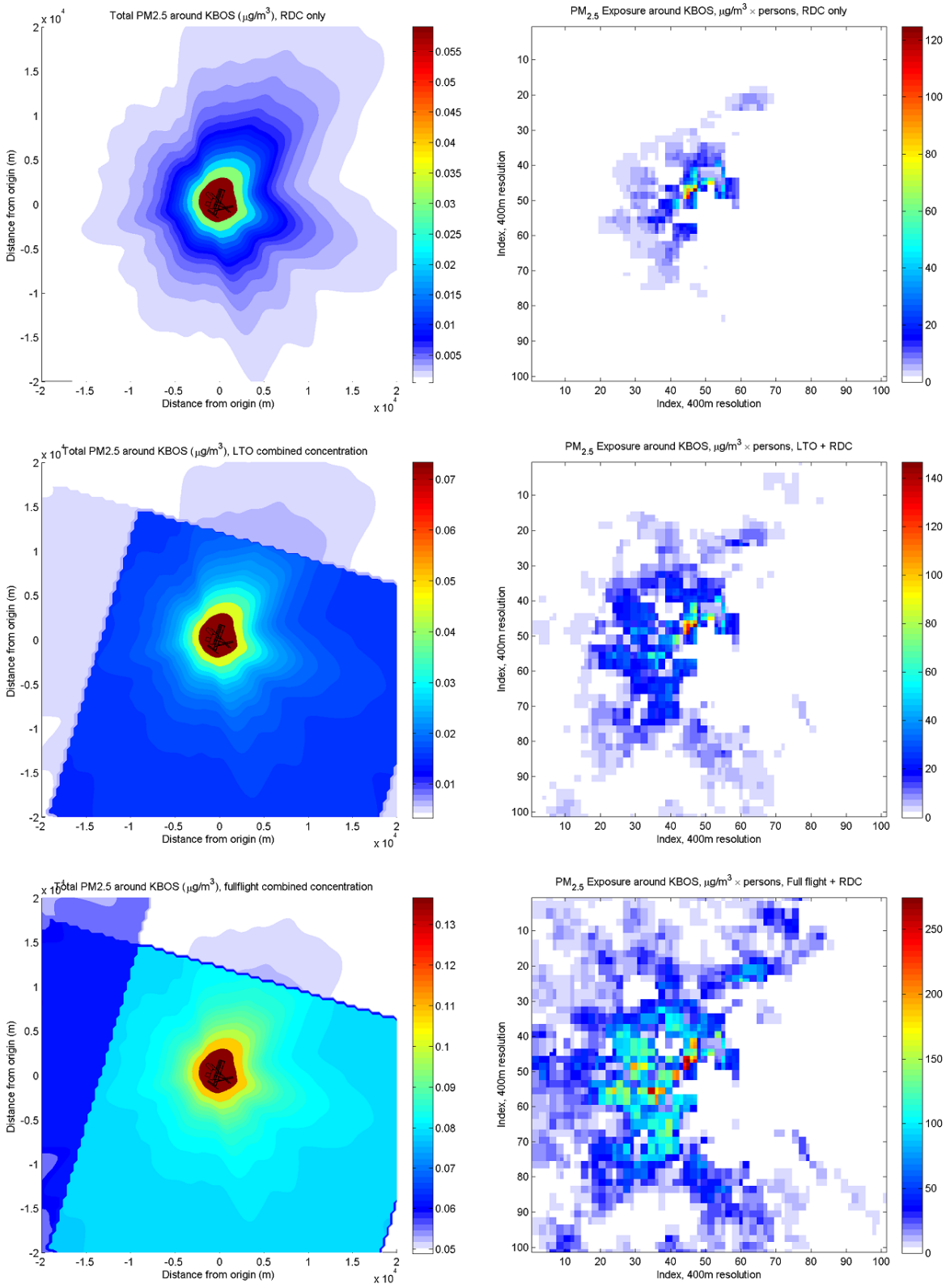

a) b)

Figure 29. Plots of a) RDC-only and combined RDC-CMAQ $PM_{2.5}$ concentration values; b) Spatial variation of local $PM_{2.5}$ exposure. With plume factor adjustment.

3-2-3 Premature Mortality Estimates for 191 Airports

Aviation-attributable premature mortality estimates for 2006 were calculated for all 191 airports. To calculate these estimates, an EPA-derived concentration-response function was applied based on a 1% / 1 $\mu g/m^3$ increase in all-cause mortalities due to long-term $PM_{2.5}$ exposure [85].

Table 11 shows the estimated premature mortalities at the local-scale from all 191 airports, without and with the plume factor adjustment. Including the plume factor adjustment decreases the estimates of RDC-only mortalities because of decreased local-scale concentrations. Two separate RDC-only totals are shown, reflecting different scaling for LTO and full-flight cases to ensure no negative combined concentrations.

The results suggest that at the local-scale near airports, ground-level-primary $PM_{2.5}$ modeled by RDC accounts for 43-65% of total local-scale premature mortalities when only LTO emissions are considered. This percentage decreases to 8-13% when full-flight emissions are considered. These results also suggest that full-flight emissions are important for assessing health impacts, even at the local-scale near airports.

	Combined RDC- LTO	**Combined RDC-Full-flight**	**RDC only, Scaled for LTO**	**RDC only, Scaled for Full-Flight**	**% of combined premature mortalities from RDC, LTO**	**% of combined premature mortalities from RDC, full-flight**
Without plume factor	88	517	57	66	65%	13%
With plume factor	88	517	38	40	43%	8%

Table 11. Premature mortality totals for combined, local-scale RDC-CMAQ results for LTO and full-flight, without and with plume factor adjustment;
Percentage of local-scale impacts from RDC for combined LTO and full-flight cases.

Table 12 shows the average percent change in premature mortality estimates, comparing totals calculated using CMAQ concentrations at each receptor to totals reflecting combined, local-scale variations in concentrations. Including local-scale variations increases premature mortality estimates by 16-27% for the LTO case and 1-2% for the full-flight case.

Table 25 in Appendix A-3 lists premature mortality totals by airport for all cases, with the plume factor adjustment. Table 26 and Table 27 in Appendix A-3 list statistics for these results.

	Average % change from including local-scale peaks, combined RDC-LTO	Average % change from including local-scale peaks, combined RDC-Full-flight
Without plume factor	+27 %	+2 %
With plume factor	+16 %	+1 %

Table 12. Average percent change over 191 airports, comparing premature mortalities per airport using only CMAQ concentrations vs. including local-scale variations.

Airport	Combined RDC-LTO	Combined RDC-Full-Flight	RDC Only, Scaled for LTO	RDC Only, Scaled for Full-Flight
KLGA	9	45	3	3
KJFK	8	35	3	3
KEWR	6	31	2	2
KLAX	9	18	6	6
KLGB	5	17	1	1
KMDW	1	16	1	1
KORD	3	16	2	2
KPHL	2	13	1	1
KDCA	1	11	1	1
KBUR	3	10	1	1
Total	47	212	20	20
% of Total for 191 Airports	53 %	41 %	53 %	51%

Table 13. Premature mortality totals for top ten airports for combined, local-scale RDC-CMAQ results for LTO and full-flight, and RDC only. With plume factor adjustment.

On average, each airport contributed 0.52% of the total estimated premature mortalities for the RDC-only cases, combined LTO case, and combined full-flight case in 2006. Airports contribute more or less depending on their concentrations and proximity to populated areas. For example, Table 13 lists the premature mortality estimates with the plume factor adjustment for the top ten airports. Together, the top ten airports account for 41-53% of premature mortalities at the local-scale. These airports are located in the densely populated New York, Los Angeles, Chicago, Philadelphia, and Washington D.C. metropolitan areas.

3-2-4 Summary of Local-Scale Results

Local-scale concentrations of long-term average $PM_{2.5}$ near airports reflect prevailing wind patterns but are also influenced by concentrations of non-ground-level primary $PM_{2.5}$ from regional-scale model results. Over 191 airports, ground-level-primary concentrations of $PM_{2.5}$ accounted for 43-65% of total local-scale $PM_{2.5}$ exposure for the combined RDC-LTO case and 8-13% for the combined RDC-full-flight case. Including local-scale variations increases premature mortality estimates at the local scale by 16-27% for the combined RDC-LTO case and 1-2% for the combined RDC-full-flight case.

3-3 Regional-Scale Results

In the following section, regional-scale concentration and health impacts results will be discussed. One of the aims of the rapid dispersion process is to improve on regional-scale estimates of health impacts by accounting for variations near airports that are not resolved in regional and global-scale models. The results shown will compare LTO and full-flight results before and after the inclusion of local-scale contributions from RDC.

3-3-1 Spatial Variations in Regional Concentrations

Figure 30 and Figure 31 show the regional, surface-level, aviation-attributable concentrations of total $PM_{2.5}$ before and after subtracting out integrated RDC contributions. The integrated RDC contributions shown in these plots are for the case with plume factor adjustment only. Integrated RDC contributions are calculated by summing the ground-level-primary $PM_{2.5}$ totals that each RDC simulation contributes to each grid cell, then subtracting these grid-cell totals.

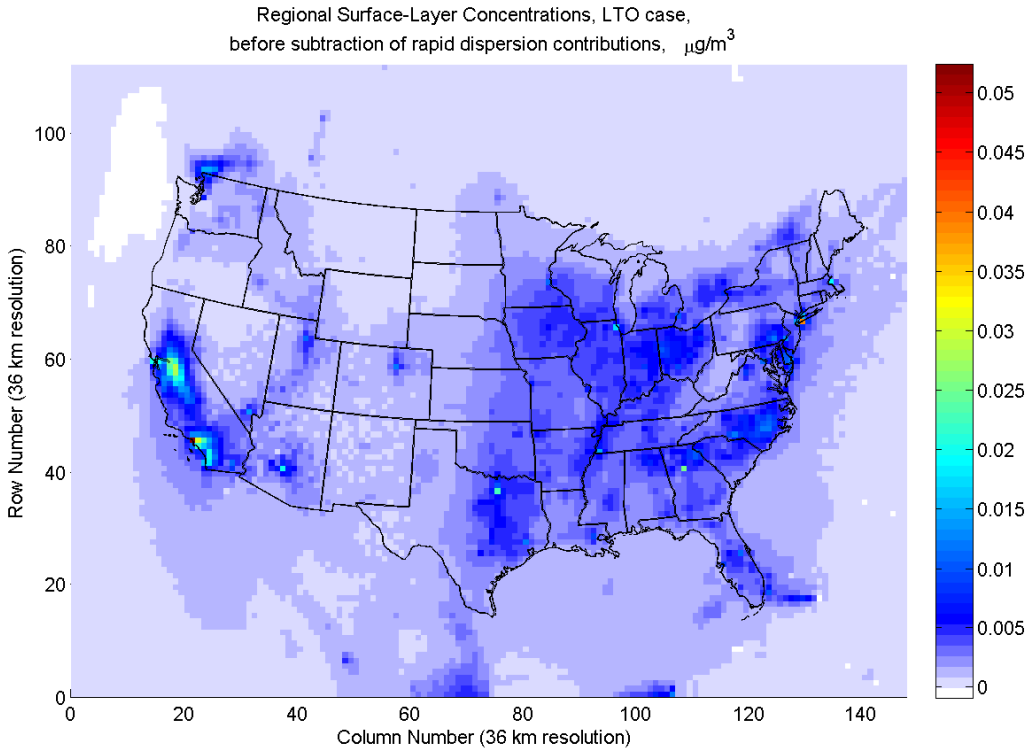

a)

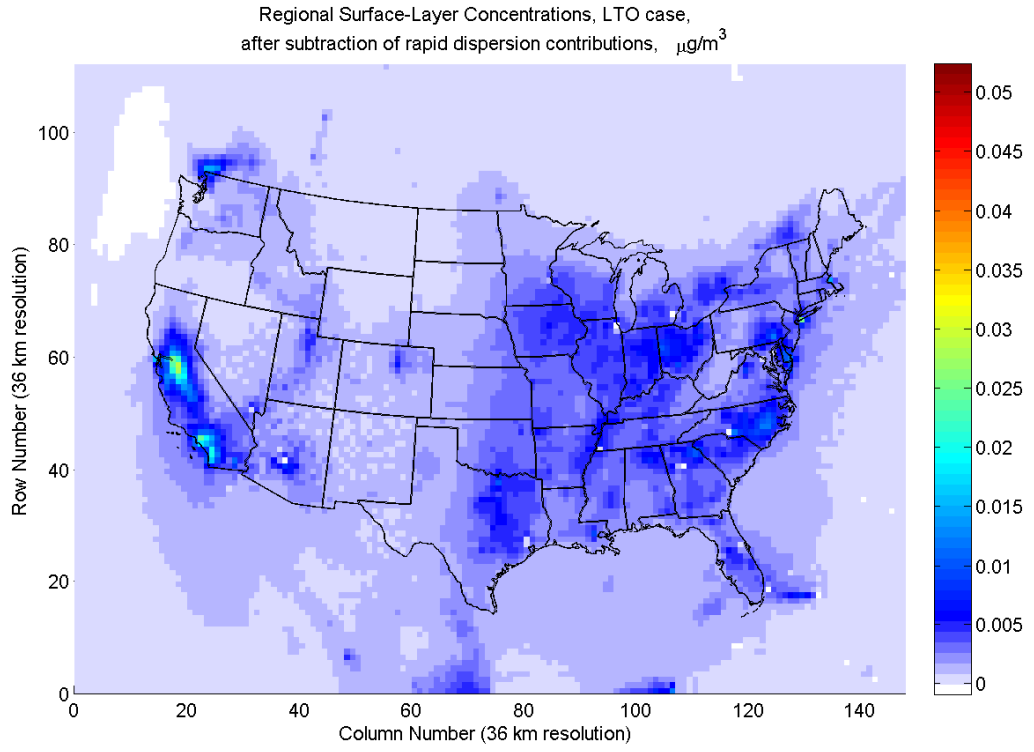

b)

Figure 30. CMAQ ground-level concentrations using LTO emissions: a) before subtraction; b) after subtraction of RDC-derived integrated ground-level primary $PM_{2.5}$. With plume factor adjustment.

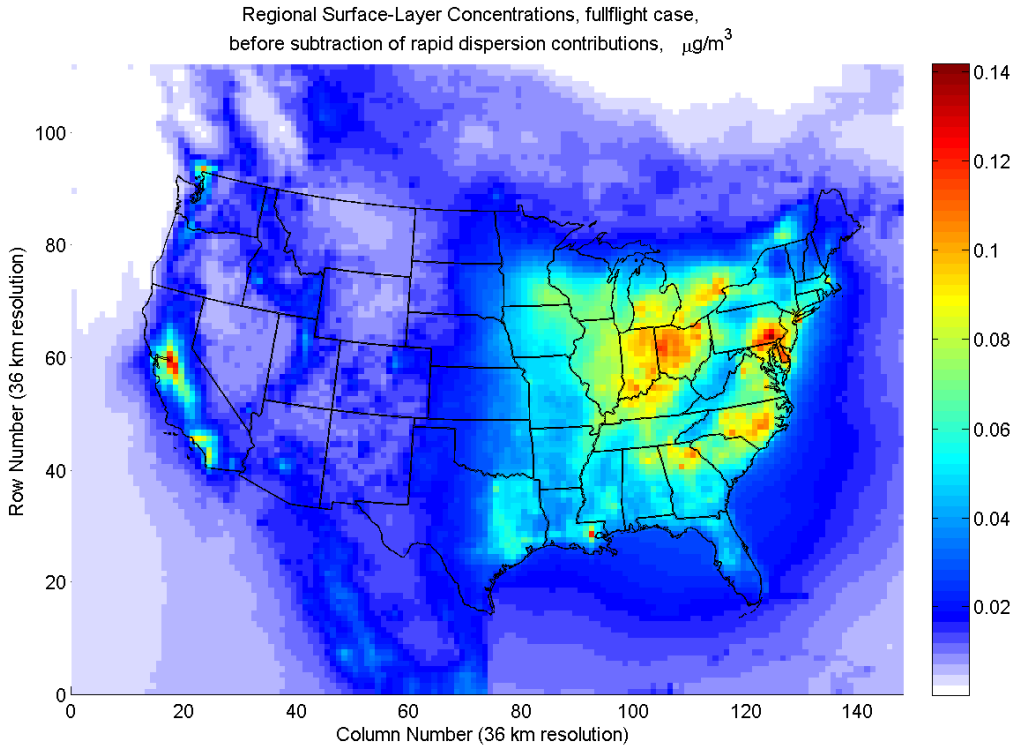

a)

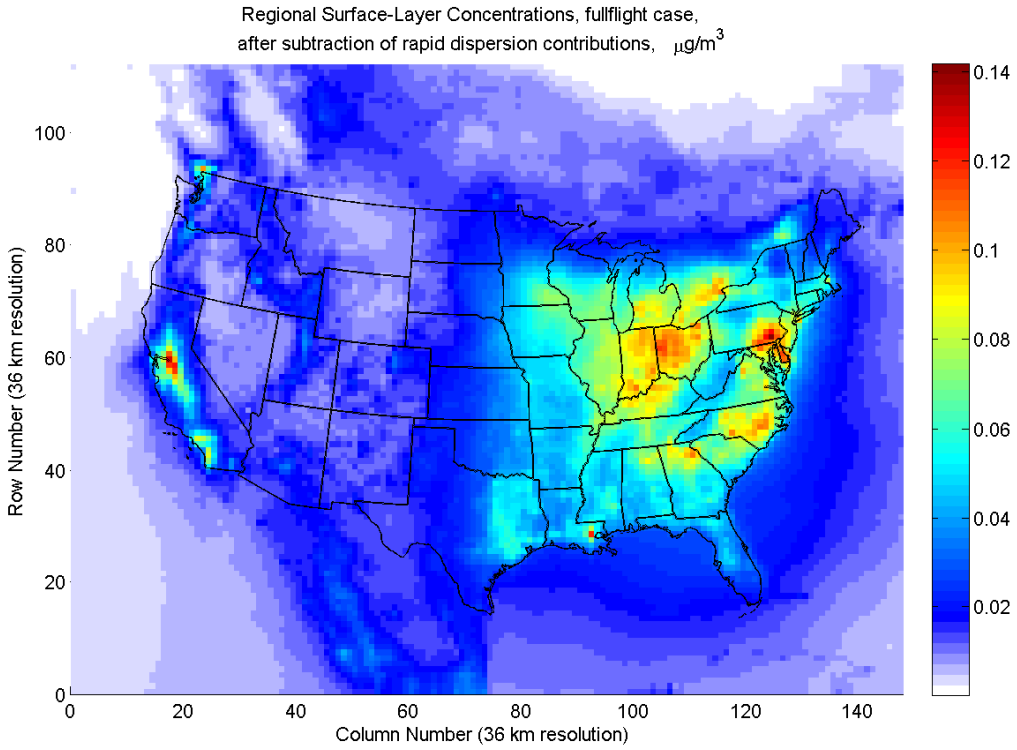

b)

Figure 31. CMAQ ground-level concentrations using full-flight emissions: a) before subtraction; b) after subtraction of RDC-derived integrated ground-level primary $PM_{2.5}$. With plume factor adjustment.

3-3-2 Spatial Variations in Regional Health Impacts

Figure 32 illustrates a sample plot of regional health impacts for the case of combined full-flight and RDC health impacts with plume factor adjustment. The result shows that aviation-attributable premature mortalities are concentrated in populated areas (locations of higher mortalities in the plot generally match locations of major cities). This pattern is similar for the LTO case and for the cases without plume factor adjustment.

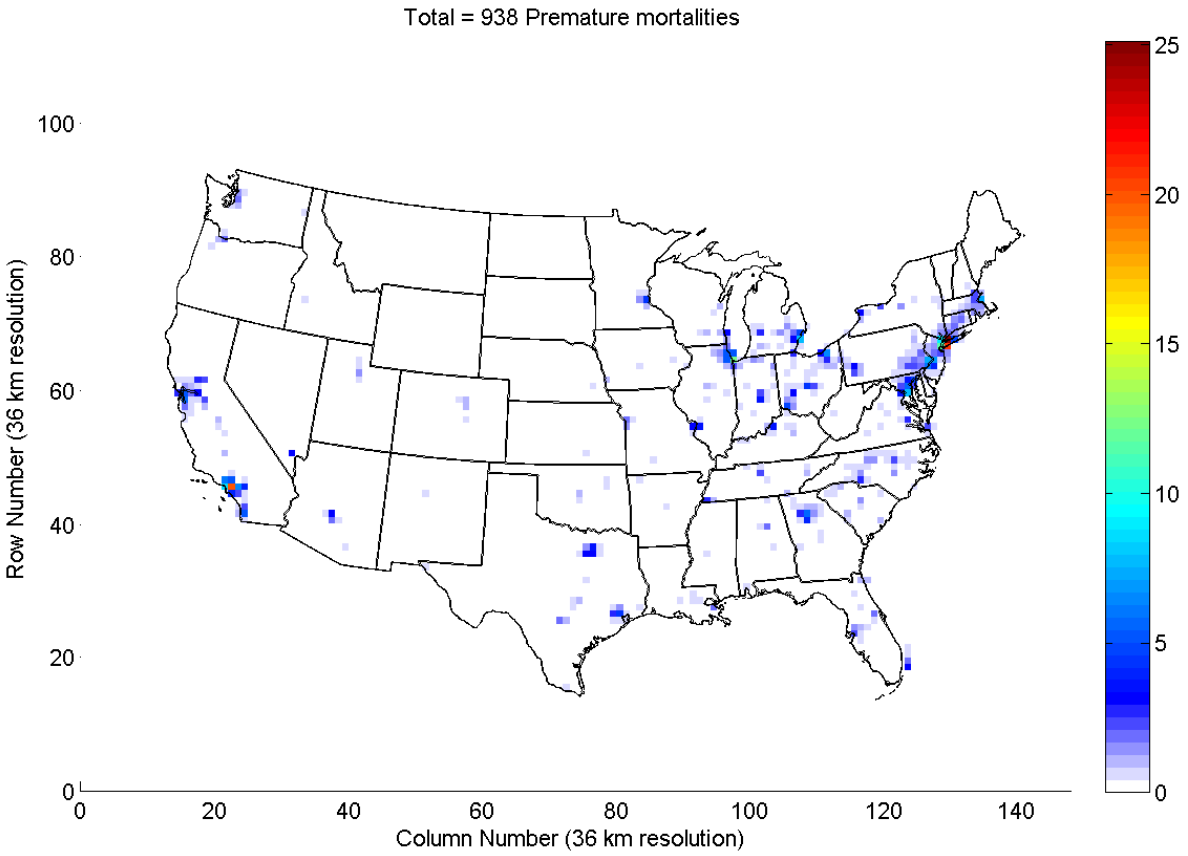

Figure 32. Example plot of regional health impacts. Combined full-flight and RDC health impacts with plume factor adjustment.

3-3-3 Comparison of Regional Health Impacts without and with Local-Scale Variations

Table 14 and Table 15 show the total number of premature mortalities without and with inclusion of local-scale variations. Including local-scale variations increases the total predicted premature mortalities by 8-12% for the LTO case and 1% for the full-flight case. For the combined health impacts, RDC-modeled ground-level-primary $PM_{2.5}$ accounts for approximately 34-50% of total health impacts for the LTO case and 4-7% for the full-flight case. Figures are higher without plume factor adjustment, as not including the plume factor will increase RDC concentrations and thus local-scale premature mortality variations.

	Without local-scale variations	**With local-scale variations**	**% change**	**Non-RDC contribution to regional total**	**RDC contribution to regional total**	**% of total health impact from RDC contributions**
LTO	103	115	+ 12 %	58	57	50 %
Full-Flight	930	943	+ 1 %	877	66	7 %

Table 14. The effect of including local-scale variations on regional premature mortality totals. Without plume factor adjustment.

	Without local-scale variations	**With local-scale variations**	**% change**	**Non-RDC contribution to regional total**	**RDC contribution to regional total**	**% of total health impact from RDC contributions**
LTO	103	111	+ 8 %	72	38	34 %
Full-Flight	930	938	+ 1 %	898	40	4 %

Table 15. The effect of including local-scale variations on regional premature mortality totals. With plume factor adjustment.

3-4 Summary of Results

The key results from this study of 191 airports are:

1) At the local-scale, ground-level-primary concentrations of $PM_{2.5}$ accounted for 38-66 premature mortalities around major airports.
2) Over these airports, ground-level-primary concentrations of $PM_{2.5}$ accounted for 43-65% of total local-scale $PM_{2.5}$ exposure for the LTO case and 8-13% when full-flight emissions are considered.
3) At the regional scale, ground-level-primary $PM_{2.5}$ contributions from RDC accounted for approximately 34-50% of the regional premature mortality total, and 4-7% of the full-flight total.
4) Inclusion of local-scale variations increased the predicted airport premature mortality estimates by an average of 16-27% for the LTO case and 1-2% for the full-flight case. Inclusion of local-scale variations increases the predicted regional total of premature mortalities by 8-12% for the LTO case and 1% for the full-flight case.

The RDMS was also demonstrated to agree with an existing regulatory dispersion model, AERMOD, on average within 5%. Using the metric mean(RDC)/mean(AERMOD), agreement with AERMOD ranged from -2% to +31%. Excluding two outlier airports, agreement with AERMOD ranged from -2% to +9%. Using RDMS saved 99.5% of the time AERMOD takes to calculate long-term average $PM_{2.5}$ concentrations, if only the RDC is considered. Including the calculation of dispersion parameters, RDMS saves 95% of the time required by AERMOD.

4. Future Developments

In the following section, future improvements to RDMS are discussed.

4-1 Diurnal Emissions Profile

To calculate long-term average $PM_{2.5}$ concentrations, the rapid dispersion calculation relies on dispersion parameters calculated from dispersion model simulations for point sources. In this work, the emissions rate for this point source was assumed constant (unit emissions rate of 1 kg/s), with emissions from individual area sources applied later to account for different emissions from different sources. However, aircraft emissions vary among hours, days, and seasons depending on aircraft traffic patterns. Because the RDMS is limited to calculating long-term averages, the effects of these temporal variations can be included in the calculation of dispersion parameters to account for any correlation between meteorology and emissions rates.

Dispersion models such as AERMOD allow for temporal variation of emissions. For future work, a normalized temporal emissions profile $e(t)$ could be specified such that:

$$\int_{8760} e(t)dt = \int_{8760} 1\ dt$$

Equation 8. Specification of temporal emissions profile.

In Equation 8, 8760 denotes the number of hours in one year and $e(t)$ is in units of kg/s. The resulting long-term average point-source concentrations would reflect temporal effects while allowing for scaling by individual area source emissions rates.

4-2 Plume Dynamics

As discussed previously, current research aims to improve understanding of the processes that determine the formation and spread of $PM_{2.5}$ within aircraft exhaust plumes. For example, Barrett estimated that including aircraft plume dynamics would result in a 40% reduction in predicted long-term average concentrations when compared to a dispersion model that assumes passive emissions sources [23]. Based on Barrett's work, in the future, concentration correction factors may be applied to long-term predictions from the rapid dispersion model to account for plume dynamics. These concentration correction factors could be calculated based on measured data for each airport (for example, LIDAR measurements) [23] but has been applied in the current work as a constant sensitivity case. Within the overall rapid dispersion process, such

concentration correction factors would be applied before the combination of RDMS results with regional or global-scale results, to avoid overestimating the impacts of aircraft on local-scale $PM_{2.5}$ concentrations. In the current results, an estimated correction factor of 0.6 was applied to the RDC results.

4-3 Estimation of Secondary Sulfate

Currently, the RDMS is limited to modeling long-term average concentrations of ground-level, primary $PM_{2.5}$ species only. Three species are accounted for in this work: primary elemental carbon; primary organic aerosol; and primary sulfates. Although combination of RDMS results with regional and global models would account for secondary $PM_{2.5}$ species, local-scale variations of these secondary species would not be captured in the final results. This variation is especially important for secondary sulfates (SO_4) that result from the emission of sulfur dioxide (SO_2).

Lewis has developed a model for estimating these local variations of secondary sulfate from dispersion models [88]. The model incorporates effects of wet and dry deposition, emissions of primary PM, SO_2, and primary SO_4, and reaction of SO_2 to form SO_4.

$$M_{SO_4} = \frac{3}{2} M_P A(0) \frac{\bar{k}_r}{\bar{k}_r + \bar{k}_d} \left[1 - \exp\left(-\left(\bar{k}_r + \bar{k}_d\right)t\right)\right] + M_P B(0)$$

$$A(0) = \frac{\text{mass emission rate of } SO_2}{\text{mass emission rate of primary fine particles}}$$

$$B(0) = \frac{\text{mass emission rate of primary sulfate, } SO_4}{\text{mass emission rate of primary fine particles}}$$

t	Time after emission from source, h *
M_P	Concentration at time t of primary fine aerosol, $\mu g/m^3$ *
M_{SO_2}	Concentration at time t of SO_2, $\mu g/m^3$ *
M_{SO_4}	Concentration at time t of total sulfate (primary and secondary), $\mu g/m^3$ *
$\bar{k}_r$	Pseudo first-order reaction rate at time t for $SO_2 \rightarrow$ sulfate, $\sim 1\%/h$
$\bar{k}_d$	Additional deposition loss rate at time t for SO_2, $\sim 2\%/h$
* time can be estimated for a particular receptor as wind speed/distance	

Equation 9. Model for calculating concentrations of secondary sulfate from Lewis [88].

In an application of this model to near-airport long-term concentrations of secondary sulfate using RDMS, known quantities include the emissions rates of primary particles, SO_2, and SO_4 and concentrations of primary PM at the receptor points. The time for transformation of SO_2 to SO_4 can be estimated for a particular receptor as wind speed/distance, although a methodology

for applying this estimate to receptors in a two-dimensional grid would need to be developed. After this is developed, the mass of secondary sulfate can be estimated at individual receptor points and added to the local-scale $PM_{2.5}$ total. These results could be combined with regional and global-scale results to calculate exposure and health impacts accounting for local-scale variations of sulfate.

4-4 Global Analysis

In this work, local-scale results from RDMS were combined with regional-scale results from the CMAQ model to obtain both local-scale and regional-scale exposure and health impacts of aviation-attributable $PM_{2.5}$ for the United States only. Future work will apply the RDMS to airports worldwide, enabling assessment of local-scale impacts of airports worldwide.

Figure 33 illustrates data sources developed for this work for using RDMS to calculate local-scale concentrations and health impacts. In addition to these data sources, to calculate health impacts, disease statistics are needed depending on the concentration-response function used. Data used for this work are listed by name as examples of the types of data generally needed for RDMS.

As shown in Figure 33, most current data sources (except taxiway data) have worldwide coverage. The RDMS in its current state of development is capable of obtaining the necessary airport-specific data and calculating local-scale health impacts for airports worldwide, provided that airports possess a unique, four-letter ICAO designation and only runway area sources are considered. Specification of taxiway sources currently requires manual processing of airport diagrams. Although this was done for a set of 191 airports, the manual determination of taxiway sources is impractical for analyses of thousands of airports worldwide.

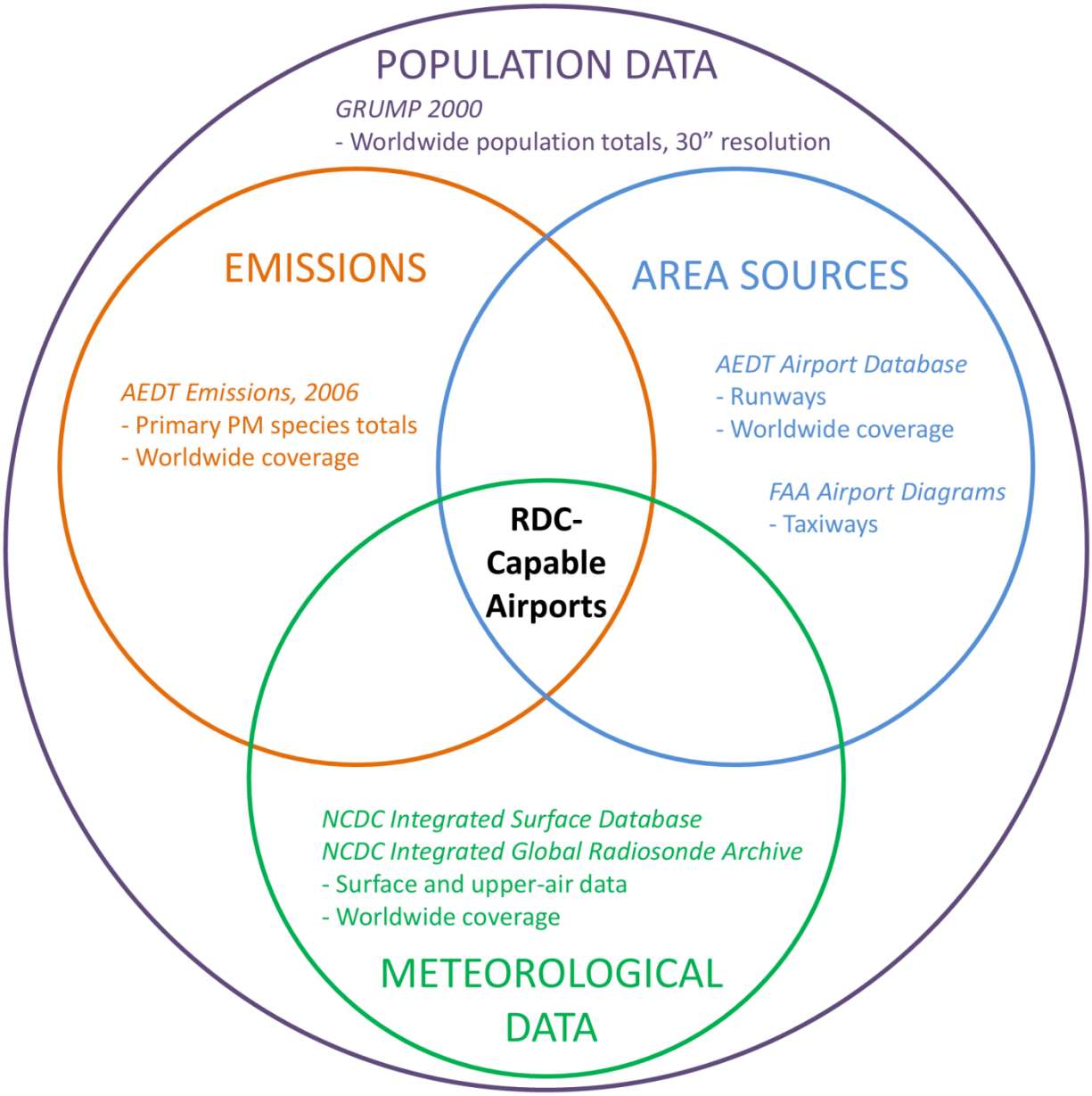

Figure 33. Data required for calculating local-scale concentrations and health impacts using the rapid dispersion calculation.

For global analyses, taxiways may be approximated as a single area source if local-scale concentrations and health impacts results do not change significantly with and without more detailed taxiway representation. Alternatively, taxiway emissions could be assigned to the runway area sources. To determine the validity of either of these approaches, the current results for the United States could be compared with results using these approximations before analyses are conducted worldwide.

Bibliography

[1] International Civil Aviation Organization, "Economic Contribution of Civil Aviation: Ripples of Prosperity," Montreal, Quebec, Canada, 2002.

[2] International Civil Aviation Organization, "ICAO Environmental Report: Aviation and Climate Change," Montreal, Quebec, Canada, 2010.

[3] Environmental Protection Agency, "Air Pollution Control Orientation Course - Effects of Air Pollutants - Health Effects," 2010. [Online]. Available: http://www.epa.gov/apti/course422/ap7a.html. [Accessed: 07-Jun-2012].

[4] C. A. Pope III and D. W. Dockery, "Health effects of Fine Particulate Air Pollution: Lines that Connect," *Journal of the Air & Waste Management Association*, vol. 56, pp. 709–742, 2006.

[5] World Health Organization, "WHO Air quality guidelines for particulate matter, ozone, nitrogen dioxide and sulfur dioxide: Global update 2005 Summary of Risk Assessment," 2005.

[6] J. I. Levy, M. Woody, B. H. Baek, U. Shankar, and S. Arunachalam, "Current and future particulate-matter-related mortality risks in the United States from aviation emissions during landing and takeoff.," *Risk Analysis*, vol. 32, no. 2, pp. 237–49, Feb. 2012.

[7] S. R. H. Barrett, R. E. Britter, and I. A. Waitz, "Global Mortality Attributable to Aircraft Cruise Emissions," *Environmental Science & Technology*, vol. 44, no. 19, pp. 7736–42, Oct. 2010.

[8] S. H. L. Yim and S. R. H. Barrett, "Public Health Impacts of Combustion Emissions in the United Kingdom," *Environmental Science & Technology*, vol. 46, no. 8, pp. 4291–6, Apr. 2012.

[9] Environmental Protection Agency, "Air Pollution Control Orientation Course - Criteria Pollutants," 2010. [Online]. Available: http://www.epa.gov/oar/oaqps/eog/course422/ap5.html. [Accessed: 07-Jun-2012].

[10] M. L. Bell, F. Dominici, K. Ebisu, S. L. Zeger, and J. M. Samet, "Spatial and Temporal Variation in PM2.5 Chemical Composition in the United States for Health Effects Studies," *Environmental Health Perspectives*, vol. 115, no. 7, pp. 989–95, Jul. 2007.

[11] Environmental Protection Agency, "The Particle Pollution Report: Current Understanding of Air Quality and Emissions through 2003," 2004.

[12] Federal Aviation Administration, “Emissions and Dispersion Modeling System (EDMS),” 2010. [Online]. Available: http://www.faa.gov/about/office_org/headquarters_offices/apl/research/models/edms_model/. [Accessed: 07-Jun-2012].

[13] Flughafen Zurich AG, “Air Quality Assessment Sensitivities - Zurich Airport Case Study,” Zurich, 2009.

[14] International Civil Aviation Organization, “ICAO Aircraft Engine Emissions Databank - Introduction,” 2012. [Online]. Available: http://easa.europa.eu/environment/edb/introduction.php. [Accessed: 07-Jun-2012].

[15] M. E. J. Stettler, S. Eastham, and S. R. H. Barrett, “Air quality and public health impacts of UK airports. Part I: Emissions,” *Atmospheric Environment*, vol. 45, no. 31, pp. 5415–5424, Oct. 2011.

[16] K. Schafer, “Remote measurement of the plume shape of aircraft exhausts at airports by passive FTIR spectrometry,” in *Proceedings of SPIE*, 2004, vol. 5270, pp. 189–198.

[17] G. R. Johnson, M. Mazaheri, Z. D. Ristovski, and L. Morawska, “A Plume Capture Technique for the Remote Characterization of Aircraft Engine Emissions,” *Environmental Science & Technology*, vol. 42, no. 13, pp. 4850–6, Jul. 2008.

[18] S. C. Herndon, T. B. Onasch, B. P. Frank, L. C. Marr, J. T. Jayne, M. R. Canagaratna, J. Grygas, T. Lanni, B. E. Anderson, D. Worsnop, and R. C. Miake-Lye, “Particulate Emissions from in-use Commercial Aircraft,” *Aerosol Science and Technology*, vol. 39, no. 8, pp. 799–809, Aug. 2005.

[19] S. C. Herndon, J. H. Shorter, M. S. Zahniser, D. D. Nelson, J. Jayne, R. C. Brown, R. C. Miake-Lye, I. Waitz, P. Silva, T. Lanni, K. Demerjian, and C. E. Kolb, “NO and NO2 Emission Ratios Measured from In-Use Commercial Aircraft during Taxi and Takeoff,” *Environmental Science & Technology*, vol. 38, no. 22, pp. 6078–84, Nov. 2004.

[20] G. Schürmann, K. Schäfer, C. Jahn, H. Hoffmann, M. Bauerfeind, E. Fleuti, and B. Rappenglück, “The impact of NOx, CO and VOC emissions on the air quality of Zurich airport,” *Atmospheric Environment*, vol. 41, no. 1, pp. 103–118, Jan. 2007.

[21] C. G. Moniruzzaman and F. Yu, “A 0D aircraft engine emission model with detailed chemistry and soot microphysics,” *Combustion and Flame*, vol. 159, no. 4, pp. 1670–1686, Apr. 2012.

[22] S. G. Perry, A. J. Cimorelli, R. J. J. Paine, R. W. Brode, J. C. Weil, A. Venkatram, R. B. Wilson, R. F. Lee, and W. D. Peters, “AERMOD: A Dispersion Model for Industrial Source Applications. Part II: Model Performance against 17 Field Study Databases,” *Journal of Applied Meteorology*, vol. 44, no. 5, pp. 694–708, May 2005.

[23] S. R. H. Barrett, R. E. Britter, and I. A. Waitz, “The impact of aircraft plume dynamics on airport local air quality,” no. August, 2012.

[24] P. F. Vohralik, L. K. Randeniya, I. C. Plumb, and S. L. Baughcum, “Effect of plume processes on aircraft impact,” *Journal of Geophysical Research*, vol. 113, no. D05312, Mar. 2008.

[25] A. Kraabol, F. Flatoy, and F. Stordal, “Impact of NOx emissions from subsonic aircraft: Inclusion of plume processes in a three-dimensional model covering Europe, North America, and the North Atlantic,” *Journal of Geophysical Research*, vol. 105, no. D3, pp. 3573–3581, 2000.

[26] M. Bennett, S. Christie, A. Graham, and D. Raper, “Lidar Observations of Aircraft Exhaust Plumes,” *Journal of Atmospheric and Oceanic Technology*, vol. 27, no. 10, pp. 1638–1651, Oct. 2010.

[27] J. Wu and S. Menon, “Aerosol Dynamics in the Near Field of Engine Exhaust Plumes,” *Journal of Applied Meteorology*, vol. 40, pp. 795–809, 2001.

[28] H.-W. Wong, P. E. Yelvington, M. T. Timko, T. B. Onasch, R. C. Miake-Lye, J. Zhang, and I. A. Waitz, “Microphysical Modeling of Ground-Level Aircraft-Emitted Aerosol Formation: Roles of Sulfur-Containing Species,” *Journal of Propulsion and Power*, vol. 24, no. 3, pp. 590–602, May 2008.

[29] Environmental Protection Agency, “The Ambient Air Monitoring Program.” [Online]. Available: http://www.epa.gov/air/oaqps/qa/monprog.html. [Accessed: 07-Jun-2012].

[30] “Nitrogen Dioxide Monitoring - Nitrogen Dioxide Monitoring Map.” [Online]. Available: http://www.massport.com/environment/environmental_reporting/PublishingImages/EDR Charts/Figure 7-9_07_EDR_Air_Quality.pdf. [Accessed: 07-Jun-2012].

[31] Los Angeles World Airports, “LAX Air Quality and Source Apportionment Study,” 2012. [Online]. Available: http://www.lawa.org/welcome_LAX.aspx?id=1060. [Accessed: 07-Jun-2012].

[32] Massport, “Nitrogen Dioxide Monitoring: Tracking Air Quality Changes at Boston Logan,” 2010. [Online]. Available: http://www.massport.com/environment/environmental_reporting/Air Quality/NitrogenDioxideMonitoring.aspx. [Accessed: 07-Jun-2012].

[33] Flughafen Zurich AG, “Zurich Airport - Air Quality,” 2010. [Online]. Available: http://www.zurich-airport.com/desktopdefault.aspx/tabid-580/. [Accessed: 07-Jun-2012].

[34] S. Hu, S. Fruin, K. Kozawa, S. Mara, A. M. Winer, and S. E. Paulson, "Aircraft Emission Impacts in a Neighborhood Adjacent to a General Aviation Airport in Southern California," *Environmental Science & Technology*, vol. 43, no. 21, pp. 8039–45, Nov. 2009.

[35] E. Carr, M. Lee, K. Marin, C. Holder, M. Hoyer, M. Pedde, R. Cook, and J. Touma, "Development and evaluation of an air quality modeling approach to assess near-field impacts of lead emissions from piston-engine aircraft operating on leaded aviation gasoline," *Atmospheric Environment*, vol. 45, no. 32, pp. 5795–5804, Oct. 2011.

[36] D. Westerdahl, S. Fruin, P. Fine, and C. Sioutas, "The Los Angeles International Airport as a source of ultrafine particles and other pollutants to nearby communities," *Atmospheric Environment*, vol. 42, no. 13, pp. 3143–3155, Apr. 2008.

[37] Y. Zhu, E. Fanning, R. C. Yu, Q. Zhang, and J. R. Froines, "Aircraft emissions and local air quality impacts from takeoff activities at a large International Airport," *Atmospheric Environment*, vol. 45, no. 36, pp. 6526–6533, Nov. 2011.

[38] H.-H. Hsu, G. Adamkiewicz, E. Andres Houseman, J. Vallarino, S. J. Melly, R. L. Wayson, J. D. Spengler, and J. I. Levy, "The relationship between aviation activities and ultrafine particulate matter concentrations near a mid-sized airport," *Atmospheric Environment*, vol. 50, pp. 328–337, Apr. 2012.

[39] R. E. Dodson, E. Andres Houseman, B. Morin, and J. I. Levy, "An analysis of continuous black carbon concentrations in proximity to an airport and major roadways," *Atmospheric Environment*, vol. 43, no. 24, pp. 3764–3773, Aug. 2009.

[40] M. Viana, T. a. J. Kuhlbusch, X. Querol, a. Alastuey, R. M. Harrison, P. K. Hopke, W. Winiwarter, M. Vallius, S. Szidat, a. S. H. Prévôt, C. Hueglin, H. Bloemen, P. Wåhlin, R. Vecchi, a. I. Miranda, a. Kasper-Giebl, W. Maenhaut, and R. Hitzenberger, "Source apportionment of particulate matter in Europe: A review of methods and results," *Journal of Aerosol Science*, vol. 39, no. 10, pp. 827–849, Oct. 2008.

[41] K. . Yu, Y. . Cheung, T. Cheung, and R. C. Henry, "Identifying the impact of large urban airports on local air quality by nonparametric regression," *Atmospheric Environment*, vol. 38, no. 27, pp. 4501–4507, Sep. 2004.

[42] UK Department for Transport, "Project for the Sustainable Development of Heathrow: Chapter 4 - Dispersion Modelling," 2007.

[43] G. Schürmann, K. Schäfer, and S. Emeis, "Apportionment of emission source strengths using optical remote sensing and dispersion modeling," in *Proceedings of SPIE*, 2004, vol. 5571, no. 5571, pp. 433–440.

[44] S. K. Das and P. A. Durbin, “Prediction of atmospheric dispersion of pollutants in an airport environment,” *Atmospheric Environment*, vol. 41, no. 6, pp. 1328–1341, Feb. 2007.

[45] J. Koo, “Adjoint Sensitivity Analysis of the Intercontinental Impacts of Aviation Emissions on Air Quality and Health,” Massachusetts Institute of Technology, 2011.

[46] Environmental Protection Agency, “Addendum: User’s Guide for the AMS/EPA Regulatory Model - AERMOD.” Environmental Protection Agency, 2012.

[47] N. S. Holmes and L. Morawska, “A review of dispersion modelling and its application to the dispersion of particles: An overview of different dispersion models available,” *Atmospheric Environment*, vol. 40, no. 30, pp. 5902–5928, Sep. 2006.

[48] European Topic Centre on Air and Climate Change, “Whole model’s catalogue.” [Online]. Available: http://pandora.meng.auth.gr/mds/strquery.php?wholedb. [Accessed: 07-Jun-2012].

[49] Cambridge Environmental Research Consultants, “ADMS-Airport,” 2012. [Online]. Available: http://www.cerc.co.uk/environmental-software/ADMS-Airport-model.html. [Accessed: 07-Jun-2012].

[50] M. Beychok, “Gaussian Plume,” 2007. [Online]. Available: http://commons.wikimedia.org/wiki/File:Gaussian_Plume_(SVG).svg. [Accessed: 07-Jun-2012].

[51] D. Carruthers, C. McHugh, M. Jackson, and K. Johnson, “Developments in ADMS-Airport to take account of near field dispersion and applications to Heathrow Airport,” in *Proceedings of the 11th International Conference on Harmonisation within Atmospheric Dispersion Modelling for Regulatory Purposes*, 2007, pp. 346–350.

[52] CMAS Center UNC Chapel Hill, “CMAQ Overview.” [Online]. Available: http://www.cmaq-model.org/index.php/cmaqoverview. [Accessed: 07-Jun-2012].

[53] M. Woody, B. Haeng Baek, Z. Adelman, M. Omary, Y. Fat Lam, J. Jason West, and S. Arunachalam, “An assessment of Aviation’s contribution to current and future fine particulate matter in the United States,” *Atmospheric Environment*, vol. 45, no. 20, pp. 3424–3433, Jun. 2011.

[54] A. Unal, Y. Hu, M. E. Chang, M. Talat Odman, and A. G. Russell, “Airport related emissions and impacts on air quality: Application to the Atlanta International Airport,” *Atmospheric Environment*, vol. 39, no. 32, pp. 5787–5798, Oct. 2005.

[55] Harvard Atmospheric Chemistry Modeling Group, “GEOS-Chem Overview,” 2011. [Online]. Available: http://acmg.seas.harvard.edu/geos/geos_overview.html. [Accessed: 07-Jun-2012].

[56] E. M. Leibensperger, L. J. Mickley, D. J. Jacob, and S. R. H. Barrett, “Intercontinental influence of NOx and CO emissions on particulate matter air quality,” *Atmospheric Environment*, vol. 45, no. 19, pp. 3318–3324, Jun. 2011.

[57] National Center for Atmospheric Research, “GCTM: Global Chemistry Transport Modeling,” 2012. [Online]. Available: http://www.acd.ucar.edu/gctm/.

[58] University of Leeds School of Earth and Environment, “The TOMCAT/SLIMCAT off-line 3D Chemical Transport Model,” 2012. [Online]. Available: http://homepages.see.leeds.ac.uk/~lecmc/slimcat.html.

[59] Janicke Consulting, “LASPORT: A program system for the calculation of airport-related pollutant emissions and concentrations in the lower atmosphere,” 2011. [Online]. Available: http://www.janicke.de/data/lasport/lasport-2.0.pdf.

[60] EUROCONTROL, “Airport Local Air Quality Studies (ALAQS),” 2006. [Online]. Available: http://www.eurocontrol.int/eec/public/standard_page/SEE_alaqs.html. [Accessed: 07-Jun-2012].

[61] H. A. Gray and G. R. Cass, “Source Contributions to Atmospheric Fine Carbon Particle Concentrations,” *Atmospheric Environment*, vol. 32, no. 22, pp. 3805–3825, 1998.

[62] J. H. Seinfeld and S. N. Pandis, “1.7 Spatial and Temporal Scales of Atmospheric Processes,” in *Atmospheric Chemistry and Physics - From Air Pollution to Climate Change (2nd Edition)*, 2nd ed., Hoboken: John Wiley & Sons, Inc., 2006, pp. 18–19.

[63] A. Riddle, D. Carruthers, A. Sharpe, C. McHugh, and J. Stocker, “Comparisons between FLUENT and ADMS for atmospheric dispersion modelling,” *Atmospheric Environment*, vol. 38, no. 7, pp. 1029–1038, Mar. 2004.

[64] National Oceanic and Atmospheric Administration, “Integrated Global Radiosonde Archive,” 2008. [Online]. Available: http://www.ncdc.noaa.gov/oa/climate/igra/. [Accessed: 07-Jun-2012].

[65] S. Barrett and R. Britter, “A Simple Approach for Rapid Operational Air Quality Modelling at Airports,” *Paper for 11th International Conference on Harmonisation within Atmospheric Dispersion Modelling for Regulatory Purposes*, 2007.

[66] S. R. H. Barrett and R. E. Britter, “Algorithms and analytical solutions for rapidly approximating long-term dispersion from line and area sources,” *Atmospheric Environment*, vol. 43, no. 20, pp. 3249–3258, Jun. 2009.

[67] S. R. H. Barrett and R. E. Britter, “Development of algorithms and approximations for rapid operational air quality modelling,” *Atmospheric Environment*, vol. 42, no. 34, pp. 8105–8111, Nov. 2008.

[68] K. Calder, "Multiple-Source Plume Models of Urban Air Pollution—Their General Structure," *Atmospheric Environment*, vol. 11, no. 5, pp. 403–414, 1977.

[69] National Oceanic and Atmospheric Administration, "Integrated Surface Database," 2008. [Online]. Available: http://www.ncdc.noaa.gov/oa/climate/isd/index.php.

[70] National Center for Atmospheric Research, "The Weather Research & Forecasting Model," 2012. [Online]. Available: http://www.wrf-model.org/index.php.

[71] National Center for Atmospheric Research, "MM5 Community Model Homepage," 2008. [Online]. Available: http://www.mmm.ucar.edu/mm5/.

[72] V. Isakov, A. Venkatram, J. S. Touma, D. Koračin, and T. L. Otte, "Evaluating the use of outputs from comprehensive meteorological models in air quality modeling applications," *Atmospheric Environment*, vol. 41, no. 8, pp. 1689–1705, Mar. 2007.

[73] A. P. Kesarkar, M. Dalvi, A. Kaginalkar, and A. Ojha, "Coupling of the Weather Research and Forecasting Model with AERMOD for pollutant dispersion modeling. A case study for PM10 dispersion over Pune, India," *Atmospheric Environment*, vol. 41, no. 9, pp. 1976–1988, Mar. 2007.

[74] S. R. Hanna, G. A. Briggs, and R. P. Hosker Jr., "Handbook on Atmospheric Diffusion." Department of Energy, Springfield, 1982.

[75] "AEDT Database Description Document - Airport Database," 2011.

[76] I. The MathWorks, "Mapping Toolbox - MATLAB," 2012. [Online]. Available: http://www.mathworks.com/products/mapping/.

[77] Federal Aviation Administration, "FAA Airport Diagrams," 2010. [Online]. Available: https://www.faa.gov/airports/runway_safety/diagrams/.

[78] "Inkscape," 2012. [Online]. Available: http://www.inkscape.org.

[79] Google Inc, "Keyhole Markup Language - Google Developers," 2012. [Online]. Available: https://developers.google.com/kml/.

[80] P. Lee and T. Nagao, "Hierarchical Description of Two Dimensional Shapes Using a Genetic Algorithm," in *Proceedings of 1995 IEEE International Conference on Evolutionary Computation*, 1995, vol. 2.

[81] S. Barrett, M. Prather, J. Penner, H. Selkirk, A. Dopelheuer, G. Fleming, M. Gupta, R. Halthore, J. Hileman, M. Jacobson, S. Kuhn, R. Miake-lye, A. Petzold, C. Roof, U. Schumann, I. Waitz, and R. Wayson, "Guidance on the use of AEDT Gridded Aircraft Emissions in Atmospheric Models Federal Aviation Administration," *Technical Report*, pp. 1–13, 2010.

[82] J. I. Hileman, R. W. Stratton, and P. E. Donohoo, "Energy Content and Alternative Jet Fuel Viability," *Journal of Propulsion and Power*, vol. 26, no. 6, pp. 1184–1195, 2010.

[83] Environmental Protection Agency, "40 CFR Part 51: Revision to the Guideline on Air Quality Models: Adoption of a Preferred General Purpose (Flat and Complex Terrain) Dispersion Model and Other Revisions," *Federal Register*, vol. 70, no. 216, pp. 68217–68261, 2005.

[84] Danish Centre for Environment and Energy, "OML: Model Description," 2012. [Online]. Available: http://www.dmu.dk/en/air/models/oml/omlmodeldescription/.

[85] S. R. H. Barrett, S. H. L. Yim, C. K. Gilmore, L. T. Murray, S. R. Kuhn, A. P. K. Tai, R. M. Yantosca, D. W. Byun, F. Ngan, X. Li, J. I. Levy, A. Ashok, J. Koo, H. M. Wong, O. Dessens, S. Balasubramanian, G. G. Fleming, M. N. Pearlson, C. Wollersheim, R. Malina, S. Arunachalam, F. S. Binkowski, E. M. Leibensperger, D. J. Jacob, J. I. Hileman, and I. a Waitz, "Public Health, Climate, and Economic Impacts of Desulfurizing Jet Fuel," *Environmental Science & Technology*, vol. 46, no. 8, pp. 4275–82, Apr. 2012.

[86] V. Isakov, J. S. Irwin, and J. Ching, "Using CMAQ for Exposure Modeling and Characterizing the Subgrid Variability for Exposure Estimates," *Journal of Applied Meteorology and Climatology*, pp. 1354–1371, 2006.

[87] Socioeconomic Data and Applications Center (SEDAC), "Gridded Population of the World - GPW v3," 2012. [Online]. Available: http://sedac.ciesin.columbia.edu/gpw/.

[88] C. W. Lewis and R. K. Stevens, "Hybrid Receptor Model for Secondary Sulfate from an SO2 Point Source," *Atmospheric Environment*, vol. 19, no. 6, pp. 917–924, 1985.

A. Appendices

A-1 Airports Covered

191 U.S. Airports were analyzed for this study, comprising 95% of air passenger traffic in the United States in 2005. Figure 34 shows the 36 km resolution CMAQ modeling domain used for the regional results in this study. Figure 35 shows the locations of the 191 airports throughout the United States. Figure 36 shows which CMAQ grid cells that overlap RDC domains.

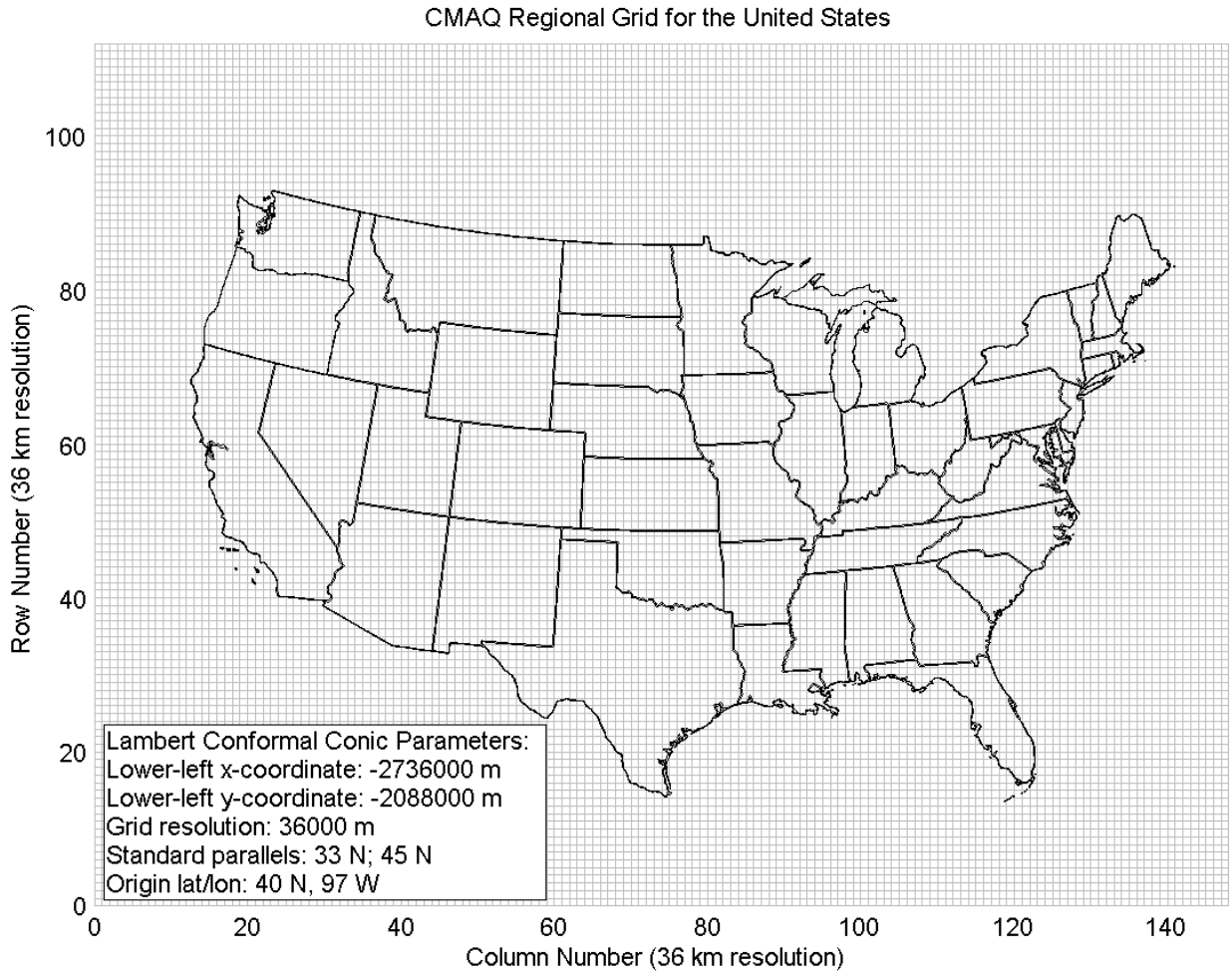

Figure 34. The CMAQ 36 km modeling domain.

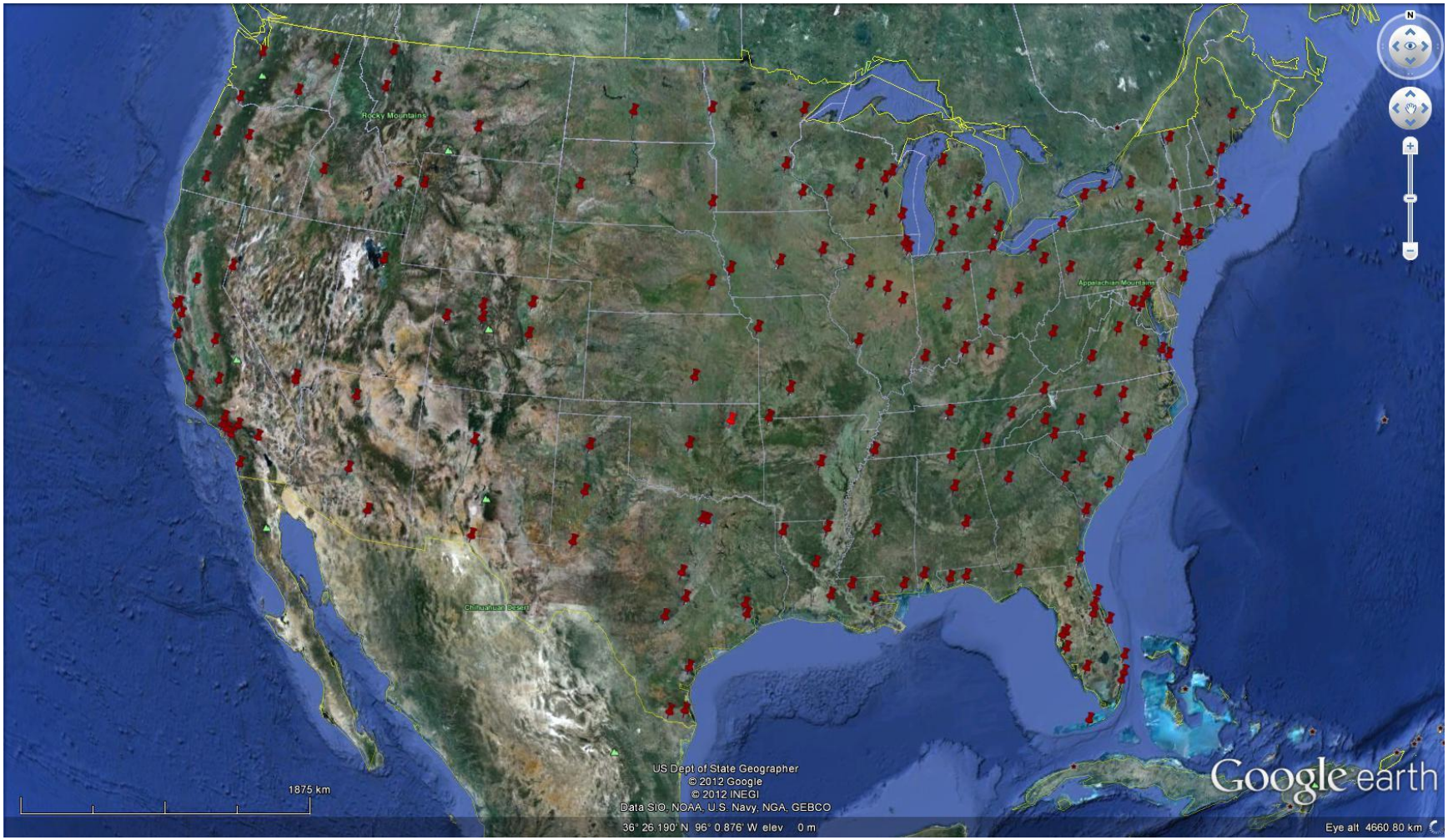

Figure 35. Google Earth™ plot of locations of 191 airports in this study.
Attribution: US Dept of State Geographer; © 2012 Google; © 2012 INEGI; Data SIO, NOAA, U.S. Navy, NGA, GEBCO.

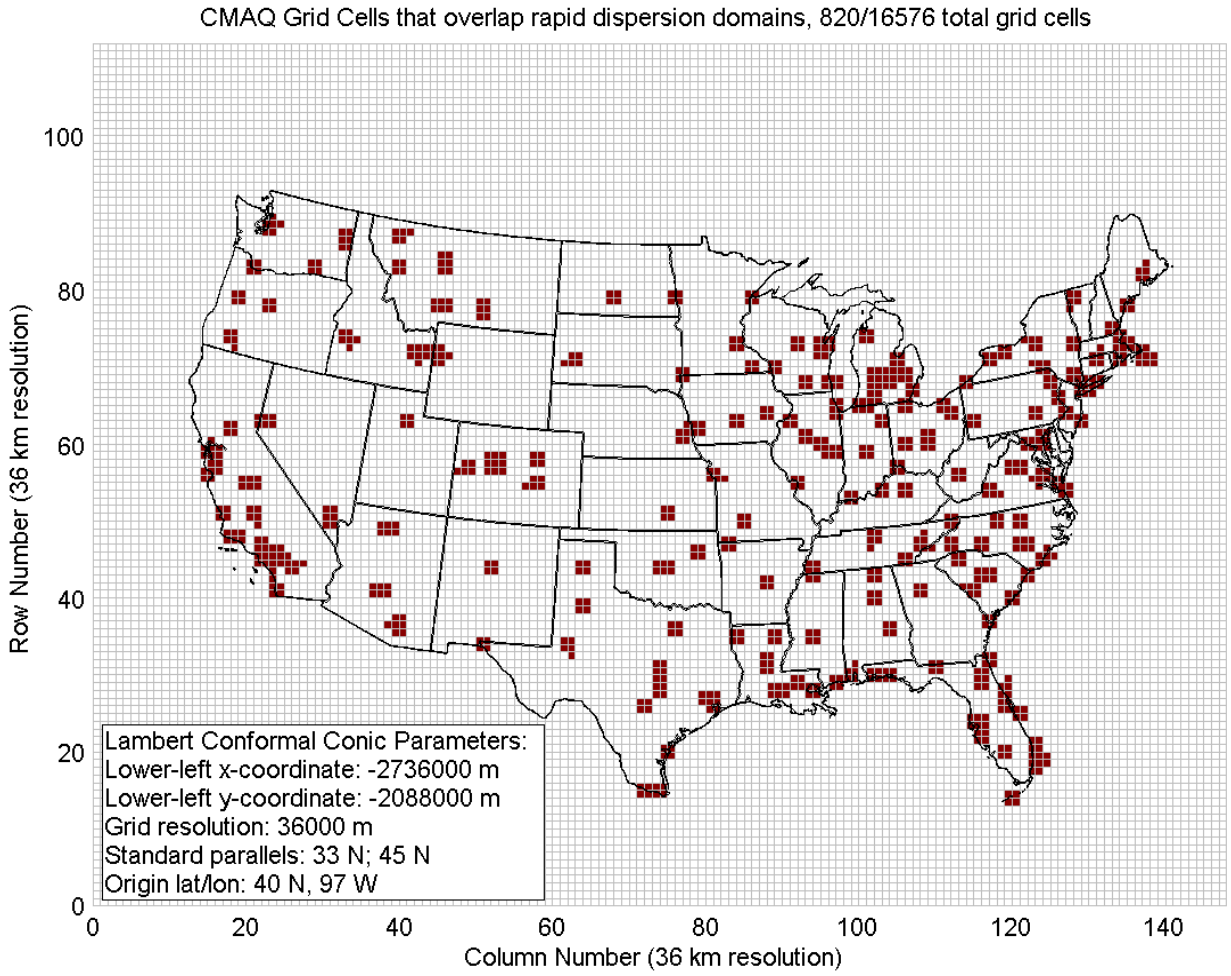

Figure 36. CMAQ grid cells that overlap rapid dispersion domains.
820/16756 grid cells overlap an RDC domain.

A-2 Comparison of RDC to AERMOD

A validation study was performed over 15 U.S. airports to assess the RDC's agreement with an existing dispersion model (AERMOD) and to determine a method of calculating dispersion parameters. Table 16 and Table 17 list different methods considered. These were developed to achieve three goals: 1) agreement between RDC and AERMOD results; 2) removal of erroneous spikes in RDC results; 3) smoothing of RDC results to account for discretized wind directions in AERMOD point-source runs. Agreement between RDC and AERMOD results is discussed in 3-1-1. The presence of erroneous spikes and the use of smoothing are discussed below.

Dispersion Parameter Calculation Method	**Description**
Method A (Default)	Locally-calculated dispersion parameters; No thresholding
Method B	Threshold by derivative of concentration
Method C	Threshold by percent change in concentration
Method D	Dispersion parameters fit over all distances in each direction
Method E	Linear interpolation of dispersion parameter s after finding cutoff distances from derivative of concentration
*All methods were calculated with and without smoothing	

Table 16. Names of dispersion parameter calculation methods compared in validation study.

Common to all methods	Point-source distances	26 logarithmically-spaced distances (more points closer to the center); min = 50m, max = 25,000m
	Point-source directions	360 linearly-spaced distances; North = 0, clockwise positive; min = 1 degree, max = 360 degrees
Thresholding of dispersion parameter values beyond certain distances	By derivative of concentration	Where derivative of concentration with respect to distance $< 1 \frac{\mu g/m^3}{m}$, calculate dispersion parameter based on concentration value at that point to the last distance (25,000m)
	By percent change in concentration	Where % change in concentration with respect to distance $< 50 \frac{\%}{km}$, calculate dispersion parameter based on concentration value at that point to the last distance (25,000m)
	Linear interpolation	Linearly interpolate dispersion parameter s from value at derivative-based cutoffs to value of *s* at farthest distance for which dispersion parameters are calculated (22,249m in logarithmically-spaced distances)*
Smoothing		Gaussian-weighted smoothing of dispersion parameters *A* and *s* over directions only; 16-degree averaging window

Table 17. Description of techniques used for methods named in Table 16.
*Dispersion parameters require two distances to calculate locally. Thus distances where parameters are defined are different from distances for which point-source concentrations are calculated.

A-2-1 Spatial Distribution of Errors and Spikes in RDC Results

Comparison of AERMOD and RDC concentration plots are shown for two airports, Pittsburgh International Airport (KPIT) and Asheville Regional Airport (KAVL). The first showed an agreement with AERMOD within 1% using the metric mean(RDC)/mean(AERMOD), while KAVL RDC results over-predicted AERMOD by 11% using the same metric. Wind roses and AERMOD results are shown for both airports in Figure 37.

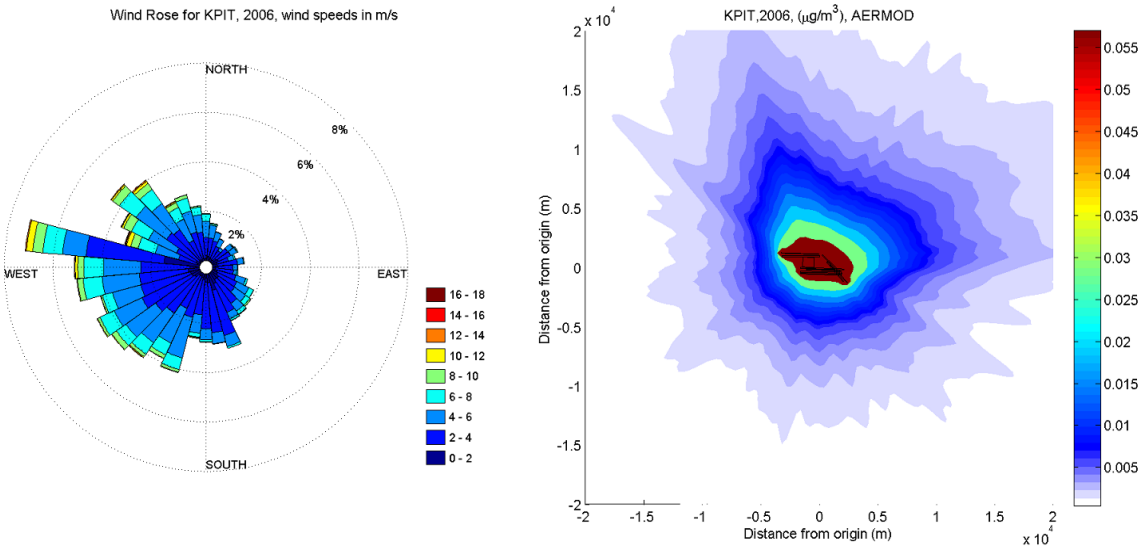

a)

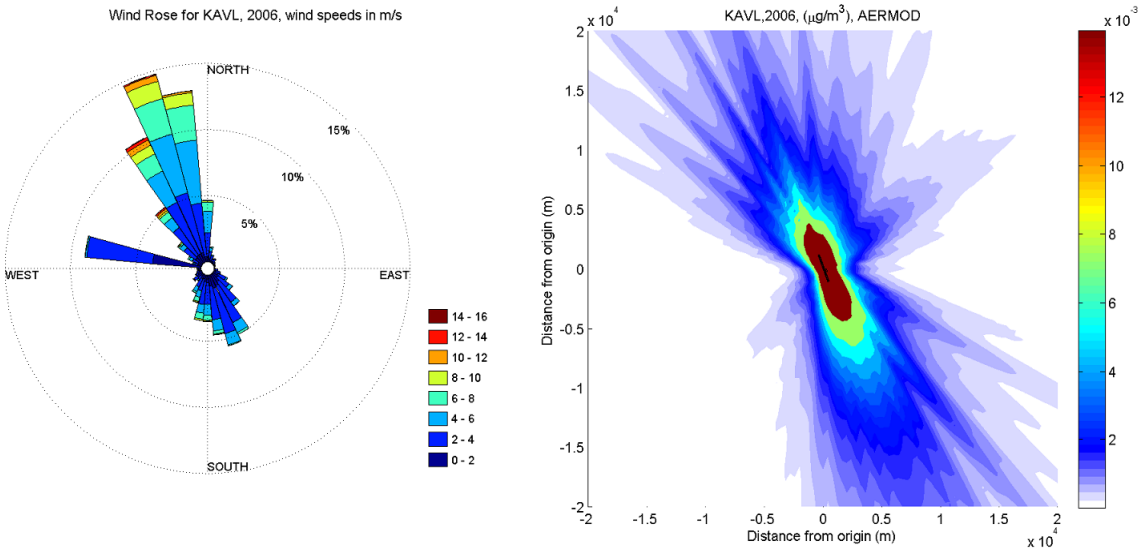

b)

Figure 37. Wind rose and full AERMOD simulation results for
a) Pittsburgh International Airport (KPIT);
b) Asheville Regional Airport (KAVL).

Figure 38 compares AERMOD simulation results for KPIT with RDC results using five different methods of calculating dispersion parameters. For KPIT, the spatial distribution of RDC results visually matches that of AERMOD results, with variations between methods. In contrast, the results for KAVL (Figure 39) show that methods A, C, and E produce spikes in the RDC-predicted concentrations where such spikes are not present in the AERMOD results. Comparison with the wind rose for KAVL shows that these spikes occur in directions with low wind speeds.

In these directions, predicted concentrations at distances away from the point source. are smaller than concentrations at the same distance for directions with larger wind speeds, due to less dispersion in these directions. Concentration values in these directions approach zero, but still decrease with distance due to the dispersion model calculation. Within the point-source simulation, a locally-calculated dispersion parameter s is calculated as follows:

$$s_\theta = \frac{\log\left(c_{1,\theta}/c_{2,\theta}\right)}{\log\left(x_2/x_1\right)} - 1$$

c_1, c_2	Point-source concentration value at locations x_1, x_2
x_1, x_2	Successive distances away from point source, $x_1 < x_2$
θ	To denote that dispersion parameter is calculated at this distance for this direction

Equation 10. Calculation of dispersion parameter *s*.

The denominator is approximately constant for logarithmically-varying distances. Thus, smaller concentration differences will result in smaller values of *s*. Since RDC calculates concentrations away from area sources approximately as a function of inverse distance to a dispersion parameter power ($\chi \sim \frac{A}{x^{s+1}}$), smaller values of *s* at larger distances away *x* will result in larger concentration values.

The different methods of calculating dispersion parameters were developed to address the problem of spikes in RDC-predicted concentrations, especially at far distances for directions with low wind speeds. All of these methods calculate parameters with a power-law curve fit and differ in the choices for points to conduct the fit over. The methods attempt to lessen the effect small changes in concentrations at far distances have on the parameter values. Methods B, C, and E employ a cut-off distance, after which the dispersion parameter is held constant for farther distances away from the point source. Method D employs a different approach by calculating dispersion parameters over all distances in one direction. This implicitly reduces the effect that small changes have on the calculated dispersion parameter by using a least-squares curve fit that will depend more on the large concentration changes closer to the point source.

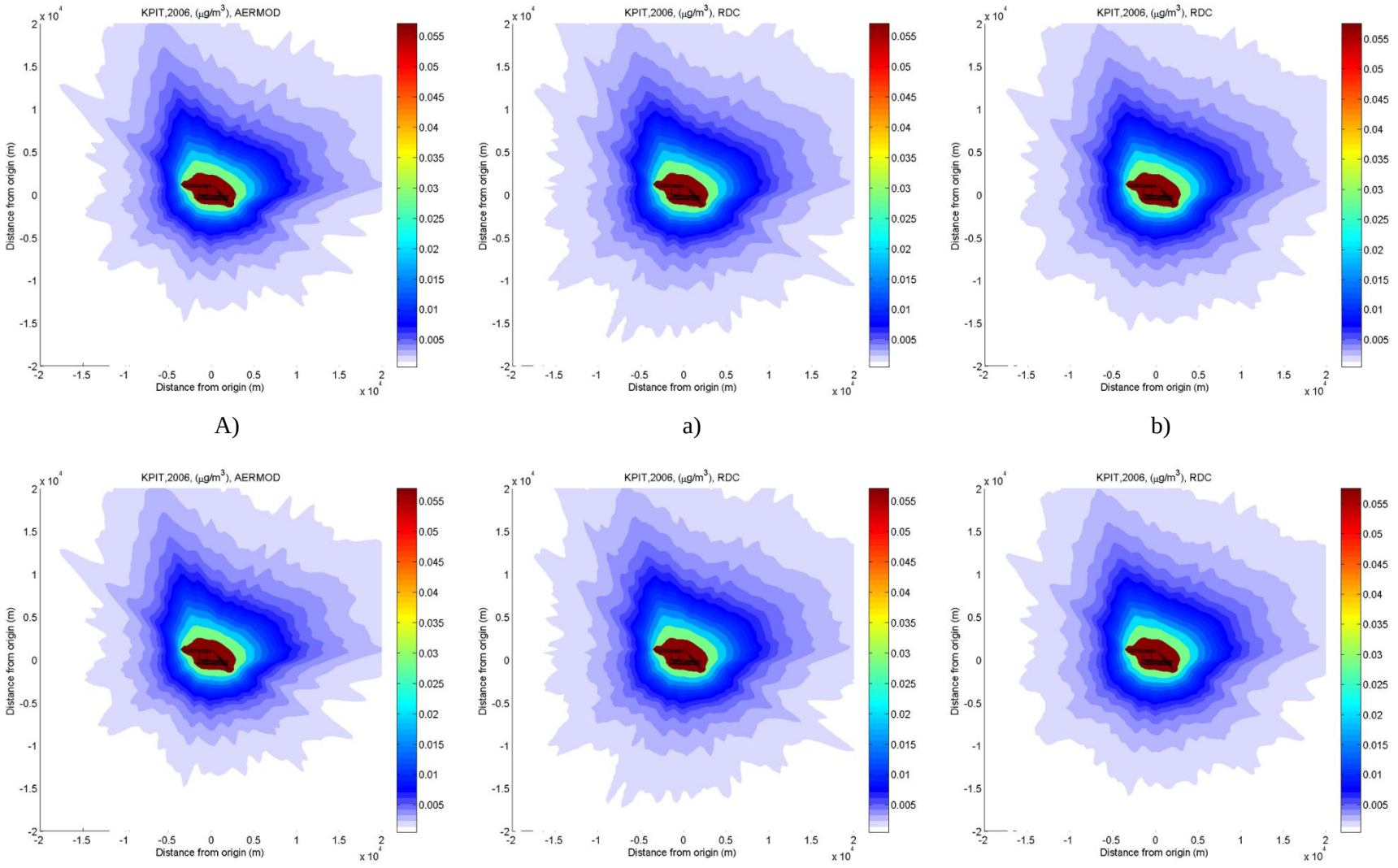

Figure 38. Comparison of full AERMOD simulations with RDC results for KPIT using unsmoothed dispersion parameters. A) AERMOD; a) Method A; b) Method B; c) Method C; d) Method D; e) Method E.

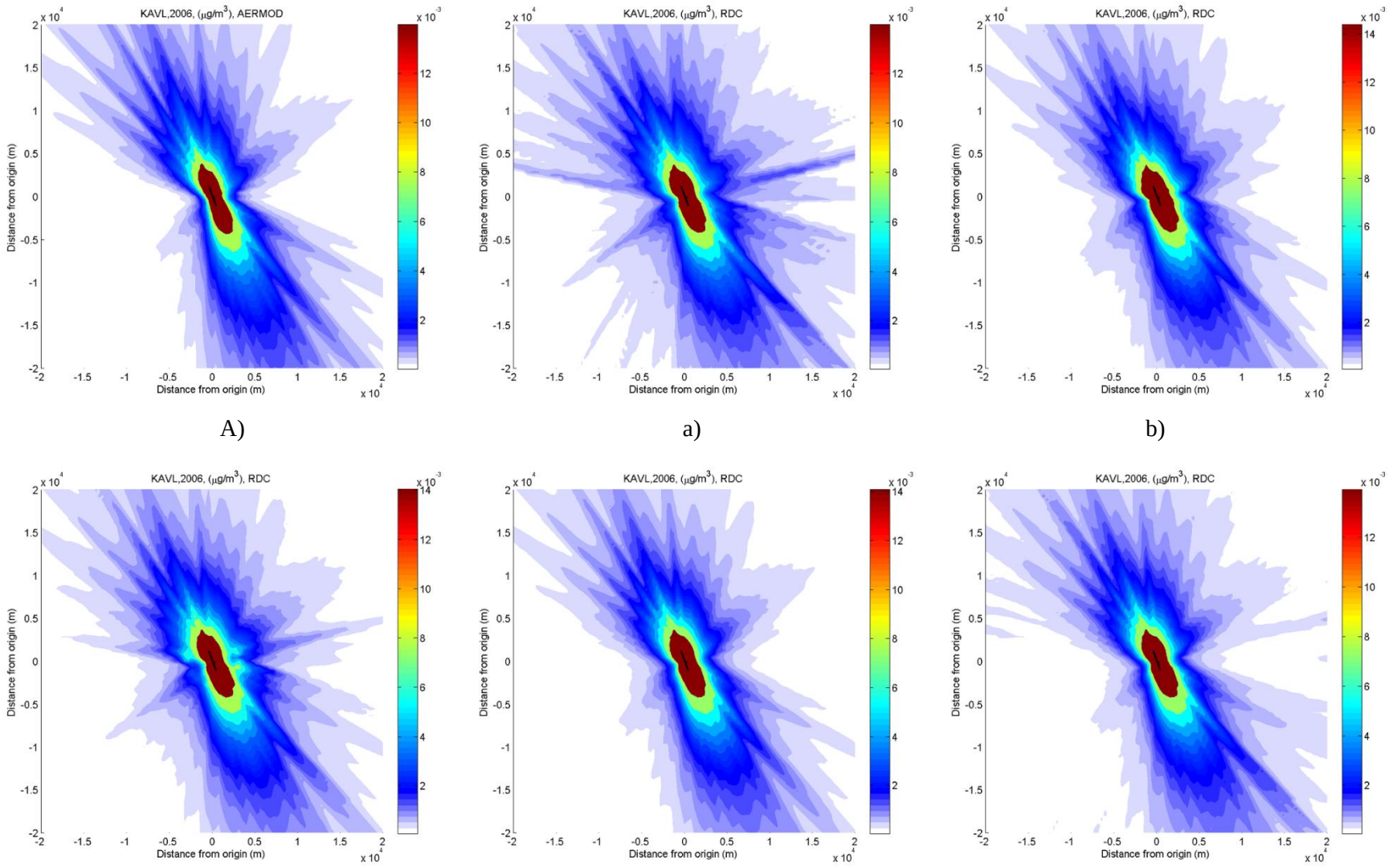

Figure 39. Comparison of full AERMOD simulations with RDC results for KAVL using unsmoothed dispersion parameters. A) AERMOD; a) Method A; b) Method B; c) Method C; d) Method D; e) Method E.

A-2-2 Smoothing

After calculating dispersion parameters at different distances and angles, a smoothing operation is applied to capture some of the smoothing effect of lateral dispersion. As described by Barrett, this can be accomplished by averaging dispersion parameters over angles [66]. In this work, a 17-degree Gaussian averaging window was applied to each direction to smooth the dispersion parameters based on Gaussian plume half-angles from Hanna [74]. In this work, this "pre-smoothing" operation introduced a <1% change in the error mean(RDC)/mean(AERMOD) compared to the unsmoothed results while smoothing out small spikes in the results, as shown in Figure 40 for KPIT.

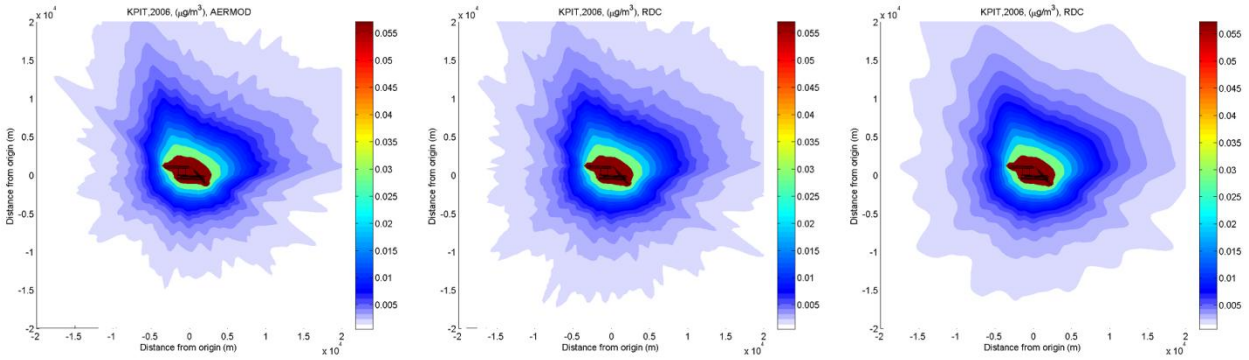

a) b) c)

Figure 40. The effect of smoothing dispersion parameters on RDC results for KPIT.
a) AERMOD results; b) RDC results for unsmoothed dispersion parameters;
c) RDC results for smoothed dispersion parameters. Calculated with Method D.

A-2-3 Agreement between RDC and AERMOD

The differences in errors among different dispersion parameter calculation methods are shown in Table 21, Table 22, and Table 23. The error means and standard deviations in Table 21 and Table 22 are calculated for all receptors over all 15 airports. The values in Table 23 are calculated by taking the mean and standard deviation on the values calculated for each airport, since mean(RDC)/mean(AERMOD) only has one value for each airport.

For the metric RDC/AERMOD over all receptors and airports, RDC on average overestimates AERMOD concentrations by 6-7%. For the metric (RDC-AERMOD)/mean(AERMOD), RDC on average overestimates AERMOD concentrations by 8-9%. For the metric mean(RDC)/mean(AERMOD), RDC on average overestimates AERMOD by 5%.

The error between RDC and AERMOD-predicted concentrations can vary by airport (Table 18, Table 19, Table 20). Nevertheless, for all airports, calculating dispersion parameters over all distances still produces better agreement than other methods of calculating dispersion parameters.

Airport	5th Percentile	Median	95th Percentile	Mean	Std
KAVL	0.761	1.092	3.868	1.532	1.799
KBDL	0.815	0.977	1.459	1.035	0.213
KBGR	0.813	0.970	1.324	1.013	0.163
KCHO	0.743	1.023	1.770	1.106	0.345
KCMI	0.821	0.956	1.147	0.962	0.097
KELP	0.854	0.968	1.134	0.981	0.089
KFAR	0.819	0.959	1.084	0.958	0.085
KGCN	0.789	1.199	2.166	1.324	0.541
KHOU	0.820	0.992	1.331	1.026	0.159
KOMA	0.815	1.052	1.330	1.060	0.167
KPDX	0.811	0.987	1.302	1.012	0.146
KPIT	0.848	0.964	1.115	0.972	0.084
KRNO	0.837	0.993	1.184	1.000	0.110
KRSW	0.838	0.999	1.288	1.023	0.158
KSGF	0.818	0.972	1.185	0.985	0.112
OVERALL MEAN	0.813	1.007	1.512	1.066	0.285

Table 18. Percentile values, means, and standard deviations of receptor ratio error for individual airports.

Airport	5th Percentile	Median	95th Percentile	Mean	Std
KAVL	-0.206	0.013	0.155	0.118	5.431
KBDL	-0.091	-0.006	0.069	0.005	1.188
KBGR	-0.083	-0.007	0.060	-0.008	0.849
KCHO	-0.218	0.005	0.143	0.065	7.894
KCMI	-0.059	-0.013	0.051	-0.003	1.562
KELP	-0.081	-0.009	0.052	-0.012	0.652
KFAR	-0.069	-0.013	0.049	0.004	0.682
KGCN	-0.272	0.020	0.238	0.309	9.970
KHOU	-0.117	-0.002	0.081	-0.002	0.933
KOMA	-0.140	0.007	0.110	0.089	2.157
KPDX	-0.105	-0.003	0.098	0.075	1.682
KPIT	-0.078	-0.010	0.057	-0.010	0.538
KRNO	-0.119	-0.002	0.084	0.020	0.963
KRSW	-0.101	0.000	0.075	0.050	2.633
KSGF	-0.095	-0.007	0.070	0.017	1.753
OVERALL MEAN	-0.122	-0.002	0.093	0.048	2.593

Table 19. Percentile values, means, and standard deviations of receptor percent error relative to mean of AERMOD for individual airports.

Airport	$\textbf{Error} = \frac{\textbf{mean(RDC)}}{\textbf{mean(AERMOD)}}$
KAVL	1.118
KBDL	1.005
KBGR	0.992
KCHO	1.065
KCMI	0.997
KELP	0.988
KFAR	1.004
KGCN	1.309
KHOU	0.998
KOMA	1.089
KPDX	1.075
KPIT	0.990
KRNO	1.020
KRSW	1.050
KSGF	1.017
OVERALL MEAN	1.048
OVERALL STD	0.080

Table 20. Ratio of mean of RDC to mean of AERMOD for individual airports.

A-2-4 Comparison of Time to run AERMOD and RDC

Table 24 shows the time to run AERMOD, RDC, and to calculate dispersion parameters. On average, RDC takes 0.4% of the time to run AERMOD, and calculating dispersion parameters takes 3.9% of the time to run AERMOD.

$\frac{\mathbf{RDC}}{\mathbf{AERMOD}}$	Mean	Std
Method A, without smoothing	1.490	2.042
Method A, with smoothing	1.748	3.842
Method B, without smoothing	1.256	0.900
Method B, with smoothing	1.299	1.120
Method C, without smoothing	1.323	1.233
Method C, with smoothing	1.421	1.962
Method D, without smoothing	1.056	0.457
Method D, with smoothing	1.066	0.530
Method E, without smoothing	1.317	1.481
Method E, with smoothing	1.478	2.910

Table 21. Mean and standard deviation of receptor ratio error over all receptors and airports.

$\frac{\mathbf{RDC - AERMOD}}{\mathbf{mean(AERMOD)}} \times \mathbf{100\%}$	Mean	Std
Method A, without smoothing	49 %	51 %
Method A, with smoothing	75 %	97 %
Method B, without smoothing	25 %	23 %
Method B, with smoothing	30 %	29 %
Method C, without smoothing	32 %	31 %
Method C, with smoothing	42 %	49 %
Method D, without smoothing	8 %	11 %
Method D, with smoothing	9 %	13 %
Method E, without smoothing	32 %	40 %
Method E, with smoothing	48 %	78 %

Table 22. Mean and standard deviation of receptor percent error relative to mean of AERMOD over all airports.

$\frac{\mathbf{mean(RDC)}}{\mathbf{mean(AERMOD)}}$	Mean	Std
Method A, without smoothing	1.199	0.089
Method A, with smoothing	1.217	0.093
Method B, without smoothing	1.185	0.084
Method B, with smoothing	1.189	0.084
Method C, without smoothing	1.187	0.084
Method C, with smoothing	1.195	0.085
Method D, without smoothing	1.050	0.082
Method D, with smoothing	1.048	0.080
Method E, without smoothing	1.165	0.077
Method E, with smoothing	1.175	0.079

Table 23. Mean and standard deviation of ratio of mean of RDC to mean of AERMOD over all airports.

Airport	# of sources	Time to complete AERMOD simulation, seconds	Time to complete RDC calculation	RDC time/ AERMOD time, %	Time to complete dispersion parameter calculation	Dispersion parameter time/ AERMOD time, %
KAVL	3	1220	7	0.57 %	125	10 %
KBDL	7	3478	14	0.40 %	158	4.5 %
KBGR	3	1497	7	0.47 %	152	10 %
KCHO	3	817	6	0.73 %	91	11 %
KCMI	9	4679	17	0.36 %	174	3.7 %
KELP	7	3970	14	0.35 %	160	4.0 %
KFAR	14	6562	25	0.38 %	169	2.6 %
KGCN	2	814	5	0.61 %	118	15 %
KHOU	14	6675	26	0.39 %	154	2.3 %
KOMA	15	7116	28	0.39 %	169	2.4 %
KPDX	8	4227	17	0.40 %	156	3.7 %
KPIT	10	5410	21	0.39 %	150	2.8 %
KRNO	7	2709	15	0.55 %	113	4.2 %
KRSW	4	2381	9	0.38 %	154	6.5 %
KSGF	10	5314	19	0.36 %	170	3.2 %
Total	116	56869	230	0.40 %	2213	3.9 %

Table 24. Comparison of tested performance between AERMOD and rapid dispersion simulations.

A-3 Local-scale Premature Mortality Estimates

Airport	Combined RDC-LTO	Combined RDC-Full-Flight	RDC only, scaled for LTO	RDC only, scaled for Full-Flight	CMAQ only, LTO	CMAQ only, Full-flight	% Change for including local-scale variations, LTO	% Change for including local-scale variations, Full-Flight
KABE	0.16	2.75	0.03	0.03	0.14	2.73	16 %	1 %
KABQ	0.10	0.60	0.05	0.05	0.07	0.57	45 %	5 %
KACK	0.00	0.01	0.00	0.00	0.00	0.01	25 %	2 %
KACY	0.05	0.88	0.02	0.02	0.04	0.87	21 %	1 %
KAEX	0.01	0.24	0.00	0.00	0.01	0.24	1 %	0 %
KAGS	0.07	1.18	0.01	0.01	0.07	1.18	5 %	0 %
KALB	0.12	1.66	0.03	0.03	0.10	1.64	19 %	1 %
KAMA	0.02	0.22	0.00	0.00	0.02	0.22	2 %	0 %
KASE	0.00	0.01	0.00	0.00	0.00	0.01	26 %	3 %
KATL	1.24	5.62	1.19	1.30	1.03	5.40	21 %	4 %
KATW	0.05	0.89	0.00	0.00	0.05	0.88	2 %	0 %
KAUS	0.20	1.33	0.06	0.06	0.15	1.28	28 %	3 %
KAVL	0.05	0.59	0.01	0.01	0.04	0.59	16 %	1 %
KAVP	0.05	1.28	0.00	0.00	0.05	1.27	5 %	0 %
KAZO	0.05	1.05	0.01	0.01	0.05	1.05	10 %	0 %
KBDL	0.14	2.15	0.05	0.05	0.12	2.14	11 %	1 %
KBFL	0.15	0.99	0.01	0.01	0.15	0.98	3 %	1 %
KBGM	0.03	0.64	0.00	0.00	0.03	0.64	0 %	0 %
KBGR	0.01	0.13	0.01	0.01	0.01	0.12	52 %	4 %
KBHM	0.16	2.09	0.06	0.06	0.13	2.06	22 %	1 %
KBIL	0.01	0.08	0.01	0.01	0.01	0.08	84 %	7 %
KBIS	0.01	0.08	0.00	0.00	0.00	0.08	47 %	2 %
KBMI	0.04	0.58	0.00	0.00	0.04	0.58	3 %	0 %
KBNA	0.20	2.64	0.12	0.12	0.20	2.64	0 %	0 %
KBOI	0.07	0.64	0.03	0.03	0.05	0.62	50 %	4 %
KBOS	1.85	8.68	0.57	0.57	1.70	8.52	9 %	2 %
KBTR	0.12	1.67	0.02	0.02	0.11	1.66	10 %	1 %
KBTV	0.03	0.29	0.01	0.01	0.02	0.28	46 %	4 %

Airport	Combined RDC-LTO	Combined RDC-Full-Flight	RDC only, scaled for LTO	RDC only, scaled for Full-Flight	CMAQ only, LTO	CMAQ only, Full-flight	% Change for including local-scale variations, LTO	% Change for including local-scale variations, Full-Flight
KBUR	2.65	10.16	0.72	0.72	2.77	10.27	- 4 %	- 1 %
KBWI	0.61	7.87	0.42	0.42	0.36	7.62	72 %	3 %
KBZN	0.00	0.05	0.00	0.00	0.00	0.05	38 %	2 %
KCAE	0.13	1.65	0.03	0.03	0.11	1.62	21 %	1 %
KCAK	0.19	3.14	0.01	0.01	0.18	3.14	3 %	0 %
KCHA	0.09	1.45	0.01	0.01	0.08	1.44	6 %	0 %
KCHO	0.03	0.53	0.00	0.00	0.02	0.53	5 %	0 %
KCHS	0.09	1.14	0.04	0.04	0.07	1.12	32 %	2 %
KCID	0.05	0.68	0.00	0.00	0.05	0.68	1 %	0 %
KCLE	0.48	5.72	0.13	0.13	0.40	5.64	20 %	1 %
KCLT	0.32	3.23	0.29	0.29	0.29	3.20	11 %	1 %
KCMH	0.45	5.96	0.13	0.13	0.37	5.88	21 %	1 %
KCMI	0.04	0.68	0.00	0.00	0.04	0.68	1 %	0 %
KCOS	0.06	0.48	0.02	0.02	0.05	0.47	11 %	1 %
KCRP	0.03	0.39	0.00	0.00	0.03	0.39	0 %	0 %
KCRW	0.02	0.54	0.00	0.00	0.02	0.54	10 %	0 %
KCVG	0.27	4.12	0.13	0.13	0.27	4.12	1 %	0 %
KCWA	0.01	0.19	0.00	0.00	0.01	0.19	1 %	0 %
KDAB	0.04	0.38	0.01	0.01	0.03	0.37	33 %	3 %
KDAL	0.63	5.61	0.13	0.13	0.73	5.70	- 13 %	- 2 %
KDAY	0.19	2.72	0.02	0.02	0.18	2.72	3 %	0 %
KDCA	0.93	10.96	0.68	0.68	0.76	10.78	23 %	2 %
KDEN	0.10	0.49	0.02	0.02	0.13	0.52	- 21 %	- 5 %
KDFW	0.87	4.31	0.52	0.52	0.74	4.18	17 %	3 %
KDLH	0.01	0.23	0.00	0.00	0.01	0.23	5 %	0 %
KDSM	0.11	1.13	0.02	0.02	0.09	1.11	19 %	2 %
KDTW	0.59	5.85	0.52	0.54	0.55	5.80	8 %	1 %
KEGE	0.00	0.01	0.00	0.00	0.00	0.01	368 %	38 %
KELP	0.14	1.31	0.06	0.06	0.10	1.27	40 %	3 %
KERI	0.03	0.74	0.00	0.00	0.03	0.74	4 %	0 %
KEUG	0.02	0.30	0.00	0.00	0.02	0.30	5 %	0 %

Airport	Combined RDC-LTO	Combined RDC-Full-Flight	RDC only, scaled for LTO	RDC only, scaled for Full-Flight	CMAQ only, LTO	CMAQ only, Full-flight	% Change for including local-scale variations, LTO	% Change for including local-scale variations, Full-Flight
KEWR	6.26	30.73	2.38	2.38	7.12	31.59	- 12 %	- 3 %
KEYW	0.00	0.03	0.00	0.00	0.00	0.03	27 %	3 %
KFAR	0.02	0.23	0.00	0.00	0.02	0.22	16 %	1 %
KFAT	0.37	1.78	0.03	0.03	0.34	1.76	7 %	1 %
KFAY	0.14	1.60	0.00	0.00	0.14	1.60	0 %	0 %
KFLL	0.44	2.42	0.34	0.34	0.69	2.67	- 36 %	- 9 %
KFNT	0.09	1.77	0.01	0.01	0.08	1.77	9 %	0 %
KFSD	0.03	0.32	0.01	0.01	0.02	0.32	27 %	2 %
KFWA	0.09	1.59	0.01	0.01	0.09	1.59	6 %	0 %
KGCN	0.00	0.00	0.00	0.00	0.00	0.00	1 %	0 %
KGEG	0.05	0.45	0.01	0.01	0.05	0.46	- 4 %	0 %
KGJT	0.01	0.10	0.00	0.00	0.01	0.10	16 %	2 %
KGNV	0.03	0.46	0.00	0.00	0.03	0.46	3 %	0 %
KGPI	0.00	0.06	0.00	0.00	0.00	0.06	4 %	0 %
KGPT	0.03	0.39	0.01	0.01	0.02	0.39	20 %	1 %
KGRB	0.05	0.90	0.01	0.01	0.05	0.89	8 %	0 %
KGRK	0.04	0.39	0.00	0.00	0.04	0.39	0 %	0 %
KGRR	0.15	2.57	0.02	0.02	0.15	2.57	- 1 %	0 %
KGSO	0.16	2.15	0.03	0.03	0.15	2.14	11 %	1 %
KGSP	0.09	1.36	0.01	0.01	0.09	1.36	6 %	0 %
KGTF	0.00	0.04	0.00	0.00	0.00	0.04	42 %	3 %
KHOU	0.29	3.65	0.19	0.19	0.32	3.68	- 10 %	- 1 %
KHPN	0.39	4.72	0.06	0.06	0.71	5.04	- 45 %	- 6 %
KHRL	0.02	0.15	0.00	0.00	0.01	0.15	9 %	1 %
KHSV	0.07	0.98	0.00	0.00	0.07	0.98	1 %	0 %
KHYA	0.02	0.22	0.00	0.00	0.02	0.21	5 %	0 %
KIAD	0.37	3.87	0.33	0.33	0.42	3.92	- 13 %	- 1 %
KIAH	0.37	3.12	0.33	0.33	0.41	3.16	- 11 %	- 1 %
KICT	0.09	0.86	0.02	0.02	0.08	0.85	15 %	1 %
KIDA	0.01	0.15	0.00	0.00	0.01	0.15	10 %	1 %
KILM	0.04	0.53	0.01	0.01	0.03	0.52	23 %	2 %

Airport	Combined RDC-LTO	Combined RDC-Full-Flight	RDC only, scaled for LTO	RDC only, scaled for Full-Flight	CMAQ only, LTO	CMAQ only, Full-flight	% Change for including local-scale variations, LTO	% Change for including local-scale variations, Full-Flight
KISP	0.21	3.00	0.02	0.02	0.21	2.99	5 %	0 %
KJAC	0.00	0.01	0.00	0.00	0.00	0.01	20 %	2 %
KJAN	0.07	0.91	0.01	0.01	0.06	0.90	10 %	1 %
KJAX	0.05	0.72	0.02	0.02	0.04	0.71	30 %	2 %
KJFK	8.49	34.63	2.97	2.97	9.65	35.79	- 12 %	- 3 %
KLAN	0.10	1.66	0.01	0.01	0.09	1.65	7 %	0 %
KLAS	1.63	3.38	1.58	2.67	0.82	2.01	100 %	68 %
KLAX	8.68	18.20	5.66	5.66	6.61	16.14	31 %	13 %
KLBB	0.03	0.28	0.00	0.00	0.03	0.28	- 3 %	0 %
KLEX	0.08	1.69	0.01	0.01	0.08	1.68	7 %	0 %
KLFT	0.05	0.69	0.01	0.01	0.04	0.68	15 %	1 %
KLGA	9.45	45.17	3.50	3.50	11.08	46.80	- 15 %	- 3 %
KLGB	5.10	16.82	0.52	0.52	7.61	19.33	- 33 %	- 13 %
KLIT	0.07	0.87	0.01	0.01	0.06	0.86	15 %	1 %
KLNK	0.04	0.52	0.00	0.00	0.04	0.52	1 %	0 %
KLSE	0.03	0.45	0.00	0.00	0.03	0.45	3 %	0 %
KMAF	0.02	0.19	0.00	0.00	0.02	0.19	0 %	0 %
KMBS	0.05	1.23	0.00	0.00	0.05	1.23	3 %	0 %
KMCI	0.10	0.97	0.02	0.02	0.11	0.98	- 8 %	- 1 %
KMCO	0.38	1.84	0.33	0.33	0.25	1.71	52 %	8 %
KMDT	0.17	2.57	0.02	0.02	0.16	2.55	10 %	1 %
KMDW	1.26	16.01	0.69	0.69	1.28	16.04	- 2 %	0 %
KMEM	0.76	3.15	0.68	0.68	0.56	2.96	34 %	6 %
KMFE	0.08	0.90	0.01	0.01	0.08	0.90	5 %	0 %
KMFR	0.01	0.16	0.00	0.00	0.01	0.16	40 %	2 %
KMGM	0.04	0.70	0.00	0.00	0.04	0.69	6 %	0 %
KMHT	0.07	1.01	0.03	0.03	0.05	0.99	38 %	2 %
KMIA	1.35	3.59	1.36	1.36	0.93	3.16	46 %	13 %
KMKE	0.25	3.51	0.13	0.13	0.21	3.47	22 %	1 %
KMLB	0.05	0.39	0.01	0.01	0.04	0.38	10 %	1 %
KMLI	0.08	1.05	0.01	0.01	0.07	1.04	5 %	0 %

Airport	Combined RDC-LTO	Combined RDC-Full-Flight	RDC only, scaled for LTO	RDC only, scaled for Full-Flight	CMAQ only, LTO	CMAQ only, Full-flight	% Change for including local-scale variations, LTO	% Change for including local-scale variations, Full-Flight
KMOB	0.04	0.78	0.01	0.01	0.04	0.78	3 %	0 %
KMRY	0.11	0.78	0.01	0.01	0.10	0.77	10 %	1 %
KMSN	0.10	1.37	0.02	0.02	0.09	1.36	9 %	1 %
KMSO	0.01	0.07	0.00	0.00	0.01	0.07	26 %	2 %
KMSP	0.94	5.58	0.79	0.79	0.79	5.43	19 %	3 %
KMSY	0.18	1.51	0.09	0.09	0.13	1.46	37 %	3 %
KMYR	0.02	0.38	0.00	0.00	0.02	0.38	12 %	1 %
KOAK	1.49	6.94	0.24	0.24	2.07	7.52	- 28 %	- 8 %
KOKC	0.14	1.18	0.02	0.02	0.13	1.17	7 %	1 %
KOMA	0.11	1.37	0.03	0.03	0.10	1.36	12 %	1 %
KONT	1.63	6.14	0.27	0.27	1.59	6.11	2 %	1 %
KORD	2.50	15.64	2.11	2.17	1.69	14.82	48 %	5 %
KORF	0.28	3.26	0.05	0.05	0.26	3.24	6 %	0 %
KPBI	0.24	1.03	0.12	0.12	0.16	0.95	52 %	9 %
KPDX	0.24	2.91	0.14	0.14	0.18	2.85	33 %	2 %
KPHF	0.11	1.51	0.02	0.02	0.11	1.51	0 %	0 %
KPHL	1.63	13.41	1.06	1.06	0.99	12.77	64 %	5 %
KPHX	1.57	4.29	1.32	1.66	1.20	3.77	31 %	14 %
KPIA	0.07	1.08	0.01	0.01	0.07	1.07	6 %	0 %
KPIE	0.23	2.70	0.02	0.02	0.41	2.87	- 43 %	- 6 %
KPIT	0.14	2.43	0.06	0.06	0.11	2.40	25 %	1 %
KPNS	0.05	0.71	0.02	0.02	0.04	0.69	49 %	3 %
KPSC	0.02	0.15	0.00	0.00	0.01	0.15	14 %	1 %
KPSP	0.08	0.31	0.02	0.02	0.06	0.29	23 %	5 %
KPVD	0.19	2.28	0.08	0.08	0.13	2.22	43 %	3 %
KPWM	0.05	0.44	0.02	0.02	0.03	0.42	81 %	5 %
KRAP	0.00	0.06	0.00	0.00	0.00	0.06	4 %	0 %
KRDM	0.00	0.04	0.00	0.00	0.00	0.03	15 %	1 %
KRDU	0.26	3.00	0.05	0.05	0.26	3.00	- 1 %	0 %
KRIC	0.14	2.49	0.03	0.03	0.14	2.49	- 3 %	0 %
KRNO	0.10	0.40	0.09	0.09	0.05	0.35	116 %	16 %

Airport	Combined RDC-LTO	Combined RDC-Full-Flight	RDC only, scaled for LTO	RDC only, scaled for Full-Flight	CMAQ only, LTO	CMAQ only, Full-flight	% Change for including local-scale variations, LTO	% Change for including local-scale variations, Full-Flight
KROC	0.22	2.41	0.11	0.11	0.15	2.34	49 %	3 %
KRST	0.03	0.47	0.00	0.00	0.03	0.47	1 %	0 %
KRSW	0.07	0.48	0.02	0.02	0.07	0.48	5 %	1 %
KSAN	1.64	5.39	0.54	0.54	1.26	5.01	31 %	8 %
KSAT	0.35	2.46	0.13	0.13	0.28	2.39	25 %	3 %
KSAV	0.03	0.50	0.01	0.01	0.03	0.50	2 %	0 %
KSBA	0.06	0.22	0.03	0.03	0.04	0.20	60 %	11 %
KSBN	0.08	1.51	0.01	0.01	0.07	1.51	5 %	0 %
KSBP	0.03	0.17	0.00	0.00	0.03	0.17	4 %	1 %
KSDF	0.43	4.72	0.25	0.25	0.27	4.57	59 %	3 %
KSEA	0.47	2.31	0.46	0.46	0.31	2.15	52 %	8 %
KSFB	0.05	0.99	0.02	0.02	0.11	1.04	- 49 %	- 5 %
KSFO	1.70	5.98	0.49	0.49	1.80	6.08	- 6 %	- 2 %
KSGF	0.05	0.61	0.00	0.00	0.05	0.61	5 %	0 %
KSHV	0.05	0.66	0.01	0.01	0.04	0.65	14 %	1 %
KSJC	1.20	6.22	0.40	0.40	1.04	6.06	15 %	3 %
KSLC	0.29	1.51	0.11	0.11	0.31	1.52	- 5 %	- 1 %
KSMF	0.36	2.52	0.03	0.03	0.37	2.53	- 2 %	0 %
KSNA	2.89	8.92	0.47	0.47	2.86	8.89	1 %	0 %
KSRQ	0.08	0.87	0.01	0.01	0.07	0.86	11 %	1 %
KSTL	0.45	4.79	0.21	0.21	0.35	4.69	27 %	2 %
KSWF	0.05	1.13	0.00	0.00	0.05	1.13	4 %	0 %
KSYR	0.12	1.53	0.03	0.03	0.11	1.51	18 %	1 %
KTLH	0.04	0.57	0.01	0.01	0.04	0.57	8 %	1 %
KTOL	0.11	1.95	0.01	0.01	0.11	1.95	- 1 %	0 %
KTPA	0.41	2.76	0.21	0.21	0.31	2.66	33 %	4 %
KTRI	0.04	0.73	0.00	0.00	0.04	0.73	6 %	0 %
KTUL	0.13	1.22	0.03	0.03	0.12	1.21	7 %	1 %
KTUS	0.13	0.69	0.07	0.07	0.10	0.65	31 %	5 %
KTVC	0.01	0.23	0.00	0.00	0.01	0.23	41 %	1 %
KTYS	0.07	1.20	0.02	0.02	0.08	1.20	- 5 %	0 %

Airport	Combined RDC-LTO	Combined RDC-Full-Flight	RDC only, scaled for LTO	RDC only, scaled for Full-Flight	CMAQ only, LTO	CMAQ only, Full-flight	% Change for including local-scale variations, LTO	% Change for including local-scale variations, Full-Flight
KVPS	0.03	0.28	0.02	0.02	0.02	0.27	86 %	5 %
KXNA	0.05	0.49	0.00	0.00	0.05	0.49	1 %	0 %
TOTAL	88	517	38	40	87	516	16 %	1 %

Table 25. Premature mortality totals for combined, local-scale RDC-CMAQ results, CMAQ-only results, and percent increase from including local-scale variations. With plume factor adjustment.

Percentile Values (%)	Combined RDC-LTO	Combined RDC-Full-Flight	RDC Only, Scaled for LTO	RDC Only, Scaled for Full-Flight
Min	0.0 %	0.0 %	0.0 %	0.0 %
10th	0.02 %	0.03 %	0.0 %	0.0 %
25th	0.04 %	0.09 %	0.01 %	0.01 %
50th	0.10 %	0.21 %	0.05 %	0.04 %
75th	0.31 %	0.52 %	0.30 %	0.26 %
90th	1.2 %	1.1 %	1.4 %	1.3 %
Max	11 %	8.5 %	14 %	14 %
Mean (%)	0.52 %	0.52 %	0.52 %	0.52 %
Std (%)	1.4 %	1.0 %	1.6 %	1.6 %
TOTAL MORTALITIES	88	517	57	66

Table 26. Premature mortality statistics for 191 airports. Percentage of total contributed by airports. Without plume factor adjustment.

Percentile Values (%)	Combined RDC-LTO	Combined RDC-Full-Flight	RDC Only, Scaled for LTO	RDC Only, Scaled for Full-Flight
Min	0.0 %	0.0 %	0.0 %	0.0 %
10th	0.01 %	0.03 %	0.0 %	0.0 %
25th	0.04 %	0.09 %	0.01 %	0.01 %
50th	0.10 %	0.21 %	0.04 %	0.04 %
75th	0.30 %	0.52 %	0.26 %	0.25 %
90th	1.4 %	1.1 %	1.4 %	1.3 %
Max	11 %	8.7 %	15 %	14 %
Mean (%)	0.52 %	0.52 %	0.52 %	0.52 %
Std (%)	1.5 %	1.0 %	1.6 %	1.6 %
TOTAL MORTALITIES	88	517	38	40

Table 27. Premature mortality statistics for 191 airports. Percentage of total contributed by individual airports. With plume factor adjustment.

A-4 Additional Results for Five Major Airports

A-4-1 Area Sources

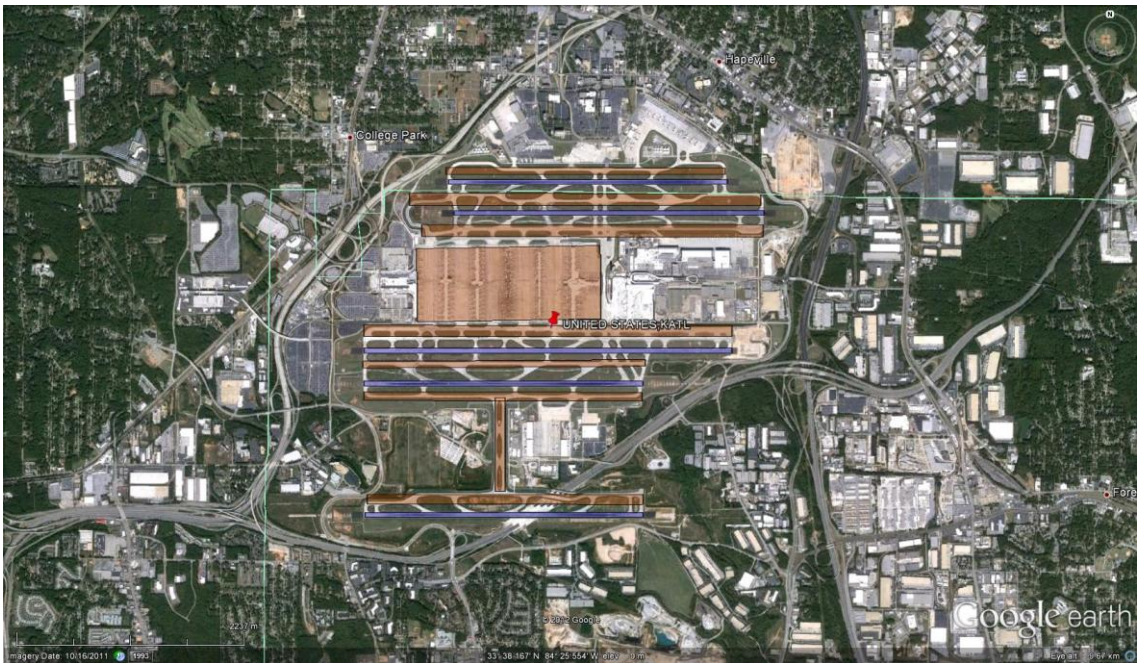

Figure 41. Complete area-source representation of Hartsfield-Jackson Atlanta International Airport (KATL) superimposed on satellite imagery in Google Earth™. Runways are blue, terminals/taxiways are orange. Attribution: © 2012 Google.

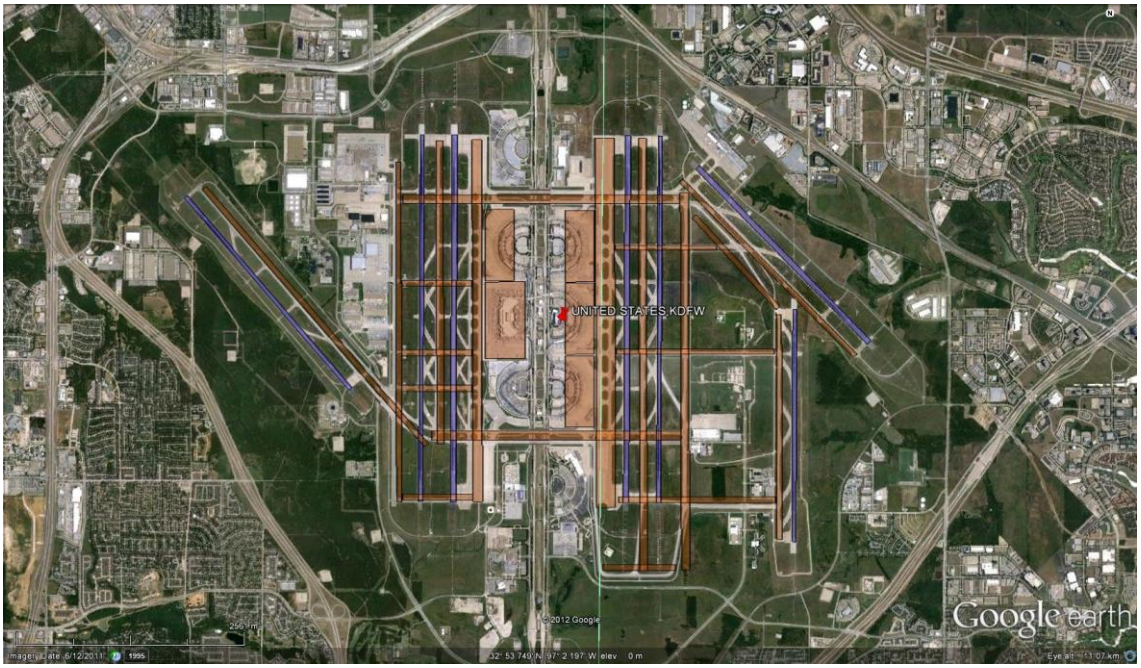

Figure 42. Complete area-source representation of Dallas/Fort Worth International Airport (KDFW) superimposed on satellite imagery in Google Earth™. Runways are blue, terminals/taxiways are orange. Attribution: © 2012 Google.

Figure 43. Complete area-source representation of John F. Kennedy International Airport (KJFK) superimposed on satellite imagery in Google Earth™. Runways are blue, terminals/taxiways are orange. Attribution: © 2012 Google.

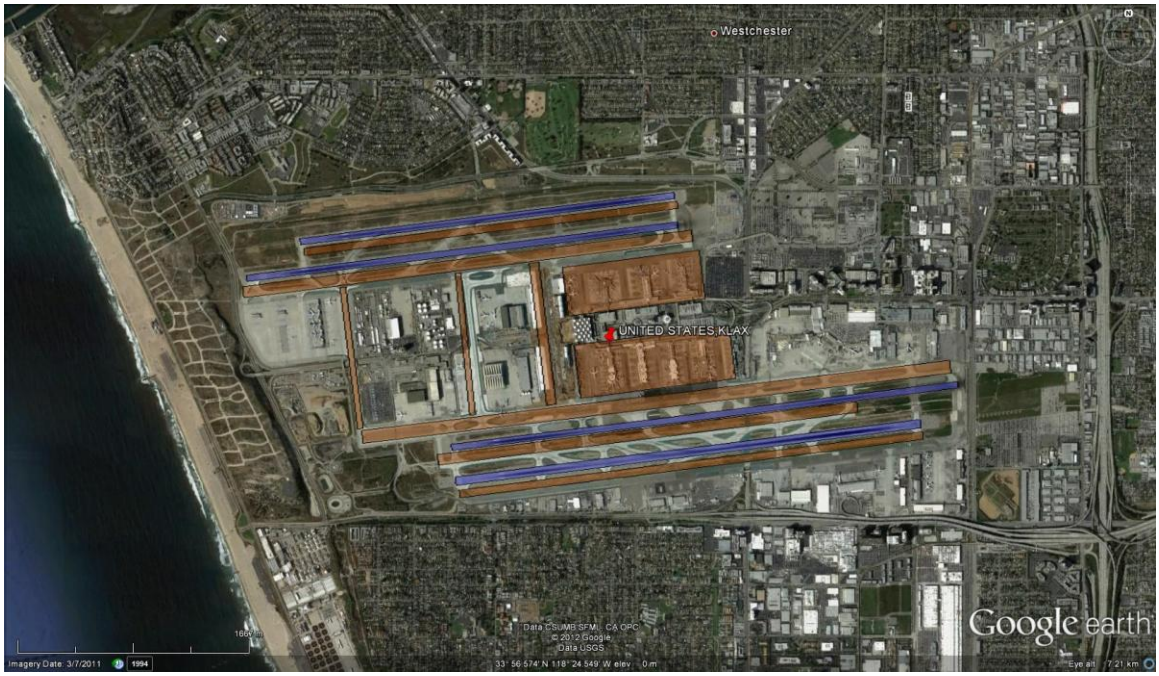

Figure 44. Complete area-source representation of Los Angeles International Airport (KLAX) superimposed on satellite imagery in Google Earth™. Runways are blue, terminals/taxiways are orange. Attribution: Data CSUMB SFML, CA OPS; © 2012 Google; Data USGS.

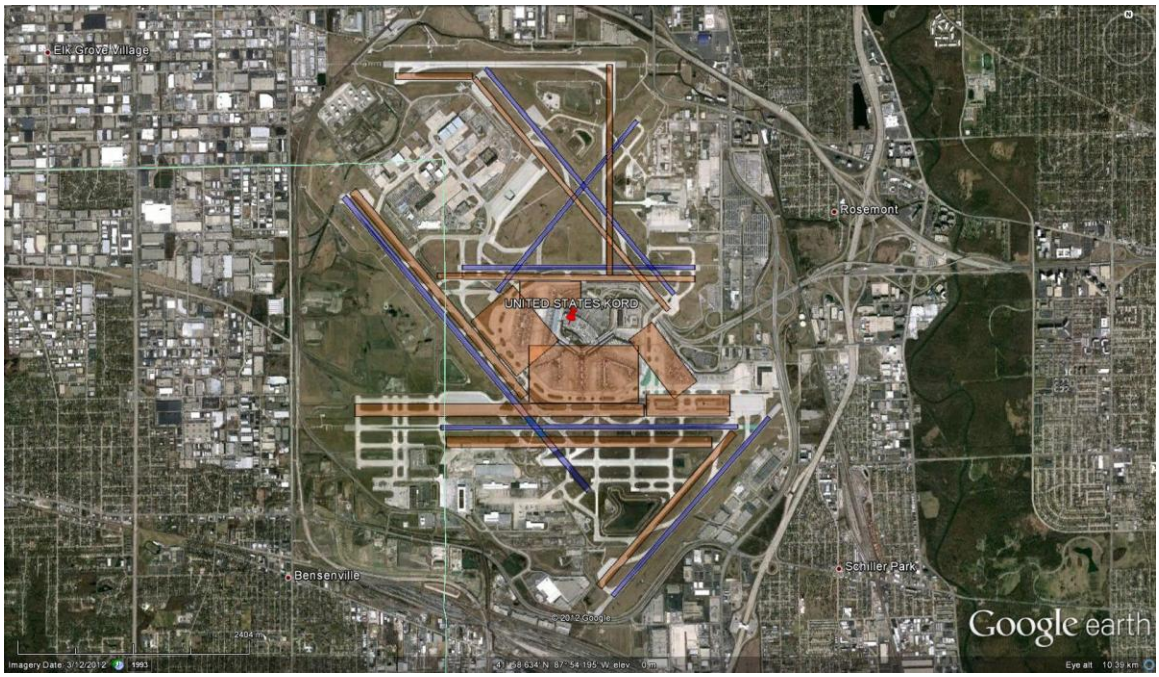

Figure 45. Complete area-source representation of Chicago O'Hare International Airport (KORD) superimposed on satellite imagery in Google Earth™. Runways are blue, terminals/taxiways are orange. Attribution: © 2012 Google.

A-4-2 Wind Roses

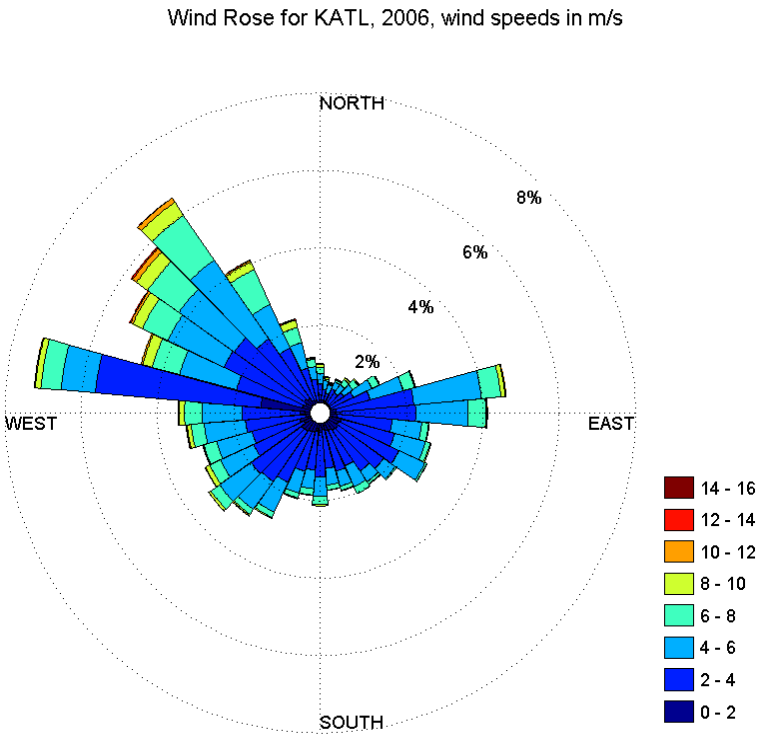

Figure 46. Wind rose for 2006 for Hartsfield-Jackson Atlanta International Airport (KATL).

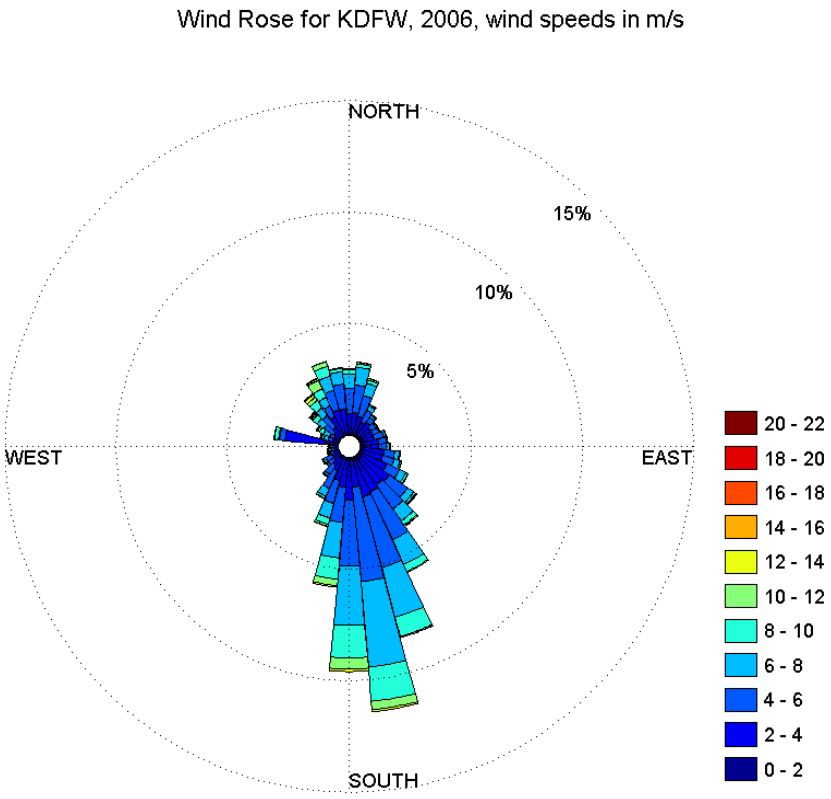

Figure 47. Wind rose for 2006 for Dallas/Fort Worth International Airport (KDFW).

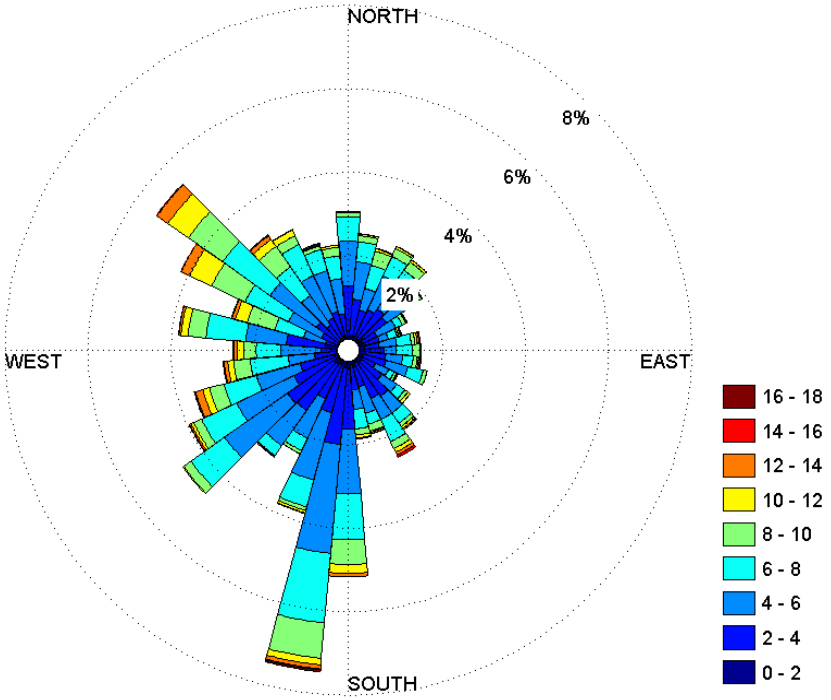

Figure 48. Wind rose for 2006 for John F. Kennedy International Airport (KJFK).

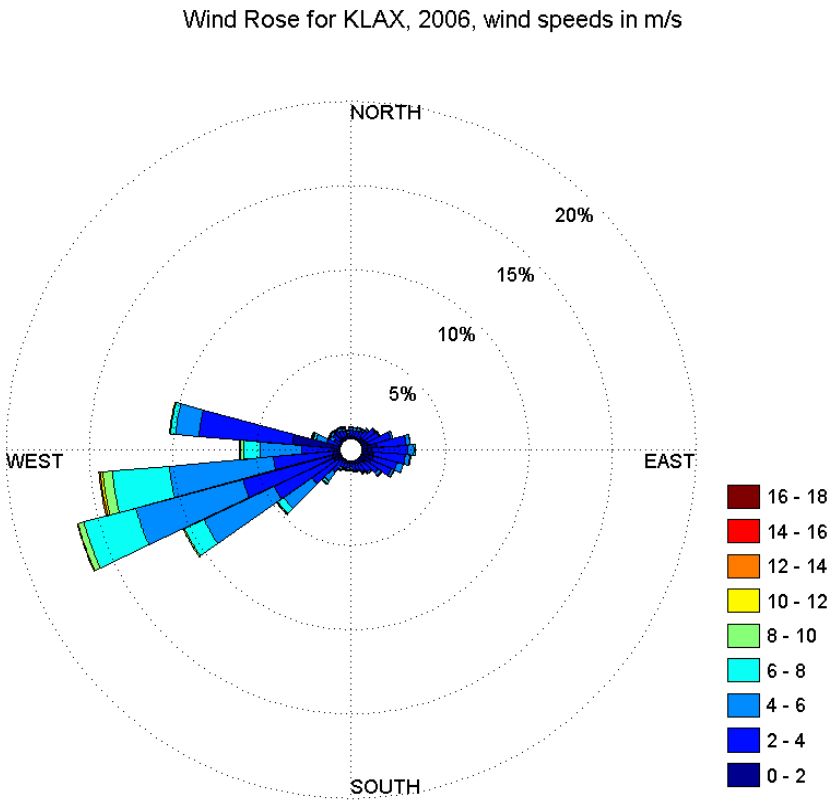

Figure 49. Wind rose for 2006 for Los Angeles International Airport (KLAX).

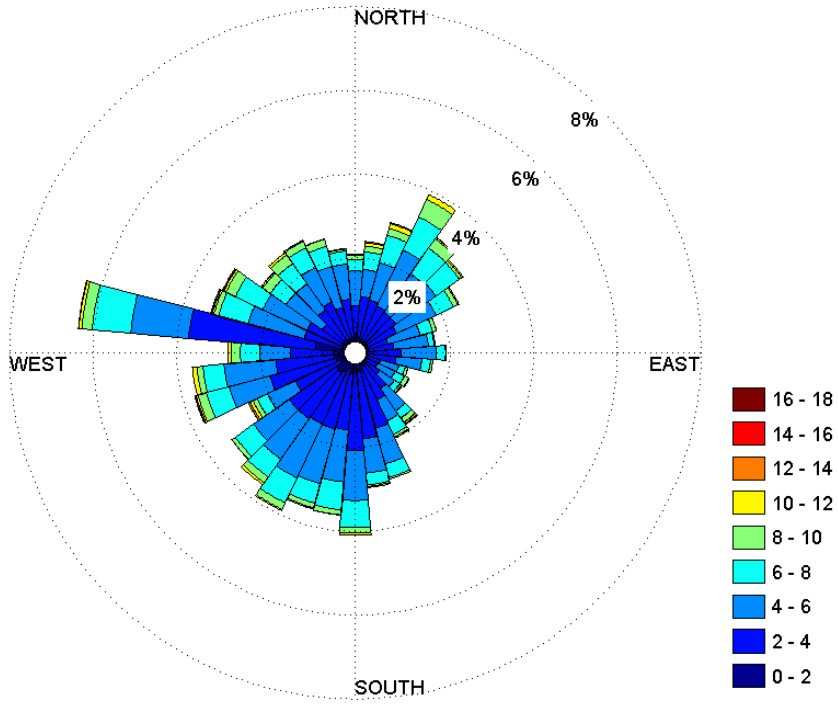

Figure 50. Wind rose for 2006 for Chicago O'Hare International Airport (KORD).

A-4-3 Concentration and Exposure Plots

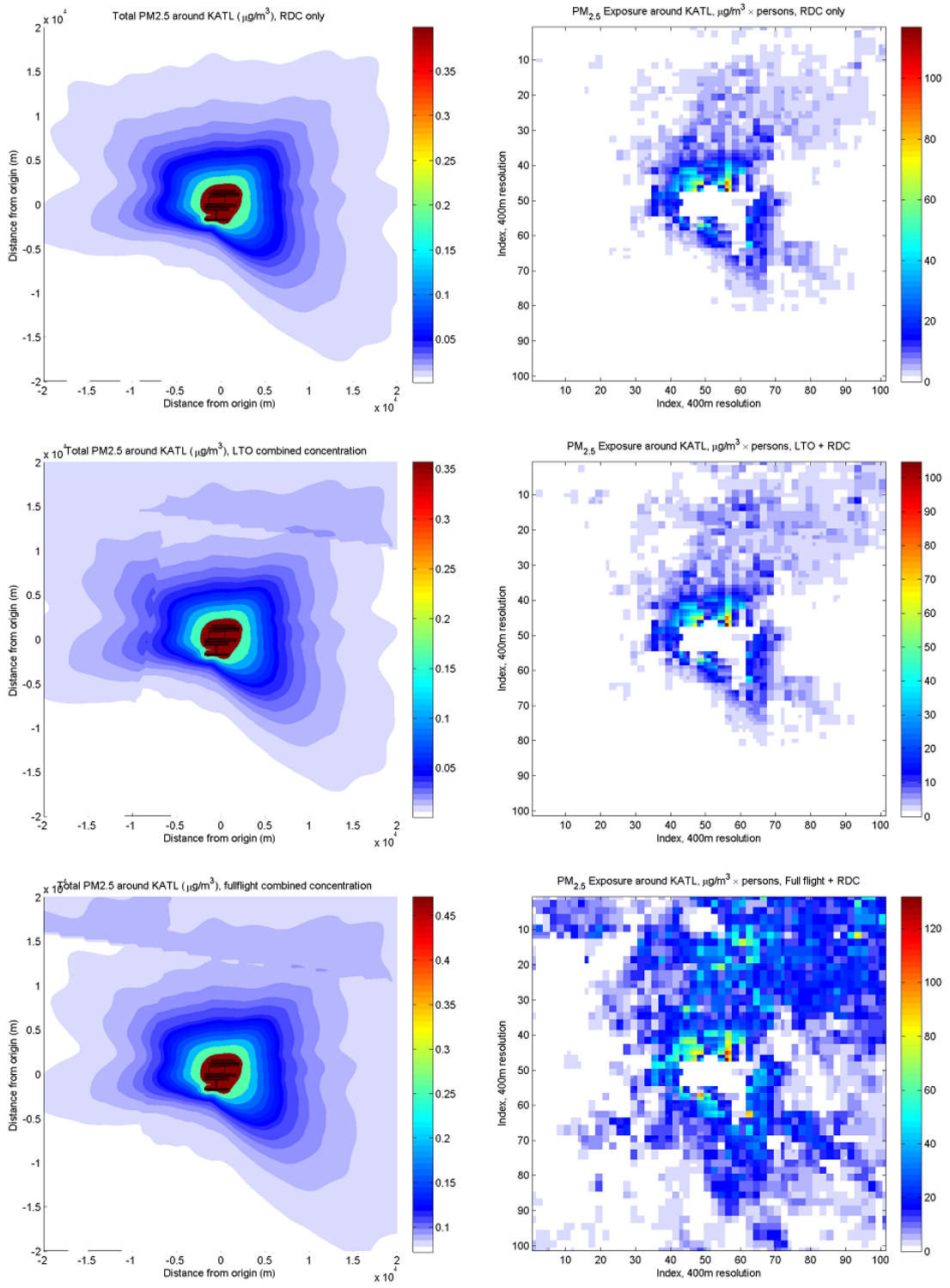

a) b)

Figure 51. Plots of a) RDC-only and combined RDC-CMAQ $PM_{2.5}$ concentration values; b) Spatial variation of local $PM_{2.5}$ exposure; for Hartsfield-Jackson Atlanta International Airport (KATL). With plume factor adjustment.

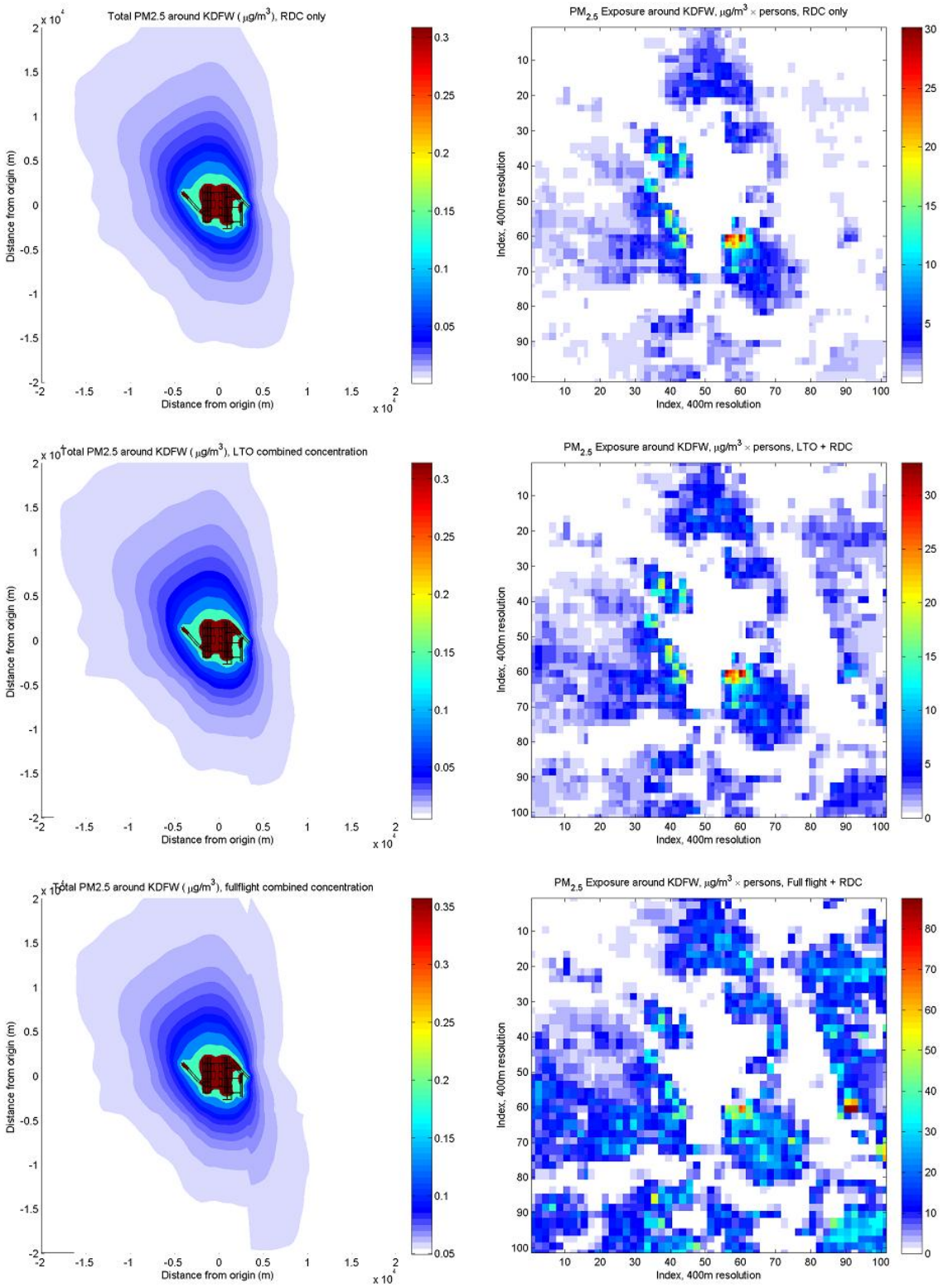

a) b)

Figure 52. Plots of a) RDC-only and combined RDC-CMAQ $PM_{2.5}$ concentration values; b) Spatial variation of local $PM_{2.5}$ exposure; for Dallas/Fort Worth International Airport (KDFW). With plume factor adjustment.

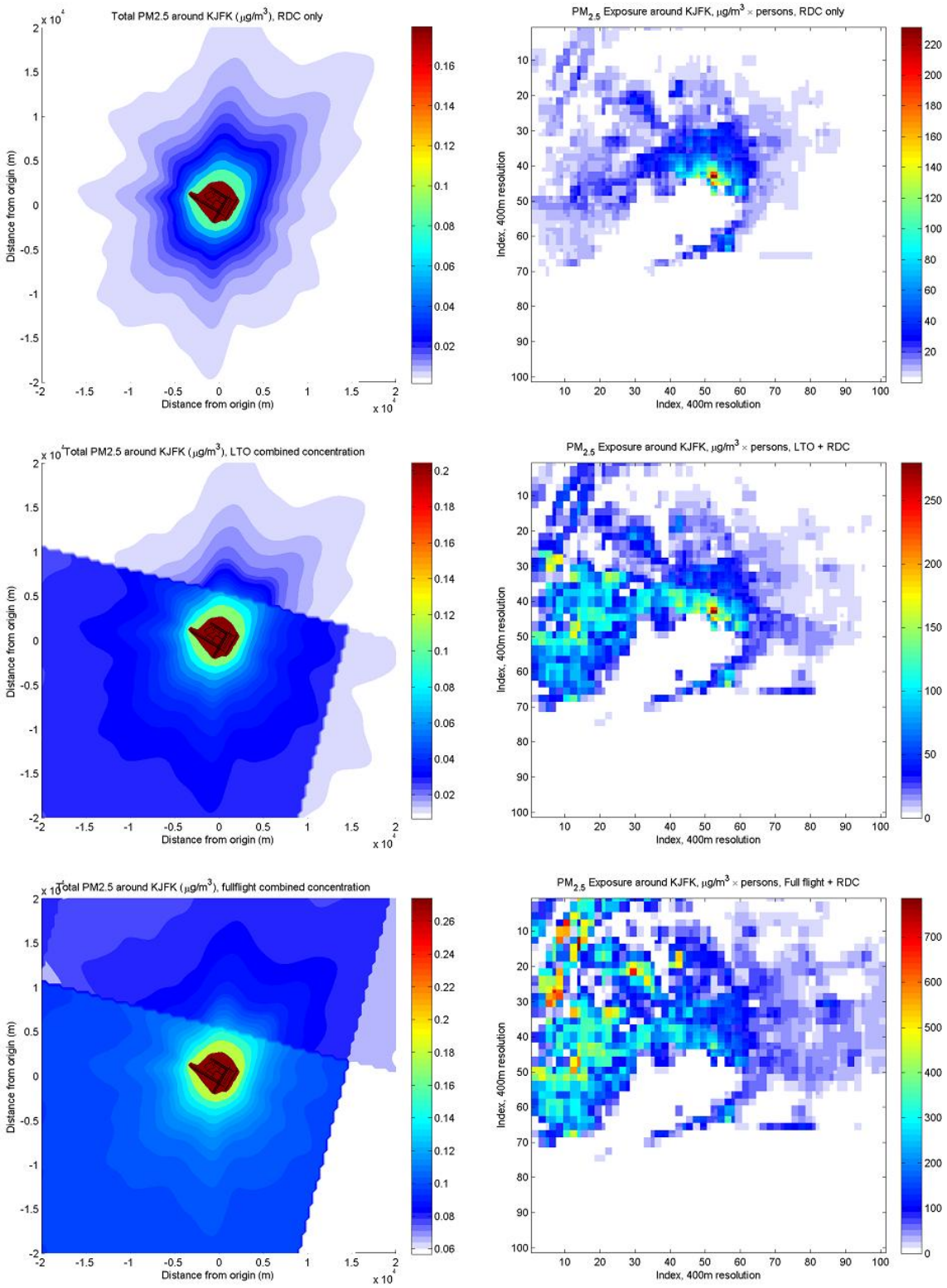

a) b)

Figure 53. Plots of a) RDC-only and combined RDC-CMAQ $PM_{2.5}$ concentration values; b) Spatial variation of local $PM_{2.5}$ exposure; for John F. Kennedy International Airport (KJFK). With plume factor adjustment.

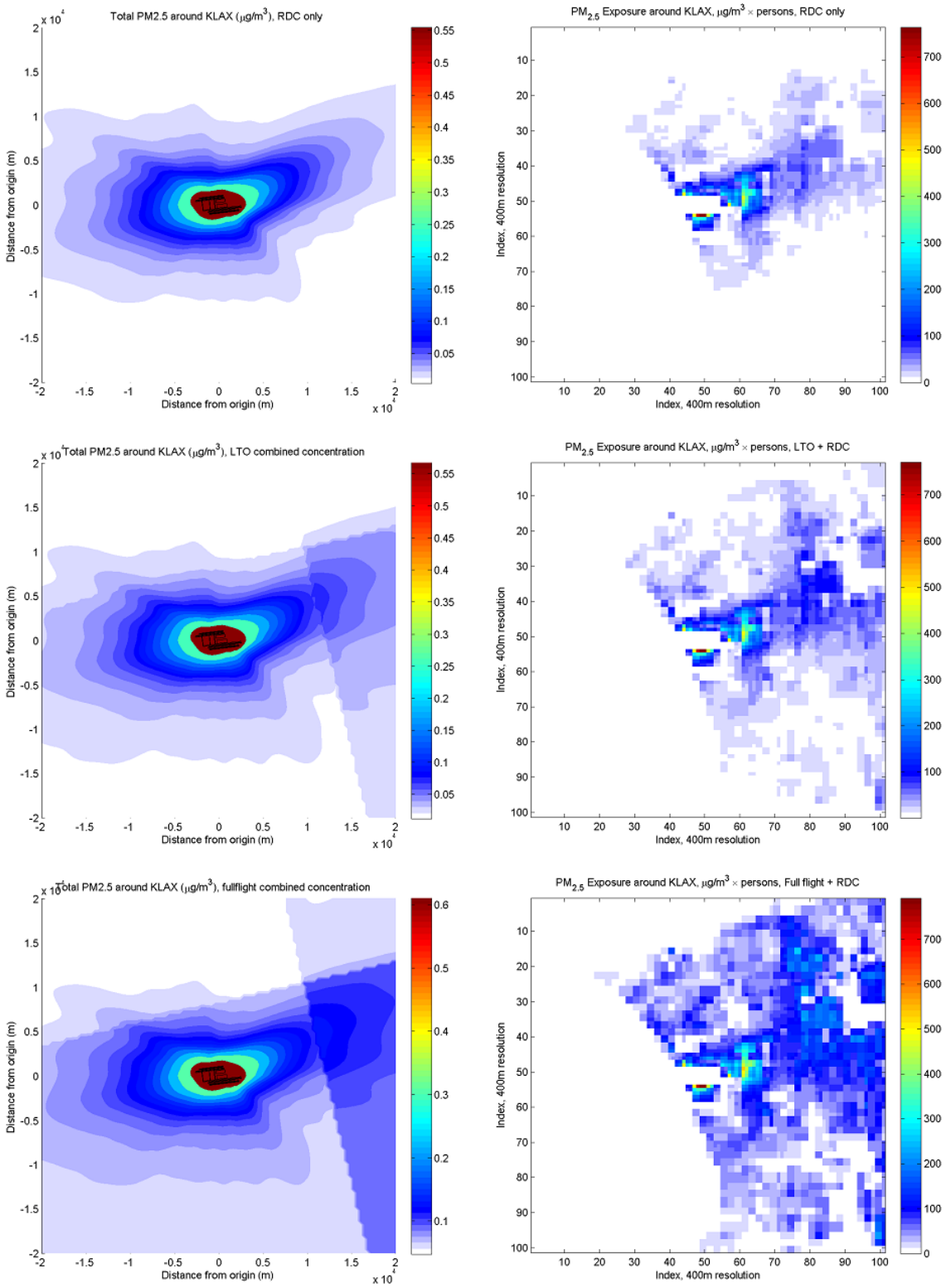

a) b)

Figure 54. Plots of a) RDC-only and combined RDC-CMAQ $PM_{2.5}$ concentration values; b) Spatial variation of local $PM_{2.5}$ exposure; for Los Angeles International Airport (KLAX). With plume factor adjustment.

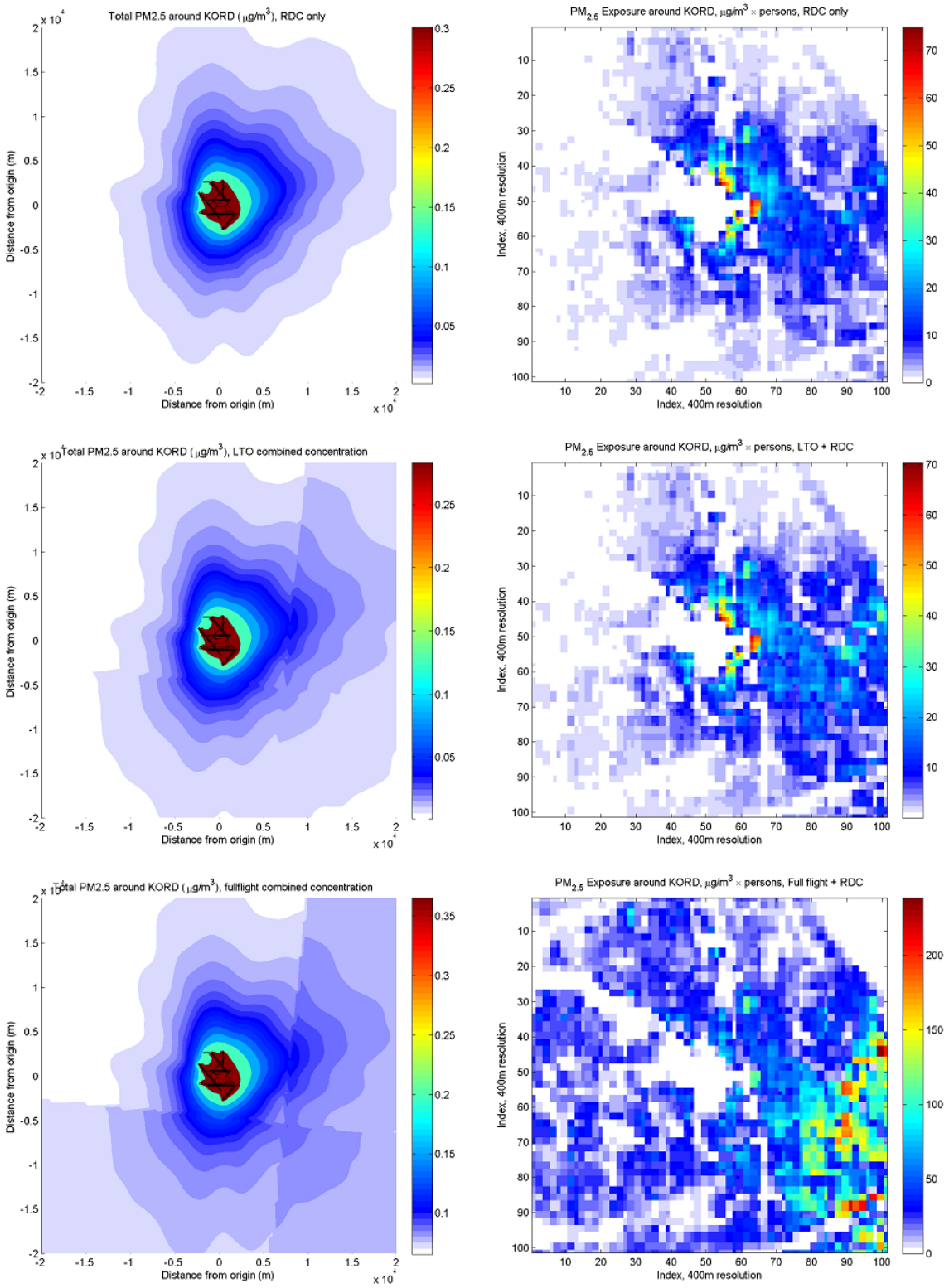

a) b)

Figure 55. Plots of a) RDC-only and combined RDC-CMAQ PM2.5 concentration values; b) Spatial variation of local $PM_{2.5}$ exposure; for Chicago O'Hare International Airport (KORD). With plume factor adjustment.